AN ABSTRACT OF THE THESIS OF

Guan Bee Ch'ng for the degree of Doctor of Philosophy in Civil Engineering presented on May 1, 1996.

Title: Aseismic Performance of a Cable-Stayed Structure with Decentralized H_∞ Control

Redacted for Privacy

Abstract approved: _____

Alan G. Hernried

The dissertation uses state-of-the-art structural engineering theories, in parallel with the modern and still-developing control theory of electrical engineering to mitigate the vibratory responses of a double-stayed bridge subjected to strong earthquake ground motions.

First, a nonlinear finite element model of the double-stayed bridge subjected to non-uniform (multi-support) earthquake excitations is developed. The model incorporates the nonlinearities from the sagging of the cables and the effects of axial forces in the members. Next, the static behaviours as well as the uncontrolled responses of this bridge subjected to three different earthquakes are studied and the effects of variations in some of the system parameters and dimensions are examined. Finally, four decentralized controllers are proposed to protect the structure from the earthquake hazard. The scheme introduced is an Algebraic-Riccati-Equation-based (ARE-based) decentralized H_∞ control strategy. Under this scheme, controllers at only four discrete points on the deck of the structure are used. With these

controllers, the overall performance is analyzed and its effectiveness is evaluated and discussed.

Aseismic Performance of a Cable-Stayed Structure with Decentralized H_∞ Control

by

Guan Bee Ch'ng

A Thesis

submitted to

Oregon State University

in partial fulfillment of
the requirements for the
degree of

Doctor of Philosophy

Completed May 1, 1996
Commencement June 1996

Doctor of Philosophy thesis of Guan Bee Ch'ng presented on May 1, 1996

APPROVED:

Redacted for Privacy

Major Professor, representing Civil Engineering

Redacted for Privacy

Chair of the Department of Civil Engineering

Redacted for Privacy

Dean of the Graduate School

I understand that my thesis will become part of the permanent collection of Oregon State University libraries. My signature below authorizes release of my thesis to any reader upon request.

Redacted for Privacy

Guan Bee Ch'ng, Author

ACKNOWLEDGMENT

At the outset, the author wishes to express his sincere gratitude to his thesis advisor, Dr. Alan G. Hernried, Professor of Civil Engineering for his invaluable guidance and expertise in every aspect. Appreciation is also given to other members of the committee, Dr. Thomas H. Miller, Dr. Solomon C. S. Yim, Dr. Molly H. Shor, and Dr. Donald C. Solmon, for their interest and participation as Graduate Committee.

The thesis investigation was supported financially by National Science Foundation under Grant Number CMS-9301464. This support is gratefully acknowledged. Financial contribution during the author's graduate study, provided by the Department of Civil Engineering at Oregon State University in the form of teaching assistantship is also greatly appreciated.

Lastly, the author would like to express his deepest and heartfelt gratitude to his family, especially his father Mr. Chin Chong Ch'ng for his constant moral support, encouragement and blessings, and his missus for her love and patience.

TABLE OF CONTENTS

TABLE OF CONTENTS (Continued)

LIST OF FIGURES

LIST OF FIGURES (Continued)

LIST OF FIGURES (Continued)

LIST OF FIGURES (Continued)

LIST OF FIGURES (Continued)

Figure | Page

LIST OF TABLES

ASEISMIC PERFORMANCE OF A CABLE-STAYED STRUCTURE WITH DECENTRALIZED H_∞ CONTROL

1. INTRODUCTION

1.1. An Overview

Like other natural hazards, earthquakes are a major concern to human beings. A strong earthquake can have devastating impacts on both mankind and the economy. During the first three quarters of this century, a source [51] reports that earthquakes have claimed an average of over ten thousand lives each year and total damage losses of more than ten billion dollars. In recent decades, damaging earthquakes such as Mexico City (1985), Loma Prieta (1989), Northridge (1994), and Hyogoken-Nanbu (1995), have contributed more to the fatalities and destruction due to earthquakes.

Long bridges are in general vulnerable to earthquakes. Among the many types of long-span bridge structures, cable supported bridges are often selected over typical, conventional designs because they are economical and aesthetically pleasing. Cable supported bridges can be broadly classified into suspension and cable-stayed bridges. In recent decades, the trend has been towards the design and construction of cable-stayed bridges rather than suspension-type bridges. The cable-stayed bridges are stiffer than the suspension bridges with the same span. The larger deflections of the suspension bridges compared to that of the cable-stayed bridges are primarily due to the flexibility of the main suspension cable.

Since first proposed by Yao [96] in 1972, the idea of using active control systems to reduce the dynamic response of civil engineering structures has received increasing consideration. This concept of active feedback control has been used for decades in the aerospace industry. Recently, it has successfully been applied to large scale civil engineering structures ([4], [5], [7], [8], [9], [10], [14], [96], etc.). Practical application includes the installation of a 400-ton tuned mass damper on the Citicorp Building in New York City to control the building's first mode. A similarly designed tuned mass damper was also introduced on the Canadian National Tower in Toronto, and on the John Hancock Building in Boston.

The idea of applying active control to a cable-stayed bridge has been discussed for more than a decade ([89], [90], [35]). The tendon control mechanism first introduced was difficult to realize or implement, due to the fact that the control actuators installed on the cables had to carry the self-weight of the structure. Recently, a double-stayed bridge configuration was proposed [35]. The advantage of this newly proposed configuration over the conventional ones is that the use of pretension stay cables above and below the guideway may provide more structural resistance to the uncontrolled vertical deflections of the guideway. Secondly, in the case of active tendon control, the actuator can be placed on either lower or upper cables, or both. This increases the flexibility of active control designs. Finally, both upper and lower cables can be pretensioned for the static dead load. For these reasons, this so-called double-stayed configuration is examined in this research.

This dissertation extends the above work to include the study of the structural behaviour of this double-stayed bridge under multi-support strong earthquake motions. Previous studies ([34], [1], [35], etc.) have constructed partial differential equations and have used the finite element method to model this type of structure. In this study, a finite element model is developed. The scope of this thesis includes

a static parametric study, dynamic parametric study, and an examination of the uncontrolled and controlled responses of the structure subjected to three different strong earthquakes. For the static parametric study, a nonlinear static equilibrium finite element method is used. This parametric study is conducted to observe the static structural behaviour of the system and to analyze the sensitivity of the response to parameter variations. For the dynamic parametric study, a nonlinear static, linear dynamic approach is used. Also examined in this study is the mitigation of seismic hazards using four decentralized controllers which are installed on the lower cables of the structure. To evaluate the aseismic performance of this controlled bridge, an advanced state-space decentralized H_∞ control scheme appropriate for this structure is considered.

1.2. Literature Reviews

Some unfortunate engineering failures of cable-supported structures have been reported due to overloadings from wind and earthquake excitations [18]. The need for more understanding of these cable-supported structures has resulted in many publications regarding their dynamic analysis. For cable-stayed bridges, work has primarily been focused on the seismic behaviour ([1], [29], [53], [54], [50], [48], [49]), and on different energy method analyses [34].

Due to the uncertain nature of dynamic loadings such as wind and earthquakes, these loadings are in general much more difficult to predict and design for than static loadings. To protect structures against these dynamic loadings, techniques for controlling and reducing the response has become a focus of attention for many researchers. In recent decades, new theoretical developments as well as possible application of active feedback control strategies to structures have grown

into an intensive research area. Categorized and outlined below are the studies done on active structural control in the past two decades [14].

New and improved control methods have been proposed. An improved control scheme was based on the Riccati equation ([58], [94]).

Applications of different proposed methods to structural control problems ([4], [5], [7], [8], [45]) using optimal control theory ([12] [56], [58], [93], [44], [91], [7], [21], [5], [87], etc.), using adaptive control ([20], [63], [64]), and using H_∞ robust control [70] have been investigated. Extensions were also made to include nonlinear problems ([9], [10])

Most theoretical and experimental control efforts on civil engineering structures were directed at buildings ([21], [23], [24], [56], [59], [62], [65], [85], [86], [88], [91], [92], [93], [94], [95], [60], etc.), and conventional highway bridges ([2], [4], [5], [8], [9], [10], [32], etc.). Only a few applications have been for cable-supported structures like cable-stayed bridges ([89], [90]), and special structures like floating structures [69].

The control mechanisms used were generally active tuned mass dampers ([14], [94], [65], [93], [91], [92], [21], etc.), and active tendon control ([5], [8], [23], [24], [59], [60], [88], [89], [90], [91], [92], [93], [94]). New control mechanisms like liquid dampers [86] can also be found in the literature. Besides the above-mentioned developments in structural control application, there are also studies on the optimal placement of the control mechanisms [3], on the optimal placement of the sensors [79], and on the investigation of the effects of uncertainties in the building parameters (e.g., stiffness, damping, etc.) on the efficiency of the optimal control [95].

Based on the overview of the previous work outlined above, little has been done on the mitigation of the dynamic response of cable-stayed bridges, and on the

investigation of the H_∞ control scheme. No efforts have been devoted to possible use of a decentralized control scheme.

1.3. Outline of this Dissertation

There are many cable configurations for cable-stayed bridges, and these configurations can be classified into a few categories or types [18]. Chapter 2 describes the configuration and physical dimensions of the bridge under study. The idealized physical model of this double-stayed guideway, and methods and approaches used to obtain the described mathematical model and response are overviewed. These methods include the finite element method (FEM), a non-linear static equilibrium approach, multiple-support excitation dynamics, and the decentralized H_∞ control scheme.

Chapter 3 presents three earthquake records that are categorized as strong motions. They are used in the subsequent simulation studies.

The uncontrolled response of this double-stayed bridge due to a moving load has been investigated ([35], [22]). Chapter 4 presents some parametric studies on the uncontrolled response of this structure subjected to strong earthquake excitations.

Chapter 5 reports the controlled response of this structure subjected to earthquake-induced support motions utilizing four decentralized H_∞ controllers.

Chapter 6 concludes the study. The effectiveness of the proposed control scheme is discussed.

2. STRUCTURAL MODELING AND COMPUTATIONAL METHODS AND APPROACHES

2.1. Ideal Physical Model of a Double-stayed Structure

Cable-stayed bridges have various cable arrangements which can be broadly classified into four basic categories [18]. They are radiating, harp, fan, and star

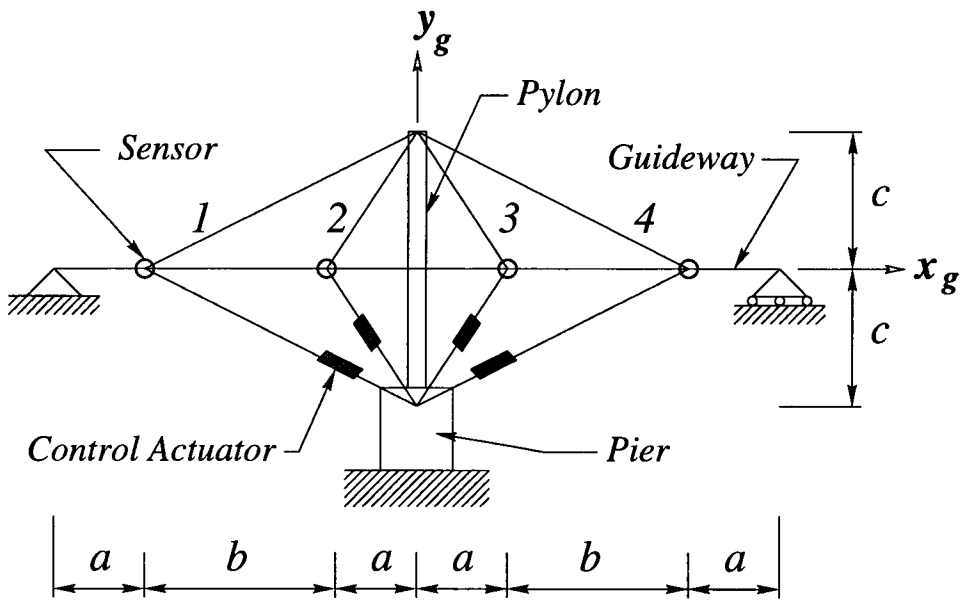

FIGURE 2.1. Ideal Physical Model of a Floating Double-Stayed Structure showing Cable Numbers, $x_g - y_g$ Coordinate System, Physical Dimensions, and Locations of Sensors and Control Actuators. ($a = L/8, b = L/4, c = 3L/16$, $L = 400\ ft$, Length of Guideway)

arrangements. No doubt, other variations and combinations are possible. Besides cable configurations, there are many different types of pylon-to-deck connections or supporting conditions [13]. The model studied in this research represents a floating

type with radiating cable configuration. A floating type connection refers to zero moment and zero shear transfers between the pylon and the deck. Figure 2.1 shows the ideal physical model of this double-stayed guideway. Also shown are the $x_g - y_g$ coordinate system, the cable numbering system, physical dimensions, and locations of sensors and control actuators. In this model, the structure is assumed to be simply supported, with a deck span of 400 ft, and the pylon is assumed to be fixed to the pier. The material and sectional properties of components of this model are listed in Table 2.1.

	Deck	Pylon	Cable
Modulus of Elasticity (ksf)	4,200,000	4,200,000	4,000,000
Cross-sectional Area (ft^2)	8.0	28.5	0.6
Moment of Inertia (ft^4)	45.0	160.0	n/a
Mass Density ($\frac{k-s^2}{ft^4}$)	0.018	0.020	0.016
Weight per unit length (klf)	4.64	18.35	0.30

TABLE 2.1. Material and Sectional Properties

2.2. The Finite Element Method (FEM)

The mathematical representation of the ideal physical model of the double-stayed guideway is obtained through the finite element method. By this method, the general analysis procedure is to first idealize or discretize the ideal physical model as a collection of finite elements connected at nodes, as shown in Figure 2.2. With the inclusion of axial deformation, each node involves three degrees of freedom (DOF).

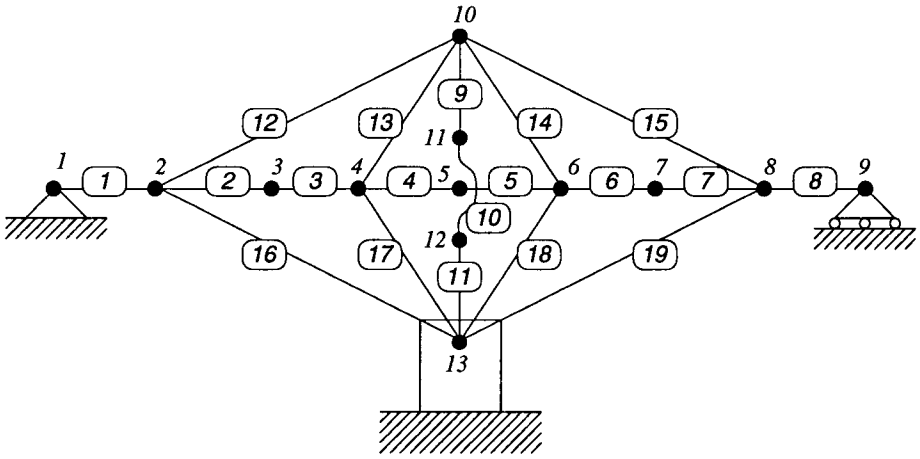

FIGURE 2.2. Finite Element Model of the Ideal Physical Model of the Floating Double-Stayed Guideway showing Node and Element Numbers, and their connectivities.

The positive sign convention for these DOF's in an arbitrarily oriented element is shown in Figure 2.3. Each element has a stiffness associated with it. There are two types of elements used to describe this model. They are beam elements for the pylon and guideway, and cable elements for the cables. A typical local beam element stiffness matrix is described below.

$$k_e^b = \begin{pmatrix} k_{11} & 0 & 0 & k_{14} & 0 & 0 \\ 0 & k_{22} & k_{23} & 0 & k_{25} & k_{26} \\ 0 & k_{32} & k_{33} & 0 & k_{35} & k_{36} \\ k_{41} & 0 & 0 & k_{44} & 0 & 0 \\ 0 & k_{52} & k_{53} & 0 & k_{55} & k_{56} \\ 0 & k_{62} & k_{63} & 0 & k_{65} & k_{66} \end{pmatrix} \tag{2.1}$$

where

$$k_{11} = k_{44} = -k_{14} = -k_{41} = \frac{A_b E_b}{L_e}$$

$$k_{22} = k_{55} = -k_{25} = -k_{52} = \frac{12 E_b I_b}{L_e^3}$$

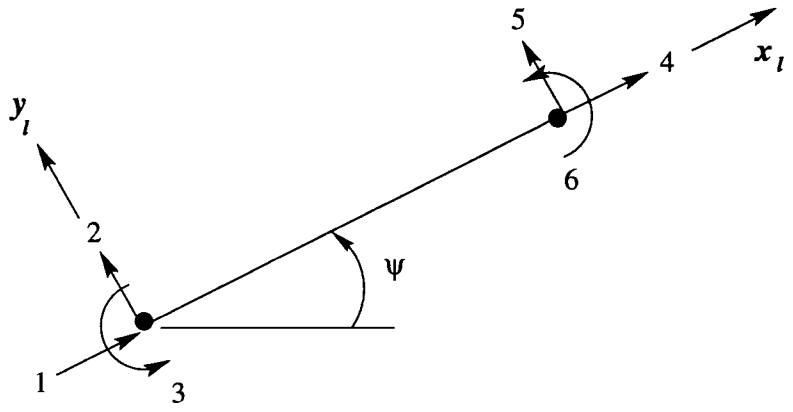

FIGURE 2.3. Positive Sign Convention in Local Coordinates, $x_l - y_l$ for a typical Finite Element

$$k_{23} = k_{32} = k_{26} = k_{62} = -k_{35} = -k_{53} = -k_{56} = -k_{65} = \frac{6E_bI_b}{L_e^2}$$

$$k_{33} = k_{66} = \frac{4E_bI_b}{L_e}$$

$$k_{36} = k_{63} = \frac{2E_bI_b}{L_e}$$

where L_e is the length of the element, A_b is the cross-sectional area, E_b is the modulus of elasticity, and I_b is the moment of inertia of the beam element. A linear local cable element stiffness matrix is described below.

$$k_e^c = \frac{A_cE_c}{L_e} \cdot \begin{pmatrix} 1 & 0 & 0 & -1 & 0 & 0 \\ 0 & 0 & 0 & 0 & 0 & 0 \\ 0 & 0 & 0 & 0 & 0 & 0 \\ -1 & 0 & 0 & 1 & 0 & 0 \\ 0 & 0 & 0 & 0 & 0 & 0 \\ 0 & 0 & 0 & 0 & 0 & 0 \end{pmatrix} \tag{2.2}$$

where L_e is the length of the element, A_c is the cross-sectional area, E_c is the modulus of elasticity of the cable.

Since the orientation of each element in the global coordinate system may be different, a transformation matrix is used to transform both the forces and displacements from the local $x_l - y_l$ coordinate system to the global $x_g - y_g$ coordinate system. This transformation matrix T is described in Equation 2.3.

$$T = \begin{pmatrix} \cos(\psi) & \sin(\psi) & 0 & 0 & 0 & 0 \\ -\sin(\psi) & \cos(\psi) & 0 & 0 & 0 & 0 \\ 0 & 0 & 1 & 0 & 0 & 0 \\ 0 & 0 & 0 & \cos(\psi) & \sin(\psi) & 0 \\ 0 & 0 & 0 & -\sin(\psi) & \cos(\psi) & 0 \\ 0 & 0 & 0 & 0 & 0 & 1 \end{pmatrix} \tag{2.3}$$

After the local beam element stiffness matrix (k_e^b) is formed for each element using Equation 2.1, the global beam element stiffness matrix (k_g^b) can be obtained by

$$k_g^b = T^T \cdot k_e^b \cdot T \tag{2.4}$$

Similarly, the global cable element stiffness matrix (k_g^c) can be obtained by

$$k_g^c = T^T \cdot k_e^c \cdot T \tag{2.5}$$

Once the global element stiffness matrices (k_g^b and k_g^c) for each element are obtained, the system or structure stiffness matrix K can be assembled. Next the boundary conditions and externally applied loadings are imposed. The system matrix K may be partitioned to separate the unknown from the known displacements, and the unknown from the known forces, as shown in Equation 2.6 below.

$$\begin{pmatrix} f_\alpha \\ f_\beta \end{pmatrix} = \begin{pmatrix} K_{\alpha\alpha} & K_{\alpha\beta} \\ K_{\beta\alpha} & K_{\beta\beta} \end{pmatrix} \cdot \begin{pmatrix} d_\alpha \\ d_\beta \end{pmatrix} \tag{2.6}$$

where f_α are the known forces, f_β are the unknown forces, d_α are the unknown displacements, and d_β are the known displacements.

The final step is to solve for the unknown forces and displacements by Equations 2.7 and 2.8.

$$f_\beta = K_{\beta\alpha} d_\alpha + K_{\beta\beta} d_\beta \tag{2.7}$$

$$d_\alpha = K_{\alpha\alpha}^{-1}(f_\alpha - K_{\alpha\beta} d_\beta) \tag{2.8}$$

To obtain the local beam element forces f_e^b (axial, shear, and bending moments), the displacements d_α need to be transformed back to the local level as follows.

$$f_e^b = k_e^b \cdot T \cdot d_\alpha \tag{2.9}$$

Similarly, the local cable element forces f_e^c can be obtained by replacing k_e^b with k_e^c in the above equation.

2.3. The Non-Linear Static Equilibrium Approach

The nonlinear behaviour of the cable-stayed bridge is primarily a result of geometric nonlinearities. The nonlinear force-deformation relationships are caused by the sagging of the inclined cable stays, and the axial-bending interactions of the pylon and deck. The sagging of the cable stays is a function of both the axial load and the self-weight of the cable.

For cables, the concept of an equivalent modulus of elasticity (E_{eq}) is employed to account for the nonlinearity in the inclined cable stays due to sagging ([29], [41], [40], [48]). By considering an equivalent straight chord member with an equivalent modulus of elasticity E_{eq} (which combines effects of both material and

geometric nonlinearities), with E_{eq} assumed to be constant if the change of tension in cable ΔT_c is not too large during each load increment, implying the axial stiffness of cable will not change significantly during each load step. The equivalent modulus of elasticity E_{eq} is given as

$$E_{eq} = \frac{E_c}{1 + \frac{(w_c H_c)^2 A_c E_c}{12 T_c^3}} \tag{2.10}$$

where A_c is the cross-sectional area of the cable, E_c is the modulus of elasticity of the cable, w_c is the weight per unit length of the cable, T_c is the cable tension before the load increment is applied, and H_c is the horizontal projected length of the cable. Equation 2.11 shows this local cable element stiffness.

$$k_{ne}^c = \frac{A_c E_{eq}}{L_e} \cdot \begin{pmatrix} 1 & 0 & 0 & -1 & 0 & 0 \\ 0 & 0 & 0 & 0 & 0 & 0 \\ 0 & 0 & 0 & 0 & 0 & 0 \\ -1 & 0 & 0 & 1 & 0 & 0 \\ 0 & 0 & 0 & 0 & 0 & 0 \\ 0 & 0 & 0 & 0 & 0 & 0 \end{pmatrix} \tag{2.11}$$

where L_e is the distance between element nodes.

To investigate the effects of the nonlinearity, two plots, one with equivalent E_{eq} versus tension in the cable with varying horizontal projected length, and the other with equivalent E_{eq} versus horizontal projected length of the cable with varying tension in the cable, are generated. They are shown in Figures 2.4 and 2.5. As can be observed from these two plots, the equivalent modulus of elasticity (E_{eq}) approaches the actual modulus of elasticity of the cable (E_c) for higher cable tensions and shorter horizontal projected lengths of the cable stay.

Nonlinearity of the axial-bending interaction due to the effect of large bending and axial deformations can be considered by employing the concept of stability

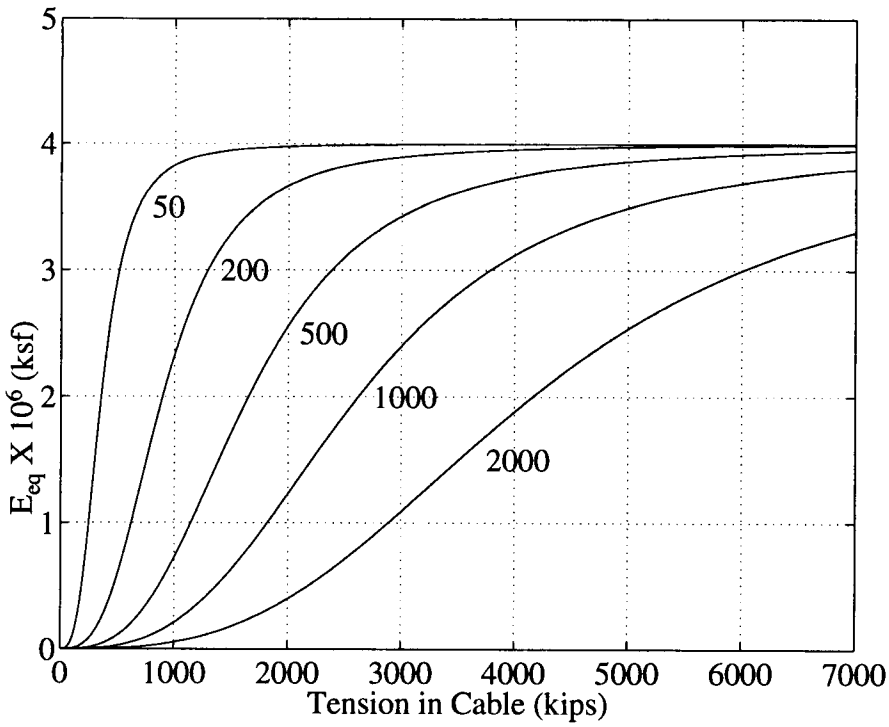

FIGURE 2.4. Equivalent E_{eq} versus Tension in the Cable with Varying Horizontal Projected Length $H_c \in \{50, 200, 500, 1000, 2000\}$ in ft.

functions ([29], [41]). The stability functions basically contain the ratio of the axial load to the critical Euler load. When this ratio is sizeable in compression, the bending stiffness will be reduced. In applying this concept, the stiffness matrix k_e^b is modified by multiplying by these stability functions, as shown in Equation 2.12

$$k_{ne}^b = \begin{pmatrix} k_{11}S_5 & 0 & 0 & k_{14}S_5 & 0 & 0 \\ 0 & k_{22}S_1 & k_{23}S_2 & 0 & k_{25}S_1 & k_{26}S_2 \\ 0 & k_{32}S_2 & k_{33}S_3 & 0 & k_{35}S_2 & k_{36}S_4 \\ k_{41}S_5 & 0 & 0 & k_{44}S_5 & 0 & 0 \\ 0 & k_{52}S_1 & k_{53}S_2 & 0 & k_{55}S_1 & k_{56}S_2 \\ 0 & k_{62}S_2 & k_{63}S_4 & 0 & k_{65}S_2 & k_{66}S_3 \end{pmatrix} \tag{2.12}$$

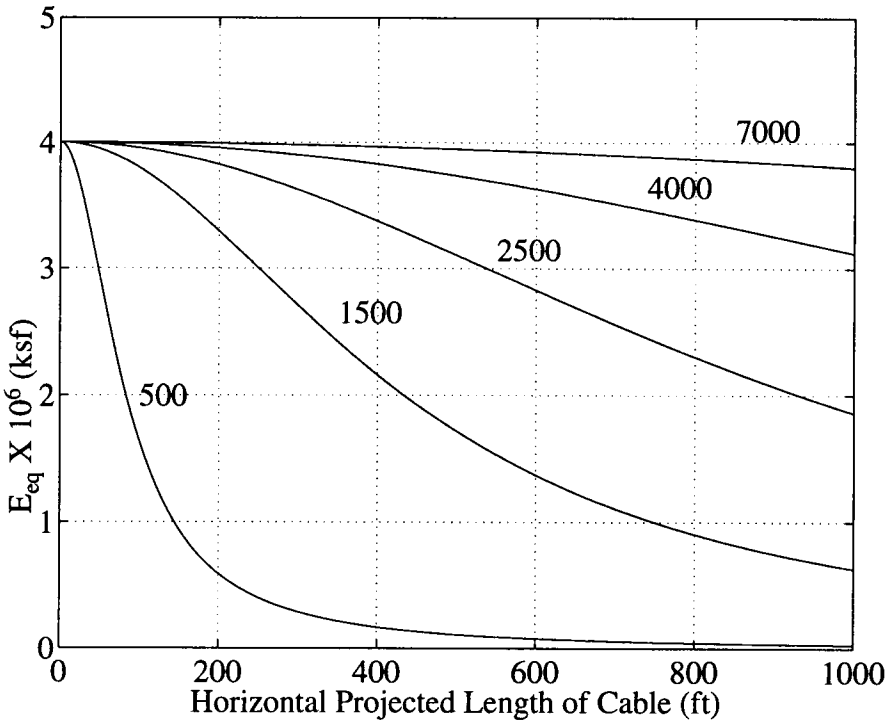

FIGURE 2.5. Equivalent E_{eq} versus Horizontal Projected Length H_c with Varying Tension in the Cable $T_c \in \{500, 1500, 2500, 4000, 7000\}$ in *kips*.

where the $k'_{ij}s$ are described in the previous section and the $S'_{ij}s$ are as described below.

For compressive axial force

$$S_1 = \frac{(x_s L_e)^3 \sin(x_s L_e)}{12 R_c}$$

$$S_2 = \frac{(x_s L_e)^2 (1 - \cos(x_s L_e))}{6 R_c}$$

$$S_3 = \frac{(x_s L_e)[\sin(x_s L_e) - x_s L_e \cos(x_s L_e)]}{4 R_c}$$

$$S_4 = \frac{(x_s L_e)[x_s L_e - \sin(x_s L_e)]}{2 R_c}$$

$$S_5 = \frac{1}{1 + \frac{E_b A_b R_{cm}}{4 P^3 L_e^2}}$$

where

$$x_s = \sqrt{\frac{P}{E_b I_b}}$$

$$R_c = 2 - 2\cos(x_s L_e) - x_s L_e \sin(x_s L_e)$$

$$R_{cm} = x_s L_e (M_{ab}^2 + M_{ba}^2)[\cot(x_s L_e) + x_s L_e \csc^2(x_s L_e)]$$

$$- 2(M_{ab} + M_{ba})^2 + (M_{ab} M_{ba})[1 + x_s L_e \cot(x_s L_e)][2 x_s L_e \csc(x_s L_e)]$$

For tensile axial force

$$S_1 = \frac{(x_s L_e)^3 \sinh(x_s L_e)}{12 R_t}$$

$$S_2 = \frac{(x_s L_e)^2 (\cosh(x_s L_e) - 1)}{6 R_t}$$

$$S_3 = \frac{(x_s L_e)[x_s L_e \cosh(x_s L_e) - \sinh(x_s L_e)]}{4 R_t}$$

$$S_4 = \frac{(x_s L_e)[\sinh(x_s L_e) - x_s L_e]}{2 R_t}$$

$$S_5 = \frac{1}{1 - \frac{E_b A_b R_{tm}}{4 P^3 L_e^2}}$$

where

$$x_s = \sqrt{\frac{P}{E_b I_b}}$$

$$R_t = 2 - 2\cosh(x_s L_e) + x_s L_e \sinh(x_s L_e)$$

$$R_{tm} = x_s L_e (M_{ab}^2 + M_{ba}^2)[\coth(x_s L_e) + x_s L_e \operatorname{csch}^2(x_s L_e)]$$

$$- 2(M_{ab} + M_{ba})^2 + (M_{ab} M_{ba})[1 + x_s L_e \coth(x_s L_e)][2 x_s L_e \operatorname{csch}(x_s L_e)]$$

A plot of these stability functions is shown in Figure 2.6. Note that at $x_s L_e = 0$, all stability functions have a value of unity, which implies that the nonlinear stiffness reduces to the linear stiffness in the absence of tensile and compressive axial load. The nonlinear static solution is obtained by a successive linear solution

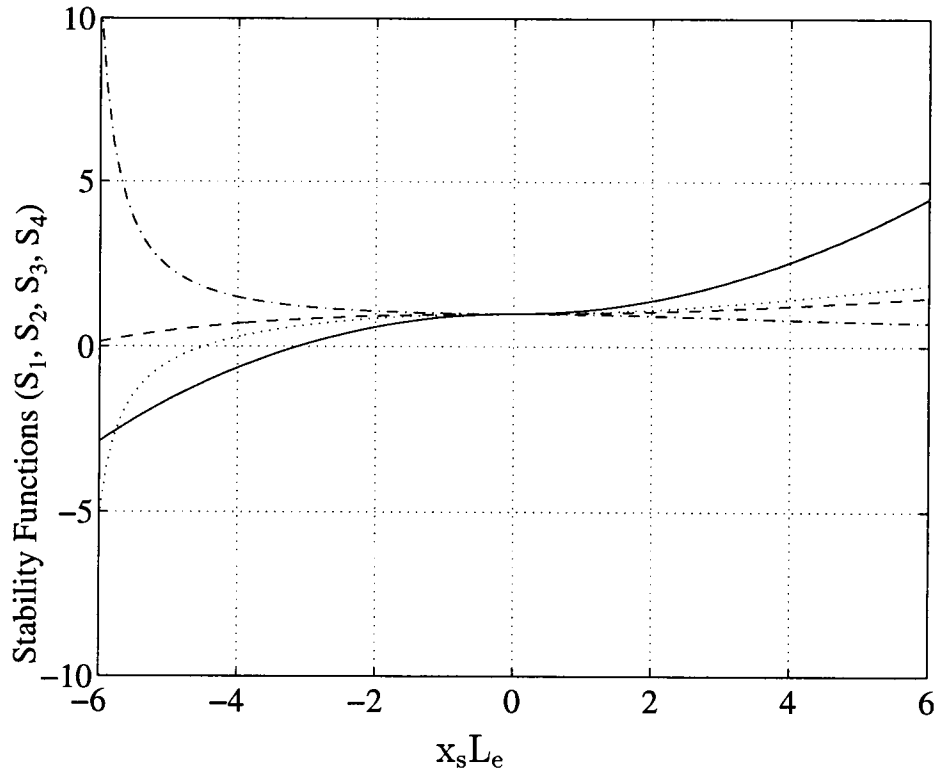

FIGURE 2.6. Stability Functions S_1 (solid line), S_2 (dashed line), S_3 (dotted line), and S_4 (dash-dotted line). Positive $x_s L_e$ indicates that the element is in tension, negative indicates compression.

approach. With this approach, the linear routine is iterated until convergence is reached. Figure 2.7 outlines this iterative approach.

2.4. Linear Dynamics with Multiple-Support Excitations

For a multi-degree-of-freedom (MDOF) system, the general equation of motion is expressed by the following matrix second order ordinary differential equation.

$$M\ddot{v} + D\dot{v} + Kv = P(t) \tag{2.13}$$

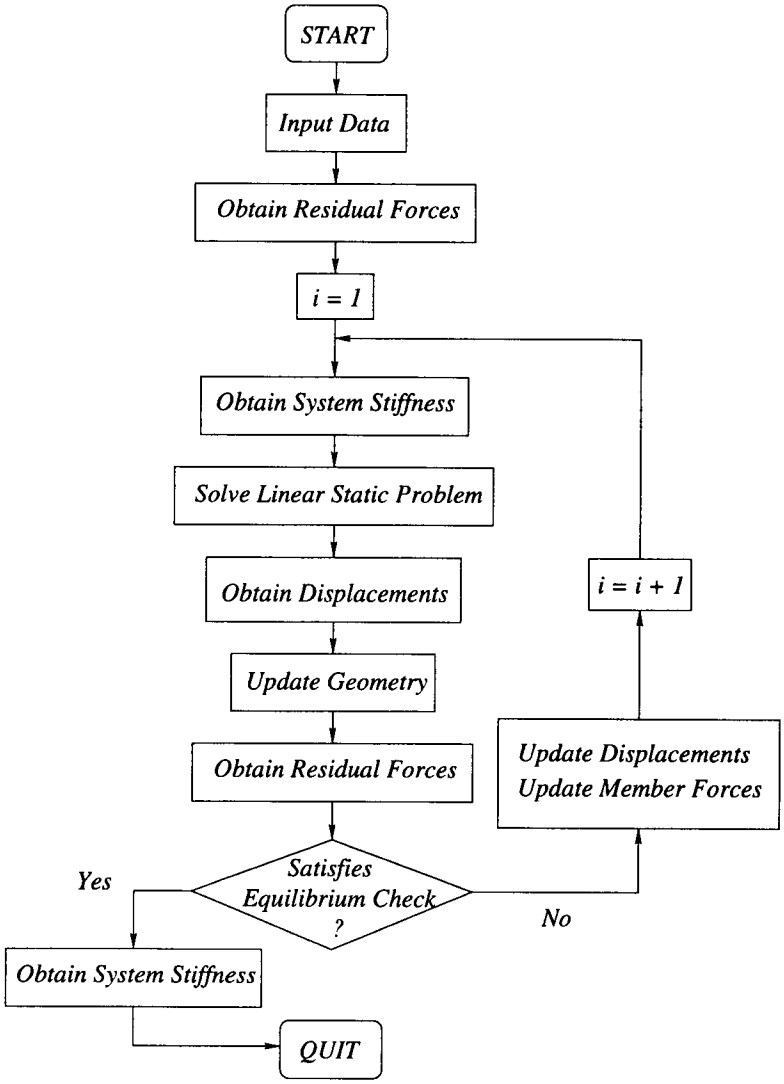

FIGURE 2.7. Flow Chart for the Nonlinear Static Equilibrium Approach

The formula describes the equilibrium of the effective forces for each degree of freedom (DOF). If there are N degrees of freedom, then M is the N by N global system mass matrix, D is the system damping matrix, K is the system stiffness matrix, and v, $\dot{v}$, $\ddot{v}$ are the displacement, velocity, and acceleration vectors, while $P(t)$ is the time dependent externally applied load vector.

The mass matrix is obtained making use of the finite element concept by a procedure similar to the analysis of the element stiffness coefficients. For a beam element with uniformly distributed mass, the consistent mass matrix ([26], [42]) is described by Equation 2.14.

$$m_e^b = \begin{pmatrix} m_{11} & 0 & 0 & m_{14} & 0 & 0 \\ 0 & m_{22} & m_{23} & 0 & m_{25} & m_{26} \\ 0 & m_{32} & m_{33} & 0 & m_{35} & m_{36} \\ m_{41} & 0 & 0 & m_{44} & 0 & 0 \\ 0 & m_{52} & m_{53} & 0 & m_{55} & m_{56} \\ 0 & m_{62} & m_{63} & 0 & m_{65} & m_{66} \end{pmatrix} \tag{2.14}$$

where

$$\begin{aligned} m_{11} = m_{44} &= \frac{\rho_b A_b L_e}{3} \\ m_{14} = m_{41} &= \frac{\rho_b A_b L_e}{6} \\ m_{22} = m_{55} &= \frac{156\rho_b A_b L_e}{420} \\ m_{23} = m_{32} = -m_{56} = -m_{65} &= \frac{22\rho_b A_b L_e^2}{420} \\ m_{33} = m_{66} &= \frac{4\rho_b A_b L_e^3}{420} \\ m_{25} = m_{52} &= \frac{54\rho_b A_b L_e}{420} \\ m_{35} = m_{53} = -m_{26} = -m_{62} &= \frac{13\rho_b A_b L_e^2}{420} \\ m_{36} = m_{63} &= -\frac{3\rho_b A_b L_e^3}{420} \end{aligned}$$

where A_b is the cross-sectional area of the beam element, E_b is the modulus of elasticity, L_e is the element length, and ρ_b is the mass density of the beam element which has units of $\frac{kip-sec^2}{ft^4}$.

Like the stiffness matrix, the global element mass matrix m_g^b is obtained by

$$m_g^b = T^T \cdot m_e^b \cdot T \tag{2.15}$$

The system damping matrix D can be constructed by specifying modal damping ratios, ξ_i and by the following matrix equation.

$$D = M \cdot \phi \cdot \hat{D} \cdot \phi^T \cdot M \tag{2.16}$$

where

$$\hat{D} = \begin{pmatrix} 2\xi_1\omega_1 & 0 & \cdots & 0 \\ 0 & 2\xi_2\omega_2 & & \vdots \\ \vdots & & \ddots & 0 \\ 0 & \cdots & 0 & 2\xi_N\omega_N \end{pmatrix} \tag{2.17}$$

and ϕ_i are the normalized mode shapes orthonormal with respect to mass and ω_i are the natural frequencies of the system, obtained by solving the following generalized eigenvalue problem.

$$K \cdot \phi_i = \omega_i^2 \cdot M \cdot \phi_i \tag{2.18}$$

Structures like cable-stayed bridges are usually supported at more than one point that are separated by long distances. Due to this, and the fact that seismic waves travel at different speeds through the earth during an earthquake, there will be a slight delay in the arrival of incoming waves to second and subsequent supports. As a result, this delay causes differential ground motions from support to support. It is assumed here that the wave velocity through rock media is $5000\frac{ft}{s}$, and that the bridge piers are supported on rock.

The equation of motion for multiple-support excitation can be obtained from the global system matrices by partitioning those degrees of freedom associated with

the ground motions from the free degrees of freedom, as shown in Equation 2.19 for the system mass matrix,

$$M\ddot{v} = \begin{pmatrix} M_{ff} & M_{fg} \\ M_{gf} & M_{gg} \end{pmatrix} \cdot \begin{pmatrix} \ddot{v}_f^t \\ \ddot{v}_g \end{pmatrix} \tag{2.19}$$

where v_f^t is the total vector of free displacements (length f), and v_g is the vector of ground displacements (length g). Rearranging system matrices M, D, and K to separate free DOF from the ground DOF, yields the following two second order matrix equations of motion.

$$M_{ff} \cdot \ddot{v}_f^t + D_{ff} \cdot \dot{v}_f^t + K_{ff} \cdot v_f^t = -M_{fg} \cdot \ddot{v}_g - D_{fg} \cdot \dot{v}_g - K_{fg} \cdot v_g \tag{2.20}$$

$$M_{gf} \cdot \ddot{v}_f^t + D_{gf} \cdot \dot{v}_f^t + K_{gf} \cdot v_f^t + M_{gg} \cdot \ddot{v}_g + D_{gg} \cdot \dot{v}_g + K_{gg} \cdot v_g = F_g \tag{2.21}$$

The term on the right hand side of Equation 2.20 is called the effective earthquake force vector $P_{eff}(t)$, and the term on the right hand side of Equation 2.21 is the support forces along the ground degrees of freedom. The displacements, velocities, and accelerations associated with the ground degrees of freedom, v_g, $\dot{v}_g$, and $\ddot{v}_g$, respectively, must all be known in order to solve the above two equations for v_f and F_g. To further simplify Equation 2.20, the total displacement vector, v_f^t, can be decomposed as a sum of both relative and static components, that is,

$$v_f^t = v_f^s + v_f \tag{2.22}$$

where v_f^s is the pseudostatic displacement vector resulting from a static-support displacement, and v_f is the relative displacement vector.

From the above, for a static case, $v_f = 0$ implies $v_f^t = v_f^s$ in Equation 2.22 and using the fact that for the static case all time derivatives are zero, Equation 2.20 reduces to

$$v_f^s = -K_{ff}^{-1} \cdot K_{fg} \cdot v_g \tag{2.23}$$

where $r = -K_{ff}^{-1} \cdot K_{fg}$ in the above equation is defined as the pseudostatic influence coefficient matrix. This matrix expresses the responses in all DOF's due to a unit displacement of each support while fixing all the other DOF's. Substituting Equation 2.22 into Equation 2.20, and assuming that the $D_{fg} + D_{ff}r$ term is negligible compared to the inertia term, one obtains the following equation of motion for multiple-support earthquake excitations

$$M_{ff} \cdot \ddot{v}_f + D_{ff} \cdot \dot{v}_f + K_{ff} \cdot v_f = -(M_{ff} \cdot r + M_{fg}) \cdot \ddot{v}_g \tag{2.24}$$

Note that if the damping matrix D is proportional to the stiffness matrix K, it can be shown that the $D_{fg} + D_{ff}r$ term vanishes. However, in a practical scenario this term will not be zero, but its contribution will be relatively small.

2.5. The ARE-based H_∞ Control Scheme

The H_∞ control technique was originally formulated by Zames [97] more than a decade ago. Traditionally, it was a complex frequency domain (transfer function) approach. In recent years, H_∞ control using the state-space technique (time domain) has begun to gain popularity among control system designers ([27], [80], etc.). One major advantage of the state-space technique over the transfer function approach is that it eases the computational complexity of the transfer function matrix for the multi-input multi-output (MIMO) system. Presented first in this section is the standard H_∞ control problem in the time domain, which is also referred to as Algebraic-Riccati-Equation-based (ARE-based) H_∞ control, followed by some discussion of the H_∞ space and norm. Lastly, the decentralized H_∞ control methodology [80] is reviewed.

The formulation of the standard H_∞ control problem for the linear, time-invariant (LTI) case generally involves a system of the following matrix form

$$\begin{aligned} \dot{x} &= Ax + \tilde{B}u + Gw_o, \\ \tilde{y} &= \tilde{C}x + \tilde{w}, \\ \tilde{z} &= \begin{pmatrix} Hx \\ \tilde{u} \end{pmatrix} \end{aligned} \tag{2.25}$$

where x is the state of the system, $\tilde{u}$ is the control input force signal, $\tilde{y}$ is the measured output, $\tilde{z}$ is the output to be regulated or controlled, w_o and $\tilde{w}$ are the square-integrable external disturbances (earthquake excitations) and sensor noises, respectively. The block diagram of this setup is shown in Figure 2.8, where the system to be controlled is boxed with the dashed lines (shaded region). The term

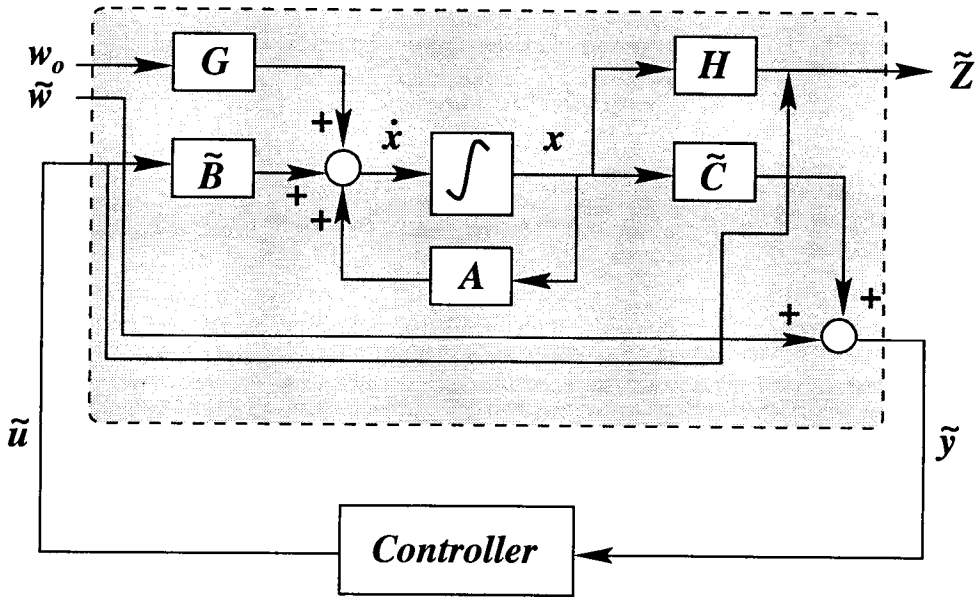

FIGURE 2.8. A standard control block diagram

H_∞ refers to the space of proper and stable transfer functions. Therefore, stating that the closed-loop transfer function $T(s)$ is in H_∞ is equivalent to saying $T(s)$ is proper and stable. A proper transfer function is a transfer function for which the degree of the denominator is greater than or equal to the degree of the numerator. The H_∞ norm of a stable and proper transfer-function matrix $T(s)$ is defined as

$$\| T(s) \|_\infty = \sup_{\|v\|_2 \neq 0} \frac{\| Tv \|_2}{\| v \|_2} = \sup_{\|v\|_2=1} \| Tv \|_2 = \sup_{\omega \in R} | T(jw) | \qquad (2.26)$$

where $Tv = z$, and $\| v(t) \|_2 = \sqrt{\int (v(t))^2 dt}$ denotes the root-integral-square norm (L_2 norm) in either the time domain or the frequency domain. From the above Equation 2.26, it is simply defined as the maximum ratio of the L_2 norm of the output z over the L_2 norm of the input v. This ratio is also known as the L_2 gain of the system. Letting $w_e = \begin{pmatrix} w_o \\ \tilde{w} \end{pmatrix}$, the objective is to design a feedback or closed-loop controller that stabilizes the overall closed-loop system (entire Figure 2.8), and obtains a small H_∞ norm of the transfer-function matrix from the disturbances w_e to the regulated output z. From the definition above, obtaining a small H_∞ norm simply means keeping the gain from $\| w_e \|_2$ to $\| z \|_2$ small. In other words, the design goal is to extremize over a space of proper and stable transfer functions, with the H_∞ norm representing the objective or cost function.

The decentralized H_∞ control setup has a more general structure than the standard H_∞ control case, and is given by the following formulation

$$\begin{aligned} \dot{x} &= Ax + \sum_{i=1}^{q} B_i u_i + G w_o \qquad (2.27) \\ y_i &= C_i x + w_i, \quad i \in \{1, 2, \ldots, q\} \\ z &= \begin{pmatrix} Hx \\ u_1 \\ \vdots \\ u_q \end{pmatrix} \end{aligned}$$

where q is the number of decentralized controllers. For convenience, the above equations 2.27 can be compactly rewritten as

$$\dot{x} = Ax + Bu + Gw_o, \tag{2.28}$$

$$y = Cx + w,$$

$$z = \begin{pmatrix} Hx \\ u \end{pmatrix}$$

where $B = \begin{pmatrix} B_1 & B_2 & \cdots & B_q \end{pmatrix}$, $u^T = \begin{pmatrix} u_1 & u_2 & \cdots & u_q \end{pmatrix}$, $y^T = \begin{pmatrix} y_1 & y_2 & \cdots & y_q \end{pmatrix}$, $C^T = \begin{pmatrix} C_1 & C_2 & \cdots & C_q \end{pmatrix}$, and $w^T = \begin{pmatrix} w_1 & w_2 & \cdots & w_q \end{pmatrix}$.

For the decentralized H_∞ control technique, a controller for each of the q control channels is designed. The local measurement y_i provides information for the i^{th} controller to generate the local control input u_i. This approach is very efficient in controlling a large scale system like the double-stayed bridge under study since each of the four independent controllers uses only the corresponding local measurement information. Each decentralized controller is designed such that the H_∞ norm of the entire system closed-loop transfer function is within a prespecified bound α.

For state-feedback control, it is assumed that all states are available for feedback. However, in a practical scenario, some of the states may not be measurable. In this case, an observer is designed to estimate the states for feedback. An observer is a device in the form of either hardware or software that uses the inputs and the outputs of the system to produce estimates of its states. In other words, it is a device that simulates the original system. The structure of the decentralized H_∞ controllers is composed of full-order observers that generate the estimates $\xi_i, i \in \{1, 2, \ldots, q\}$, of the states x for feedback. Full-order here denotes that the order of each observer is exactly the same as the order of the system. In which case, the resulting closed-loop system has an order of $(q+1)n$. To simulate the dy-

namics of the original system, these observers should have the following dynamical structure,

$$\dot{\xi}_i = A\xi_i + \sum_{j=1}^{q} B_j u_j + Gw_o + L_i(y_i - C_i\xi_i) \tag{2.29}$$

where ξ_i are the estimates of the states and L_i are the observer gains. Since the disturbance w_o is not available to the observers, it is replaced by the following estimates.

$$\hat{w}_o^i = \frac{1}{\alpha^2} G^T X \xi_i \tag{2.30}$$

where α is the predetermined H_∞ norm bound (found by trial and error). Similarly, in the i^{th} observer, the j^{th} controller, $u_j, j \neq i$, is replaced by

$$\hat{u}_j^i = -B_j^T X \xi_i \tag{2.31}$$

Doing so, Equation 2.29 becomes

$$\dot{\xi}_i = (A + \frac{1}{\alpha^2} GG^T X - SX - L_i C_i)\xi_i + L_i y_i \tag{2.32}$$

and the control estimates used for the feedback are

$$u_i = -B_i^T X \xi_i \tag{2.33}$$

The above two equations (2.32 and 2.33) represent the decentralized feedback control law. The term X in the above equations is the positive semi-definite ($X \geq 0$) solution to the following controller Algebraic-Riccati-Equation (ARE)

$$A^T X + XA + \frac{1}{\alpha^2} XGG^T X - XSX + H^T H = 0 \tag{2.34}$$

The gains of the observer, L_i are obtained from the following equation

$$L_i = W_{ii} C_i^T \tag{2.35}$$

where W_{ii} are the diagonal blocks of W,

$$W = \begin{pmatrix} W_{11} & \cdots & W_{1q} \\ \vdots & \ddots & \vdots \\ W_{q1} & \cdots & W_{qq} \end{pmatrix} \tag{2.36}$$

which is the positive definite ($W > 0$) solution to the following estimator Riccati-like algebraic equation.

$$WA_c^T + A_cW + W(\frac{1}{\alpha^2}X_cB_cB_c^TX_c - C_c^TC_c)W + G_cG_c^T + (W - W_D)C_c^TC_c(W - W_D) = 0 \tag{2.37}$$

where $A_c = A_{\alpha c} + I_cBB_c^TX_c, A_{\alpha c} = diag(A_\alpha, A_\alpha, \ldots, A_\alpha), A_\alpha = A + \frac{1}{\alpha^2}GG^TX - SX, I_c = \begin{pmatrix} I & I & \cdots & I \end{pmatrix}, B_c = diag(B_1, B_2, \ldots, B_q), X_c = diag(X, X, \ldots, X), C_c = diag(C_1, C_2, \ldots, C_q), G_c = I_cG$, and $W_D = diag(W_{11}, W_{22}, \ldots, W_{qq})$.

With q the number of decentralized controllers, the $(q+1)n$ order closed-loop system is described by the following

$$\begin{pmatrix} \dot{x} \\ \dot{\xi} \end{pmatrix} = \begin{pmatrix} A & -BB_c^TX_c \\ L_cC & A_{\alpha c} - L_cC_c \end{pmatrix} \cdot \begin{pmatrix} x \\ \xi \end{pmatrix} + \begin{pmatrix} G & 0 \\ 0 & L_c \end{pmatrix} \cdot \begin{pmatrix} w_o \\ w \end{pmatrix} \equiv F_ex_e + G_ew_e \tag{2.38}$$

$$z = \begin{pmatrix} H & 0 \\ 0 & -B_c^TX_c \end{pmatrix} \cdot \begin{pmatrix} x \\ \xi \end{pmatrix} \equiv H_ex_e \tag{2.39}$$

where $L_c = diag(L_1, L_2, \ldots, L_q)$

Associated with the observer is the notion of observability. Observability is loosely defined as the ability to estimate the system states from a record of output measurements. A weaker version of observability is referred to as detectability. A system is said to be detectable if the unstable modes are observable or equivalently the unobservable modes are stable. To ensure a stabilizing controller, the pair (A, H) has to be detectable, the solution X to the ARE (Equation 2.34) has to be positive

semi-definite ($X \geq 0$), $A_\alpha \equiv A + \alpha^{-2}GG^TX - SX$ has to be Hurwitz (or stable), $A_\alpha + SX$ has to have no $j\omega$-axis eigenvalues, and the solution W to the Riccati-like Algebraic Equation (Equation 2.37) has to be positive definite ($W > 0$). Satisfying the above conditions, the decentralized feedback control law (Equations 2.32 and 2.33) stabilizes the system of Equation 2.27, and the closed-loop transfer-function matrix

$$T(s) = H_e(sI - F_e)^{-1}G_e$$

from w_e to z satisfies

$$\| T \|_\infty \leq \alpha$$

Figure 2.9 shows the decentralized H_∞ control scheme in block diagram, where $A_d = diag(A, A, \ldots, A), S_d = diag(S, S, \ldots, S), G_d = diag(G, G, \ldots, G)$, $A_d + \frac{1}{\alpha^2}G_dG_d^TX_c - S_dX_c \equiv A_{\alpha c}$, and the shaded area represents the observer-based controllers.

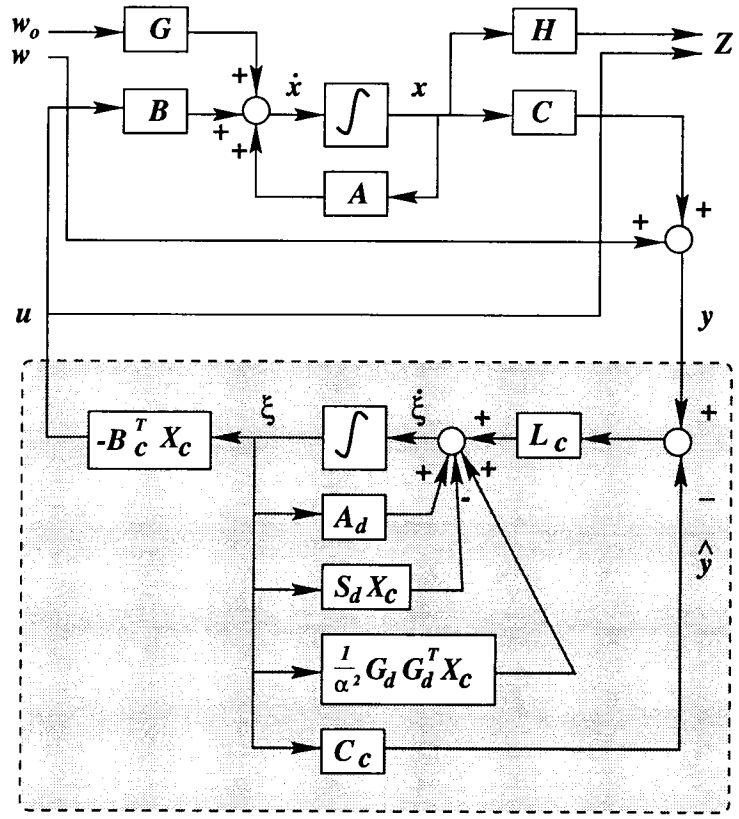

FIGURE 2.9. The Schematic Block Diagram of Decentralized H_∞ Control

3. EARTHQUAKE DATA RECORDS WITH ENGINEERING SIGNIFICANCE FOR SIMULATIONS

The earthquake records selected as excitations for the uncontrolled and controlled behaviours of the double-stayed structure are obtained from a set of short-listed earthquake data reported by Naeim and Anderson [52]. According to that report, the severity and damage potential of an earthquake ground motion is characterized by the following parameters. These parameters are Richter magnitude (M), peak ground acceleration (PA), peak ground velocity (PV), peak ground displacement (PD), maximum incremental velocity (IV), maximum incremental displacement (ID), effective peak acceleration (EPA), effective peak velocity (EPV), and the bracketed duration ($[D]$). In each of these parameter categories (except magnitude and bracketed duration), Naeim and Anderson arranged the database to obtain an ordered 30 earthquake records. This database contained records of earthquakes occuring between 1933 and 1992. From this information, the only two earthquakes that are in the top 30 list in every parameter category mentioned above are the 1971 San Fernando earthquake recorded at the Pacoima Dam station, and the 1992 Petrolia earthquake recorded at the Cape Mendocino station. In the 0.3g bracketed duration ($[D]_{0.30g}$) parameter category, the 1985 Mexico City earthquake recorded at the Infiernillo N-120 station contains the longest duration of 21.7 seconds. This 0.3g bracketed duration refers to the time duration between the first and the last occurrences of accelerations equal to or greater than 0.3g. Since these three earthquakes are classified as carrying significant engineering values, they are chosen for the studies of uncontrolled and controlled behaviour of the double-stayed structure. The properties and characteristics of each of these earthquakes are tabulated

in Tables 3.1, 3.2, and 3.3, with the above-mentioned parameters, including such information as the epicenter distance (D) and the focal depth (H). Strong motion portions of the time history plots (two components) for each of these earthquakes, and their frequency contents are also shown in the following pages.

Components	Horizontal	Vertical
Epicenter Distance, H in mi (km)	8.08 (13)	8.08 (13)
Foci Depth, F in mi (km)	4.97 (8)	4.97 (8)
Richter Magnitude, M	6.6	6.6
Orientation, Deg (°)	164	vert
Peak Acceleration, PA in g	1.15	0.71
Peak Velocity, PV in ft/s (cm/s)	3.71 (113.09)	1.85 (56.47)
Peak Displacement, PD in ft (cm)	1.26 (38.28)	0.61 (18.57)
Incremental Velocity, IV in ft/s (cm/s)	4.56 (138.88)	2.07 (63.17)
Incremental Displacement, ID in ft (cm)	1.58 (48.05)	1.13 (34.46)
Effective Peak Acceleration, EPA in g	0.84	0.61
Effective Peak Velocity, EPV in ft/s (cm/s)	2.17 (66.23)	0.65 (19.79)
Duration, $[D]_{0.05g}$ (sec)	33.9	32.0
Duration, $[D]_{0.10g}$ (sec)	33.1	n/a
Duration, $[D]_{0.20g}$ (sec)	8.0	n/a
Duration, $[D]_{0.30g}$ (sec)	7.3	n/a

TABLE 3.1. Characteristics of 1971 San Fernando Earthquake

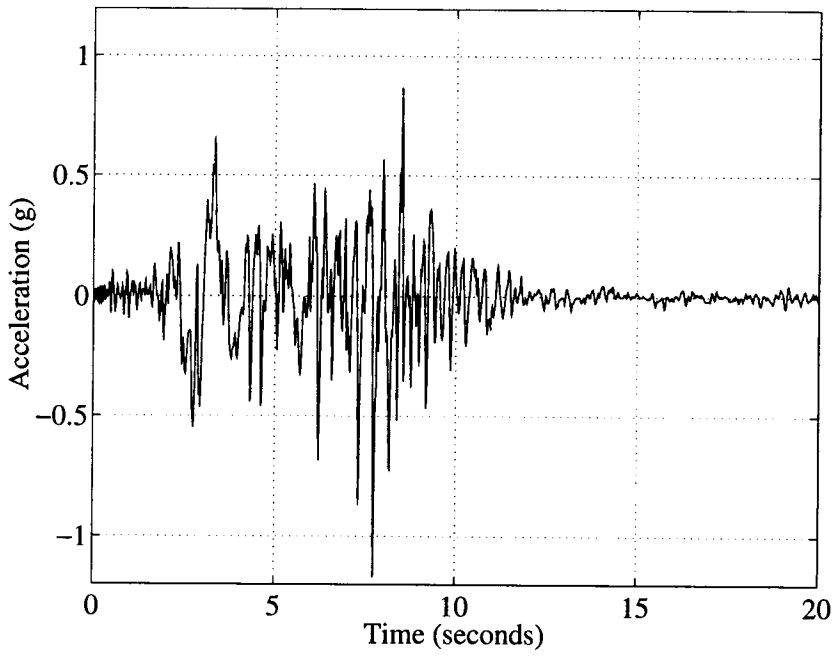

FIGURE 3.1. 1971 San Fernando S16E (horizontal) component

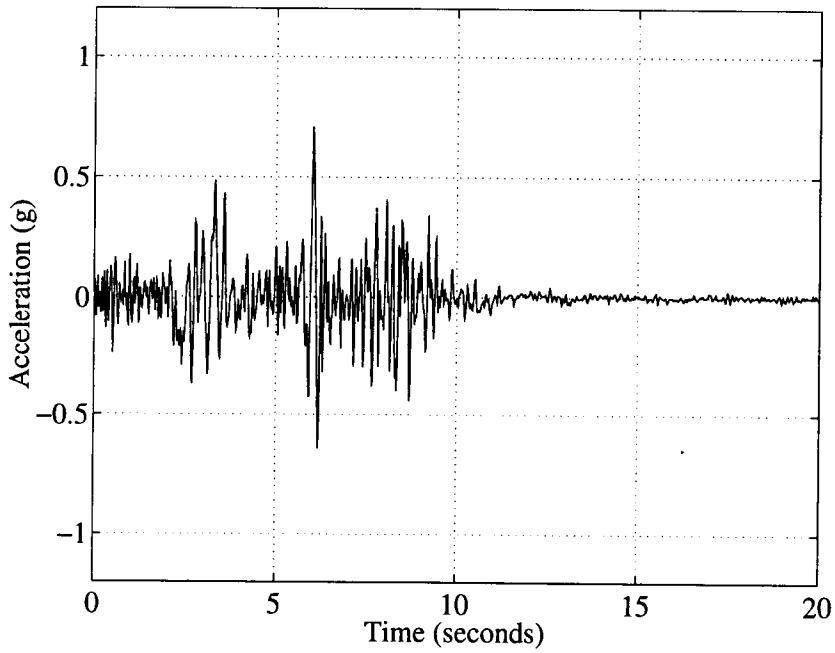

FIGURE 3.2. 1971 San Fernando vertical component

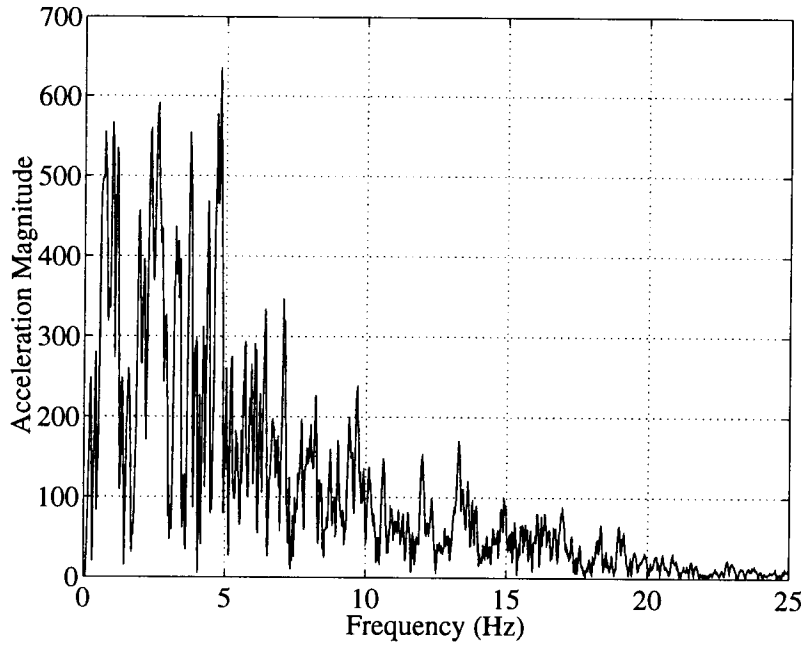

FIGURE 3.3. Fourier Transform of 1971 San Fernando S16E component

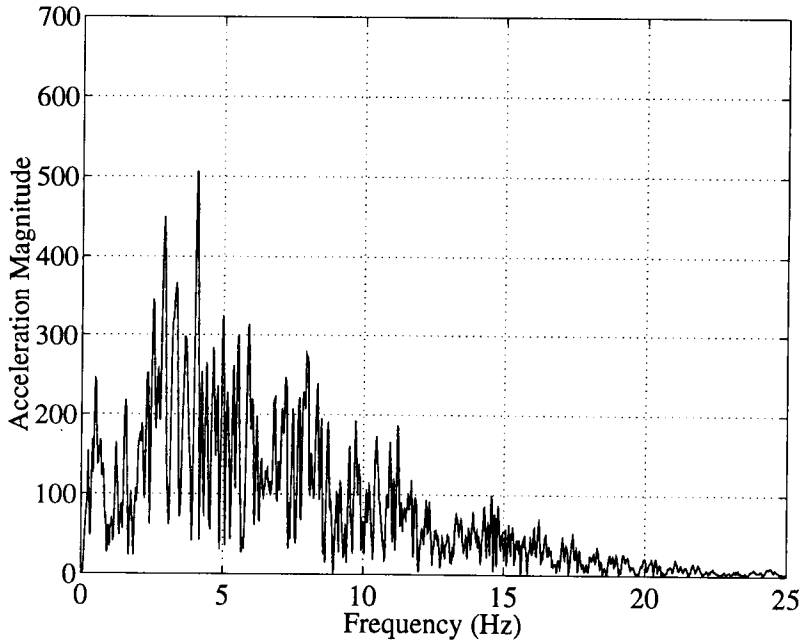

FIGURE 3.4. Fourier Transform of 1971 San Fernando vertical component

Components	Horizontal	Vertical
Epicenter Distance, H in mi (km)	17.40 (28)	17.34 (27.9)
Foci Depth, F in mi (km)	55.92 (90)	55.92 (90)
Richter Magnitude, M	8.1	8.1
Orientation, Deg (°)	335	vert
Peak Acceleration, PA in g	0.38	0.29
Peak Velocity, PV in ft/s (cm/s)	0.54 (16.45)	0.36 (10.92)
Peak Displacement, PD in ft (cm)	0.17 (5.23)	0.22 (6.81)
Incremental Velocity, IV in ft/s (cm/s)	0.89 (27.2)	0.55 (16.9)
Incremental Displacement, ID in ft (cm)	0.18 (5.49)	0.35 (10.76)
Effective Peak Acceleration, EPA in g	0.43	0.25
Effective Peak Velocity, EPV in ft/s (cm/s)	0.36 (11.03)	0.21 (6.30)
Duration, $[D]_{0.05g}$ (sec)	76.0	61.0
Duration, $[D]_{0.10g}$ (sec)	54.1	n/a
Duration, $[D]_{0.20g}$ (sec)	33.2	n/a
Duration, $[D]_{0.30g}$ (sec)	21.7	n/a

TABLE 3.2. Characteristics of 1985 Mexico Earthquake

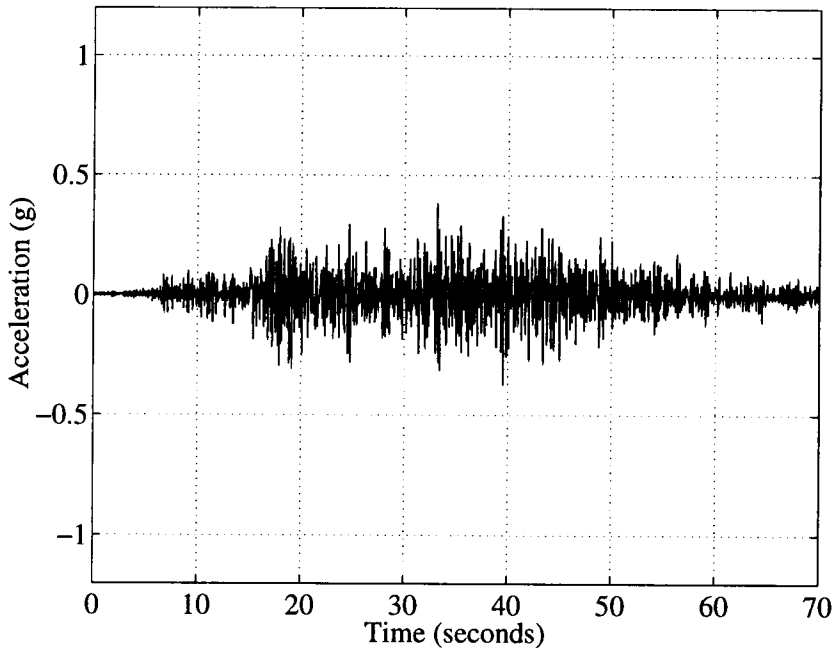

FIGURE 3.5. 1985 Mexico 335° (horizontal) component

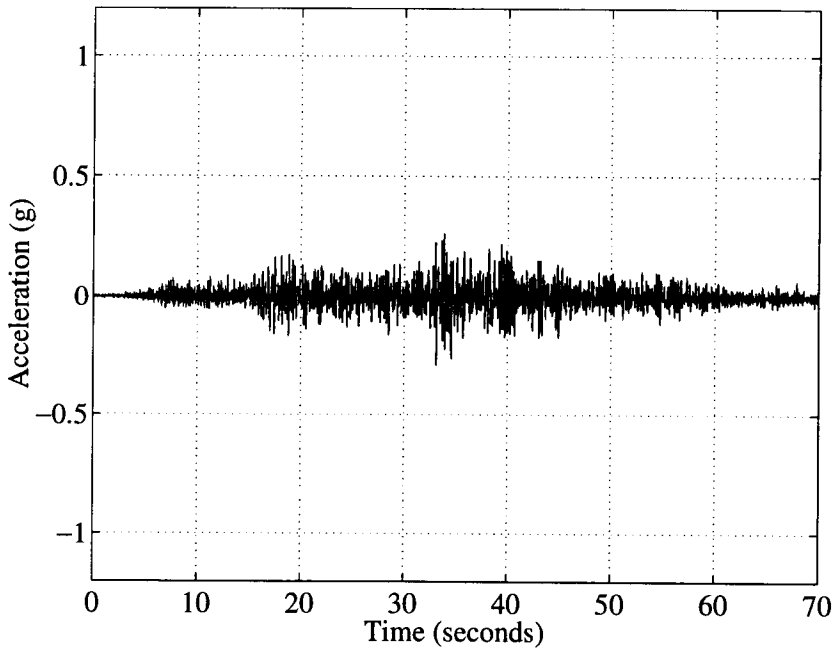

FIGURE 3.6. 1985 Mexico vertical component

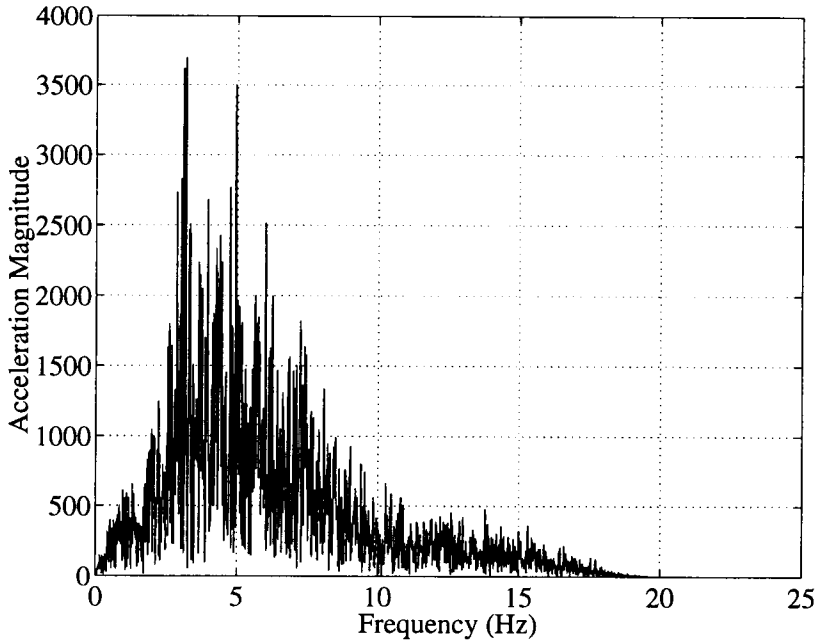

FIGURE 3.7. Fourier Transform of 1985 Mexico 335° component

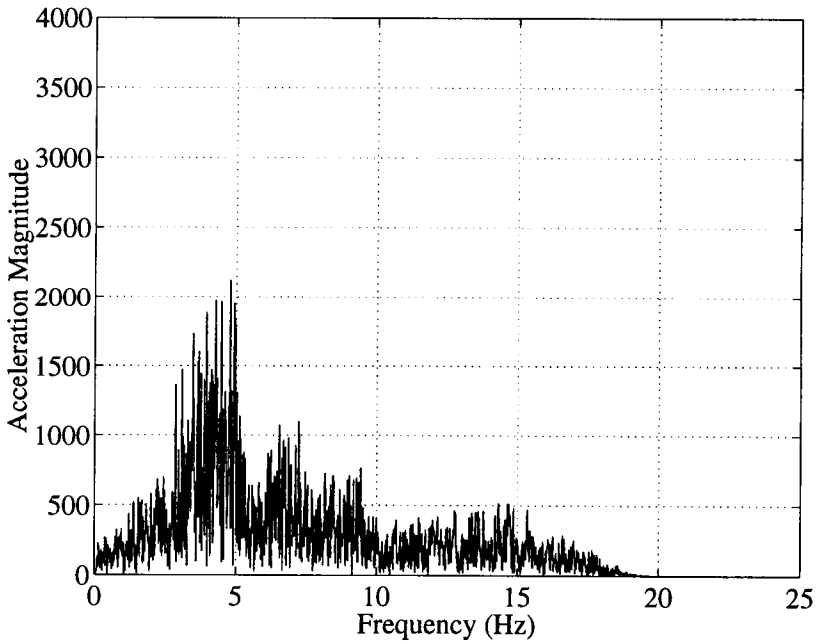

FIGURE 3.8. Fourier Transform of 1985 Mexico vertical component

Components	Horizontal	Vertical
Epicenter Distance, H in mi (km)	9.32 (15)	9.32 (15)
Foci Depth, F in mi (km)	3.11 (5)	2.86 (4.6)
Richter Magnitude, M	6.9	6.9
Orientation, Deg (°)	0	vert
Peak Acceleration, PA in g	1.50	0.75
Peak Velocity, PV in ft/s (cm/s)	4.14 (126.12)	1.98 (60.32)
Peak Displacement, PD in ft (cm)	1.18 (36.07)	2.19 (66.75)
Incremental Velocity, IV in ft/s (cm/s)	3.86 (117.52)	1.52 (46.31)
Incremental Displacement, ID in ft (cm)	2.06 (62.85)	3.53 (107.45)
Effective Peak Acceleration, EPA in g	0.98	0.39
Effective Peak Velocity, EPV in ft/s (cm/s)	1.94 (59.16)	0.55 (16.79)
Duration, $[D]_{0.05g}$ (sec)	37.9	7.9
Duration, $[D]_{0.10g}$ (sec)	33.7	n/a
Duration, $[D]_{0.20g}$ (sec)	17.1	n/a
Duration, $[D]_{0.30g}$ (sec)	4.0	n/a

TABLE 3.3. Characteristics of 1992 Petrolia Earthquake

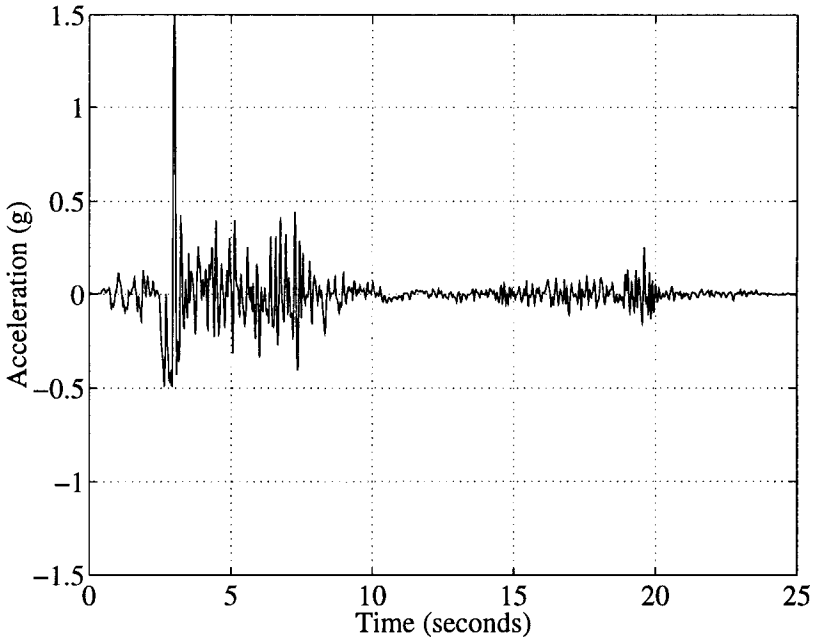

FIGURE 3.9. 1992 Petrolia 0° (horizontal) component

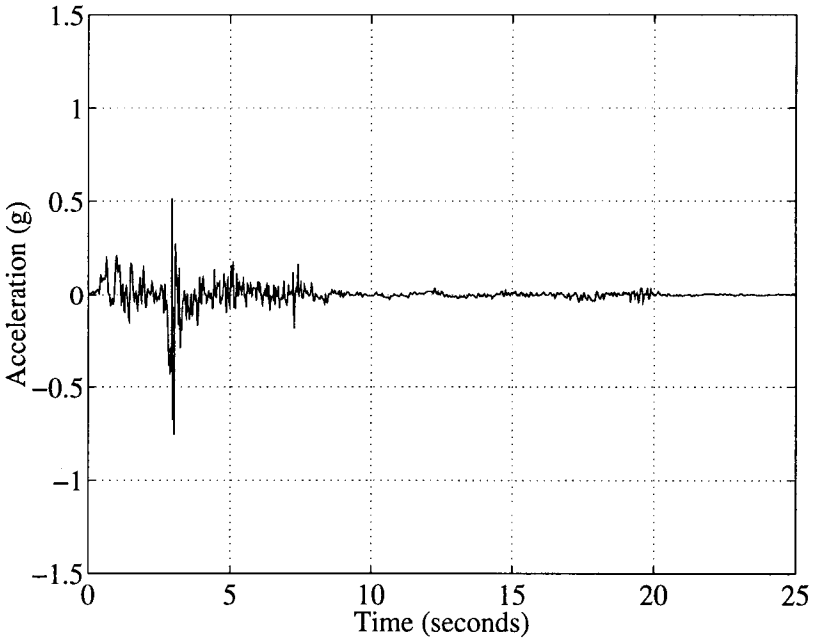

FIGURE 3.10. 1992 Petrolia vertical component

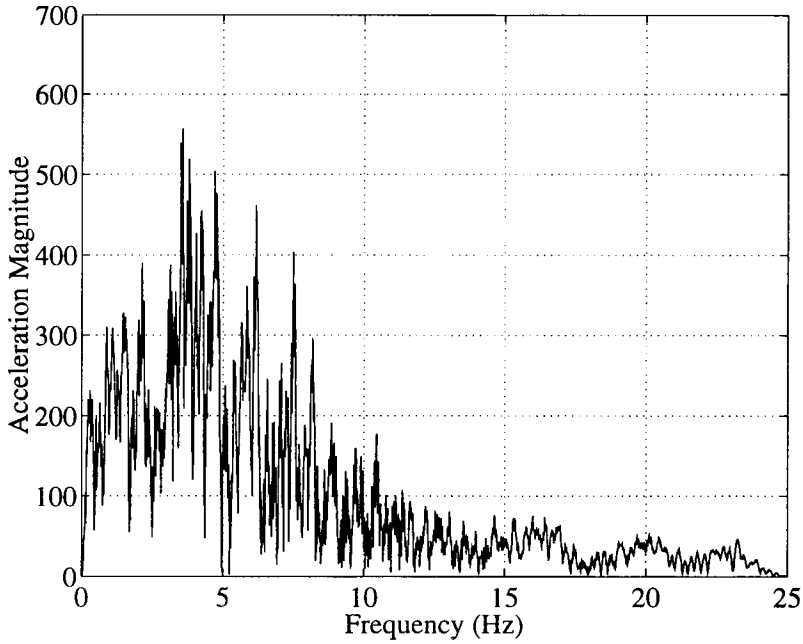

FIGURE 3.11. Fourier Transform of 1992 Petrolia 0° component

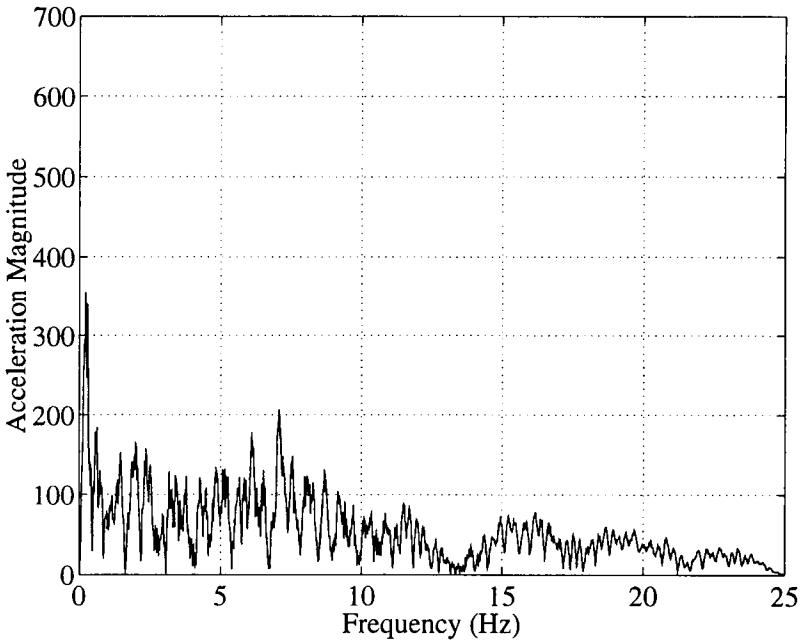

FIGURE 3.12. Fourier Transform of 1992 Petrolia vertical component

4. UNCONTROLLED BEHAVIOUR OF THE DOUBLE-STAYED STRUCTURE

4.1. Uncontrolled Static Parametric Study

This section presents the influences of some important structural properties of the double-stayed system on the overall static structural behaviour. In particular, the influences of upper and lower cable pretensions, the presence of the lower cables, the moments of inertia of the deck and pylon, as well as the influences of the span length and system nonlinearities are presented. Since the bending moments are most likely to be the controlling structural strength design factor for this long span structure (shear is likely to control the design for short, deep beam type structures), and excessive deflections will usually govern the serviceability requirement, the structural behaviours observed and presented here are limited to the maximum bending moments of the deck and pylon, the maximum absolute deflections of the deck and pylon, and the maximum deflections of the deck normalized by the maximum deflections of the pylon.

The static loading is a result of the structure's dead-weight. For the analysis, this distributed self-weight loading is replaced by equivalent nodal loads and equivalent moments at both ends of the span. The equivalent nodal forces are assigned to each node according to their tributary areas. The nonlinear static equilibrium finite element analysis approach used to analyze the static responses in the following subsections is described in Chapter 2. The pretensions in the upper cable 1 (and 4), in the upper cable 2 (and 3), in the lower cable 1 (and 4), and in the lower cable 2 (and 3), used in the analysis are 800, 600, 600, 450 *kips*, respectively.

4.1.1. Influence of pretension of upper cable 1 (and 4)

The pretension in the cables has some influence on the structural behaviour of the double-stayed bridge. By changing the pretensions of upper cables 1 and 4 while holding all others constant, the following behaviours can be seen. In general, the maximum moments and the maximum absolute deflections in the deck decrease as the pretension in upper cable 1 (and 4) increases up to a certain value. Beyond this value, increases in the maximum moments and the deck deflections are observed. The maximum moments and maximum absolute deflections of the pylon increase for all cases considered. These behaviours are plotted in Figures 4.1 (a) - (d). As can be seen in these plots, for design purposes a pretension of 1500 *kips* and greater is not recommended since beyond this value the maximum deck moments and the cable stress increase.

Also, from these illustrations, it is observed that the maximum moments respond less sensitively to variations in the neighborhood of the pretension of upper cable 1 (and 4) under study (800 *kips*). For example, a 10 % change in the pretension of upper cable 1 (and 4) causes an approximately 7 % change in the maximum moments in the deck and pylon, as well as in the maximum deflections of the deck. An even smaller percentage change (4 %) in the maximum deflections of the pylon is also observed.

4.1.2. Influence of pretension of upper cable 2 (and 3)

By changing the pretensions of upper cables 2 and 3 while keeping the pretensions in the other cables fixed, the maximum positive moments of the deck remain almost unchanged while the maximum negative moments of the deck experience an increase. The maximum moments of the pylon also increase. However, the maxi-

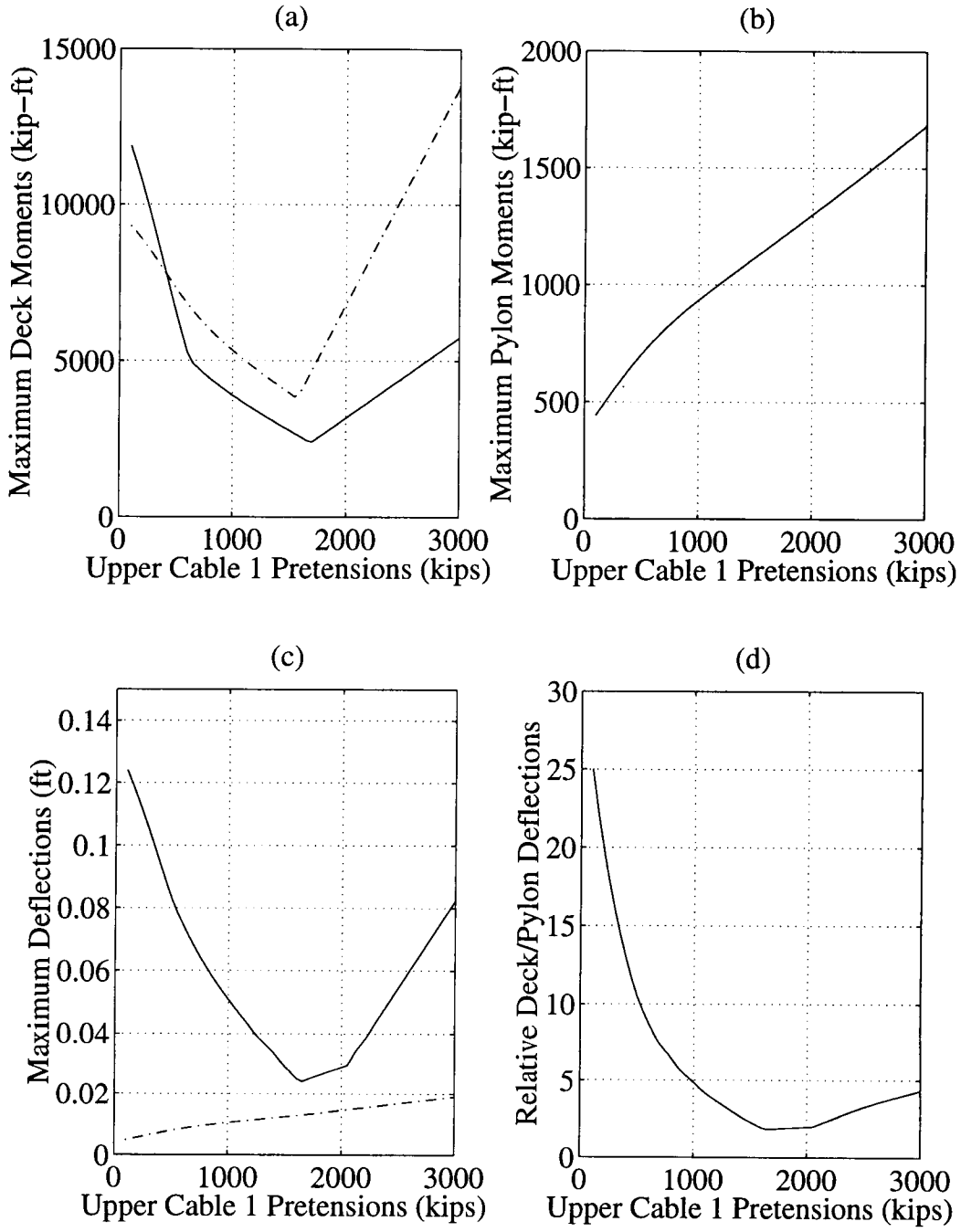

FIGURE 4.1. Influence of pretension of upper cable 1 (and 4). (a) Solid and dash-dotted lines represent positive and negative maximum moments of deck, respectively. (c) Solid and dash-dotted lines represent maximum deflections of deck and pylon, respectively.

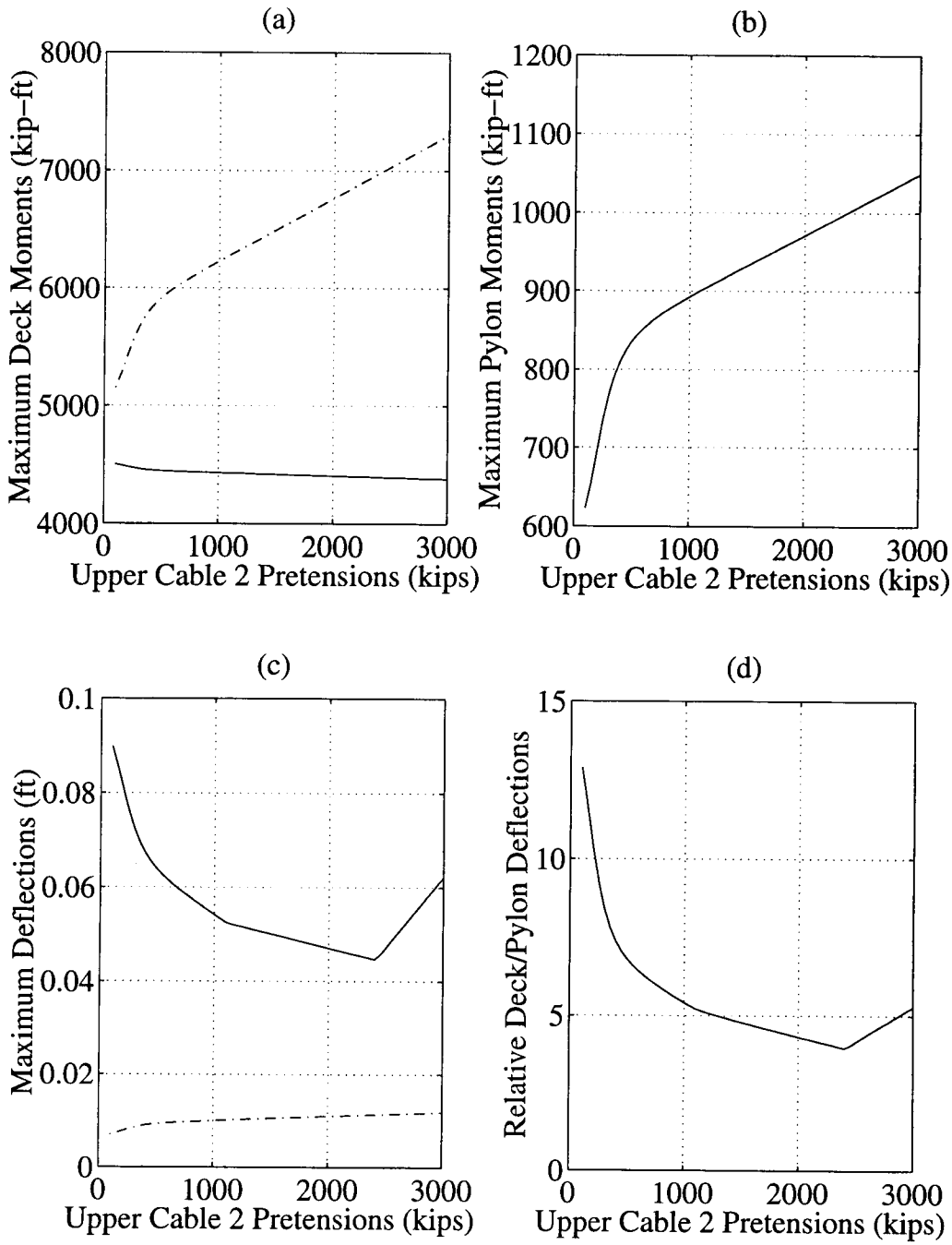

FIGURE 4.2. Influence of pretension of upper cable 2 (and 3). (a) Solid and dash-dotted lines represent positive and negative maximum moments of deck, respectively. (c) Solid and dash-dotted lines represent maximum deflections of deck and pylon, respectively.

mum absolute deflections of the deck decrease until a certain pretension value and then start to increase beyond that. The relative deflections between the deck and the pylon also follow the same behaviour, due to the almost unchanged maximum absolute deflections of the pylon. These behaviours are plotted in Figures 4.2 (a) - (d).

Based on these figures, it is noticed that the maximum forces in the deck and pylon react less sensitively to variations in the pretension of the upper cable 2 (and 3) under study (600 *kips*), compared to that from a variation in the pretension in the upper cable 1 (and 4) presented in the previous section. For example, a 10 % change in the pretension of upper cable 2 (and 3) corresponds to less than a 1 % change in the maximum moments of the deck and pylon, and less than a 3 % change in the maximum deflections of both the deck and pylon.

4.1.3. Influence of pretension of lower cable 1 (and 4)

As the pretension of lower cables 1 and 4 increases, it is observed that the maximum positive and negative moments in the deck, the maximum moments in the pylon, the maximum absolute deflections of the deck and the pylon, as well as the maximum deflections of the deck normalized by the maximum deflections of the pylon, increase. The increases in both the negative and positive moments of deck result mainly from the fact that the relatively high stiffness of lower cables 1 and 4 causes 'U' shaped deflection in the deck at stations 1 and 4, and an inverted 'U' shaped at stations 2 and 3. These behaviours are plotted in Figures 4.3 (a) - (d).

Also, from these figures, it can be seen that the maximum forces in the deck and pylon also respond insensitively to variation of the pretension in the lower cable 1 (and 4) under study (600 *kips*). For instance, a 10 % variation in the pretension of

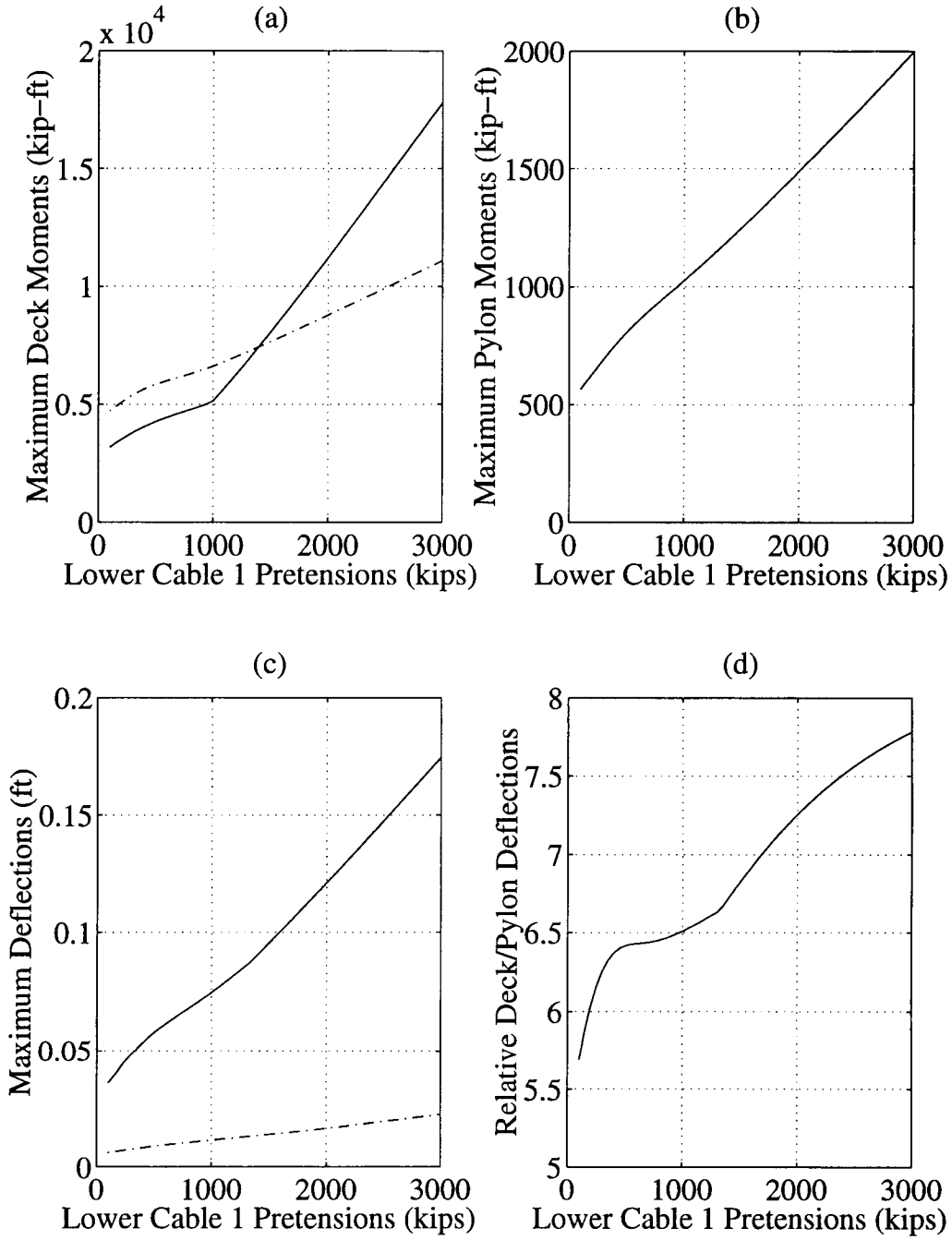

FIGURE 4.3. Influence of pretension of lower cable 1 (and 4). (a) Solid and dash-dotted lines represent positive and negative maximum moments of deck, respectively. (c) Solid and dash-dotted lines represent maximum deflections of deck and pylon, respectively.

the lower cable 1 (and 4) causes less than a 4 % variation in the maximum moments and maximum deflections in both the deck and the pylon.

4.1.4. Influence of pretension of lower cable 2 (and 3)

As the pretension of lower cables 2 and 3 increases, it is observed that the maximum positive moment of the deck and maximum moment of the pylon increase while the maximum negative moment of the deck decreases. This behaviour may be explained by the fact that the larger stiffness of the lower cable (2 and 3) causes a downward pull on the deck, thus decreasing the negative moments and at the same time increasing the positive moments. For design purposes this relatively high value of pretension is not recommended. Also, it is observed that the maximum absolute deflections of the deck increase while the maximum absolute deflections of the pylon are almost unaffected. The maximum deflections of the deck normalized by the maximum deflection of the pylon show a decrease up to a certain pretension value, and an increase beyond that point. These behaviours are plotted in Figure 4.4(a) - (d).

It is also observed that the structure responds insensitively to the changes in the neighborhood of the pretension under study (450 *kips*). In this case, a 10 % change in the pretension of the lower cable 2 (and 3) corresponds to less than a 2 % change in the maximum moments and maximum deflections of both the deck and the pylon.

4.1.5. Influence of presence of lower cables

The maximum positive moments of the double-stayed structure are higher than for the system without lower cables for low pretension of upper cable 1 (and

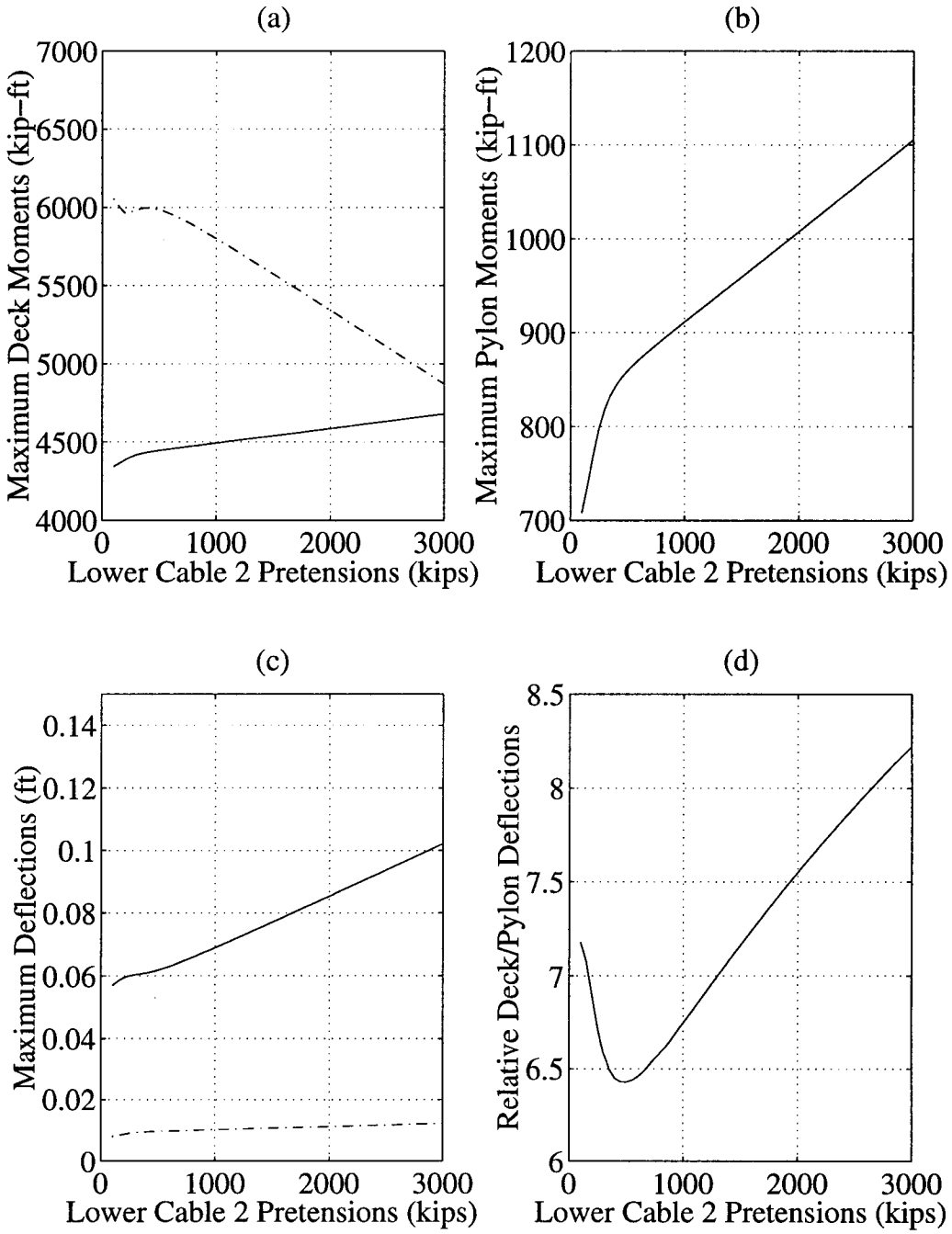

FIGURE 4.4. Influence of pretension of lower cable 2 (and 3). (a) Solid and dash-dotted lines represent positive and negative maximum moments of deck, respectively. (c) Solid and dash-dotted lines represent maximum deflections of deck and pylon, respectively.

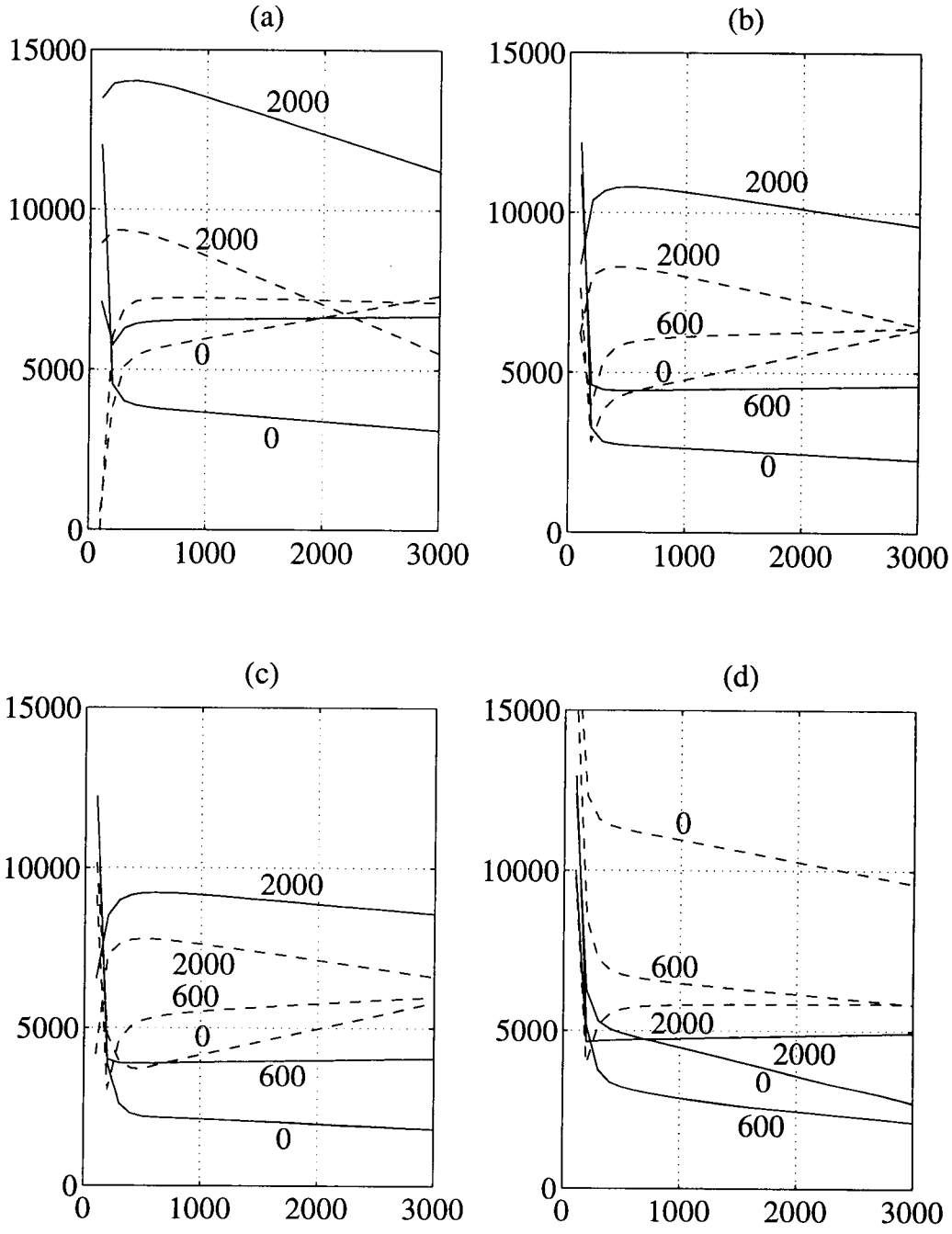

FIGURE 4.5. Influence of cable pretensions on maximum moments of deck with varying pretensions of lower cable 1. Solid and dashed lines represent positive and negative moments, respectively. (Horizontal axis represents pretensions of upper cable 2 in *kips*, and vertical axis represents the maximum moments of deck in $kip - ft$). (a), (b), (c), and (d) show graphs with pretensions of 500, 800, 1000, and 2000 *kips* in the upper cable 1, respectively.

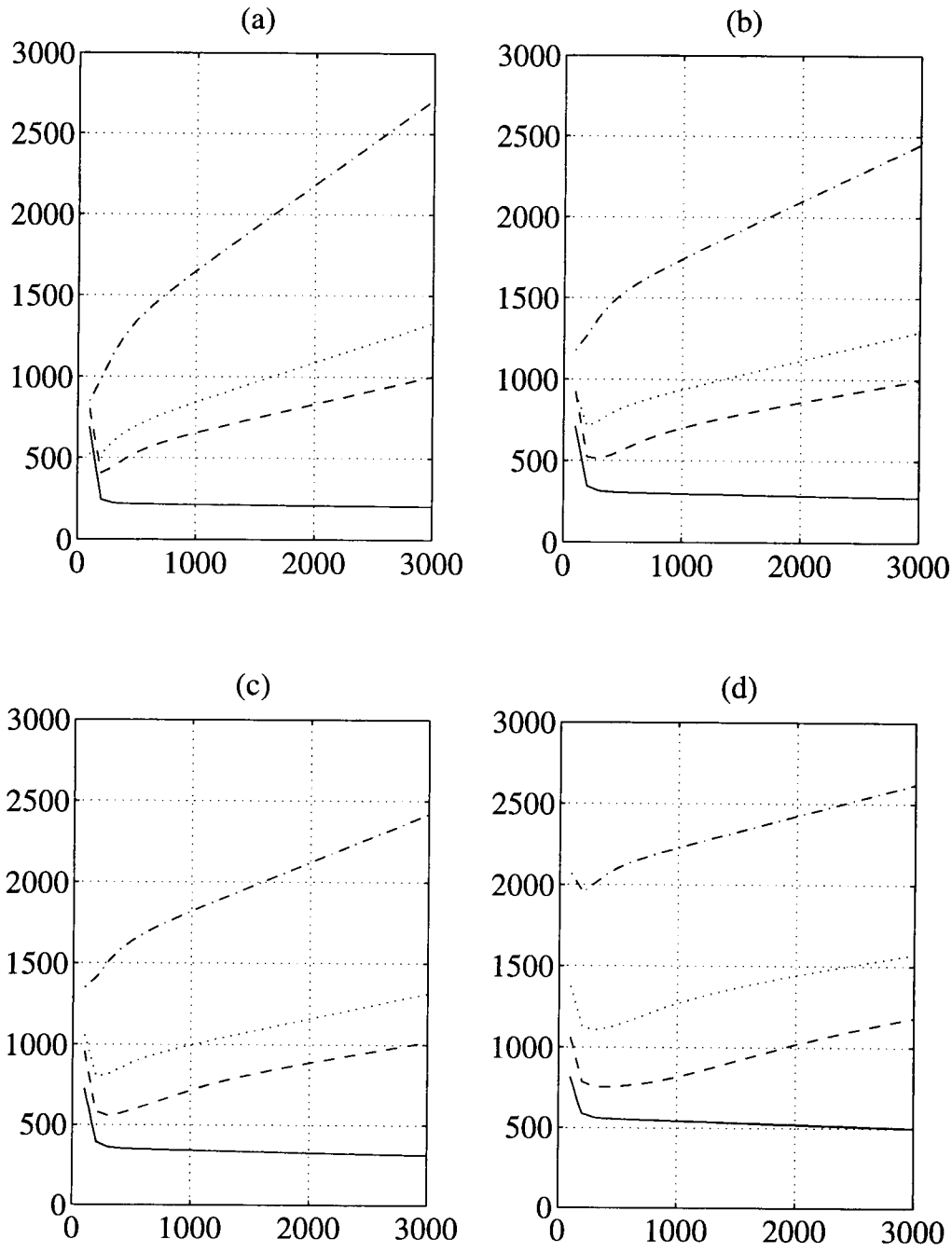

FIGURE 4.6. Influence of cable pretensions on maximum moments of pylon with varying pretensions of lower cable 1. Solid, dashed, dotted, and dash-dotted lines represent pretensions of 0, 300, 600, and 2000 *kips* in lower cable 1, respectively. (Horizontal axis represents pretensions of upper cable 2 in *kips*, and vertical axis represents the maximum moments of pylon in $kip - ft$). (a), (b), (c), and (d) show graphs with pretensions of 500, 800, 1000, and 2000 *kips* in the upper cable 1, respectively.

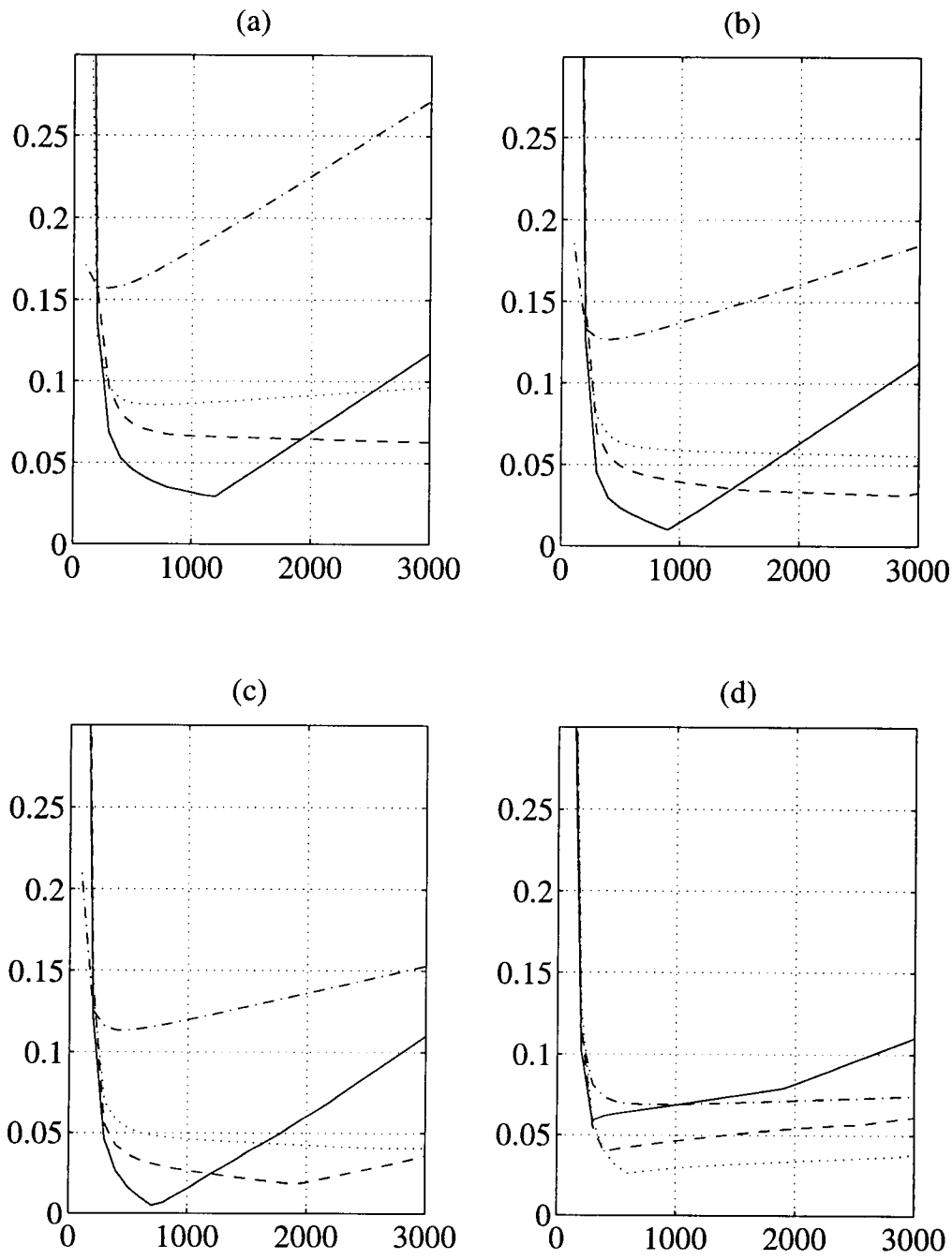

FIGURE 4.7. Influence of cable pretensions on maximum deflections of deck with varying pretensions of lower cable 1. Solid, dashed, dotted, and dash-dotted lines represent pretensions of 0, 300, 600, and 2000 *kips* in lower cable 1, respectively. (Horizontal axis represents pretensions of upper cable 2 in *kips*, and vertical axis represents the maximum deflection of deck in $kip - ft$). (a), (b), (c), and (d) show graphs with pretensions of 500, 800, 1000, and 2000 *kips* in the upper cable 1, respectively.

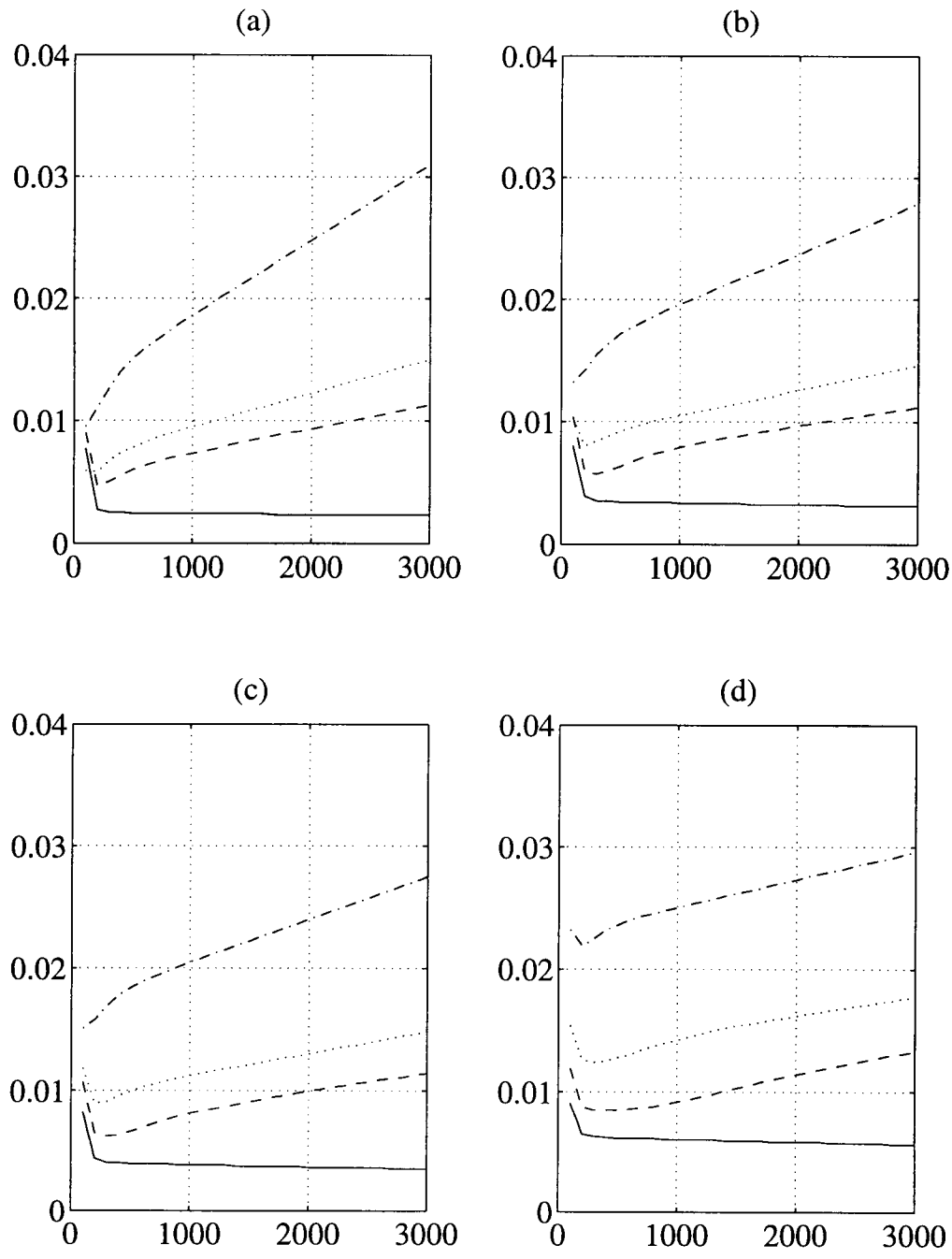

FIGURE 4.8. Influence of cable pretensions on maximum deflections of pylon with varying pretensions of lower cable 1. Solid, dashed, dotted, and dash-dotted lines represent pretensions of 0, 300, 600, and 2000 *kips* in lower cable 1, respectively. (Horizontal axis represents pretensions of upper cable 2 in *kips*, and vertical axis represents the maximum deflections of pylon in $kip - ft$). (a), (b), (c), and (d) show graphs with pretensions of 500, 800, 1000, and 2000 *kips* in the upper cable 1, respectively.

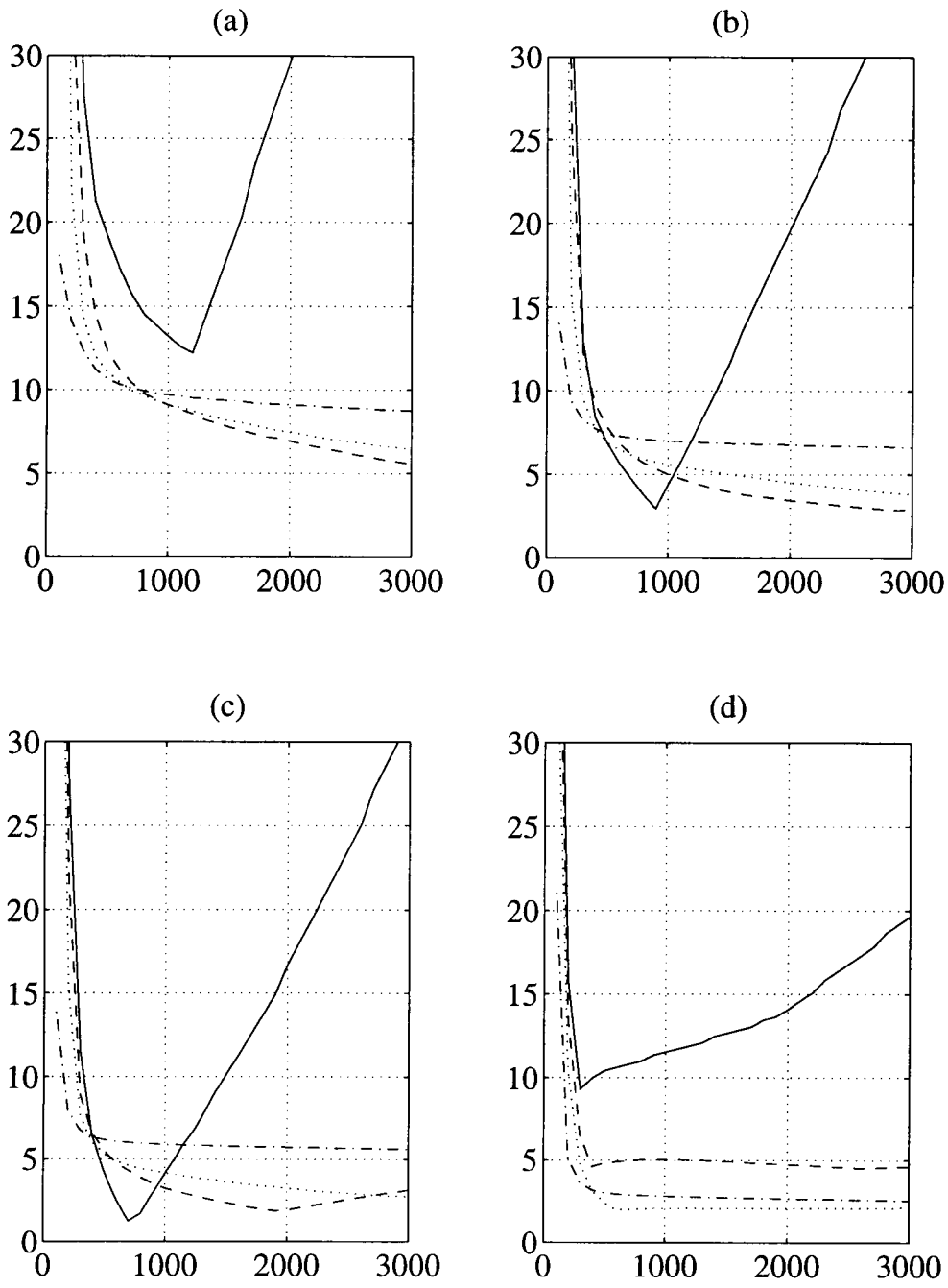

FIGURE 4.9. Influence of cable pretensions on maximum relative deflections between deck and pylon with varying pretensions of lower cable 1. Solid, dashed, dotted, and dash-dotted lines represent pretensions of 0, 300, 600, and 2000 *kips* in lower cable 1, respectively. (Horizontal axis represents pretensions of upper cable 2 in *kips*, and vertical axis represents the ratio of maximum deflections of deck over pylon). (a), (b), (c), and (d) show graphs with pretensions of 500, 800, 1000, and 2000 *kips* in the upper cable 1, respectively.

4) and lower for high pretension of upper cable 1 (and 4). However, the maximum moments and maximum deflections in the pylon are in general higher for the system with lower cables than for that without lower cables. The maximum deflections in the deck are higher for low pretensions in the upper cable 1 (and 4) and high pretensions in lower cable 1 (and 4), and are lower otherwise. This response may be explained by the fact that low pretension in the upper cable 1 (and 4) causes some negative deformation in the deck of the system without the lower cables. The presence of the lower cables creates a further downward pull on the deck resulting in higher negative deflections. These behaviours can be observed in Figures 4.5 - 4.9. As a comparison between the maximum responses of a double-stayed system with and without lower cables, Table 4.1 shows their response percentage difference. From this table, it may be concluded that the presence of the lower cables significantly affects the maximum static behaviour of the system.

4.1.6. Influence of moment of inertia of deck

The increase of the moment of inertia increases the stiffness of the deck. Since stiffer members carry a proportionally larger load, as the moment of inertia of the deck increases the maximum positive moments in the deck increase. The negative moments of the deck increase to a peak and then decrease. Dramatic changes in both positive and negative moments occur in the range of 5 to approximately 60 ft^4 (see Figure 4.10). Within this range, one also observes a dramatic decrease in maximum moments in the pylon (see Figure 4.11), a dramatic decrease in maximum absolute deflection of the deck, pylon, and the maximum deflection of the deck normalized by the maximum deflection of the pylon (Figures 4.12 - 4.14). Beyond this range

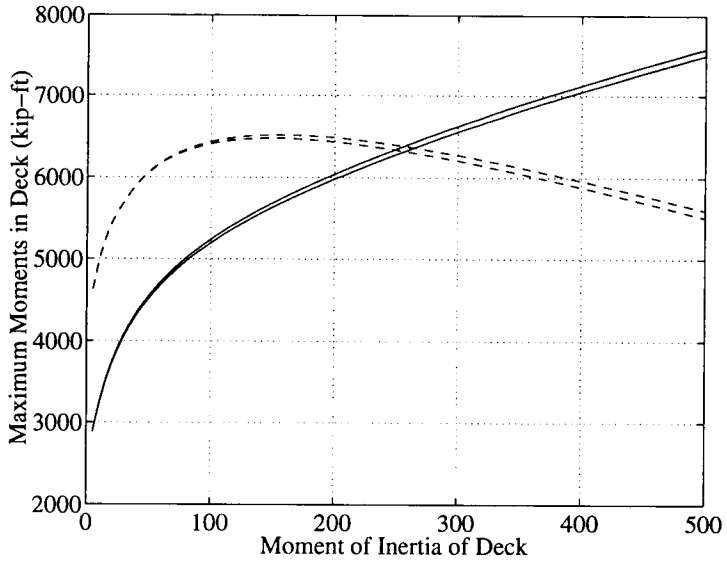

FIGURE 4.10. Influence of moment of inertia of deck on maximum moments of deck with varying moments of inertia of pylon. Solid and dashed lines represent positive and negative moments, respectively. Upper and lower curves of both solid and dashed lines correspond to $I_{pylon} = 10$, and $400 ft^4$, respectively.

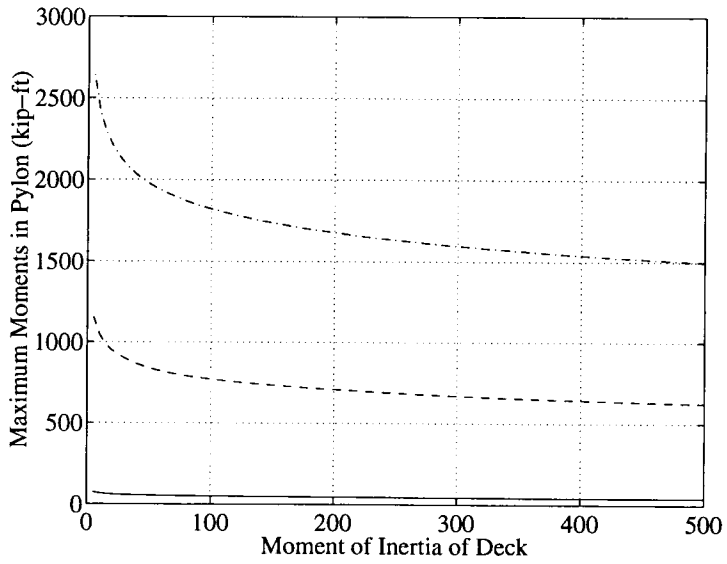

FIGURE 4.11. Influence of moment of inertia of deck on maximum moments of pylon with varying moments of inertia of pylon. Solid, dashed, and dash-dotted lines represent $I_{pylon} = 10, 160$, and 400 ft^4, respectively.

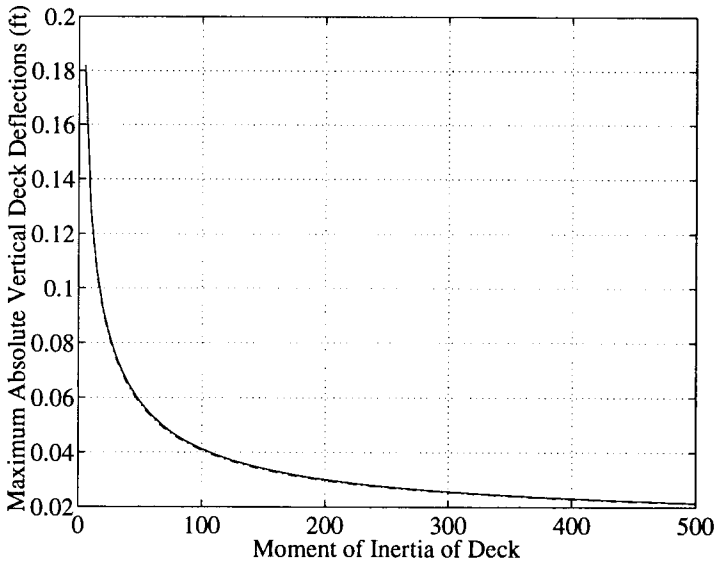

FIGURE 4.12. Influence of moment of inertia of deck on maximum deflection of deck with varying moments of inertia of pylon. Solid, and dash-dotted lines represent $I_{pylon} = 10$, and $400ft^4$, respectively.

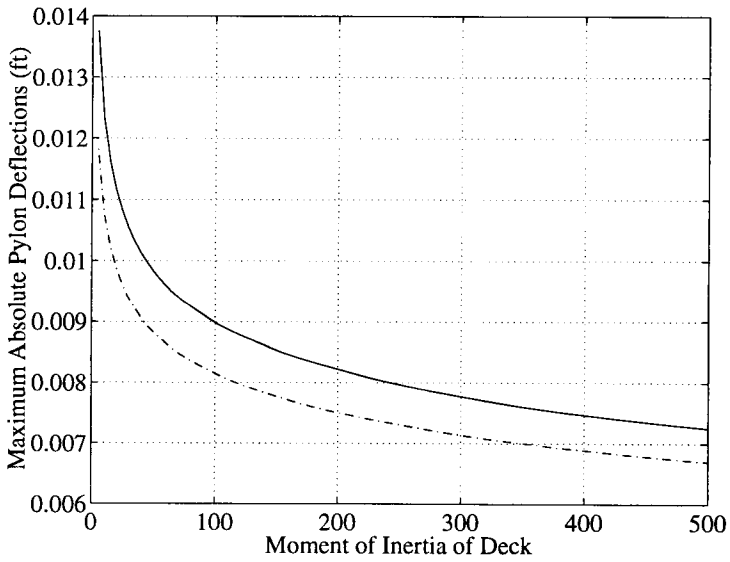

FIGURE 4.13. Influence of moment of inertia of deck on maximum deflection of pylon with varying moments of inertia of pylon. Solid, and dash-dotted lines represent $I_{pylon} = 10$, and $400ft^4$, respectively.

	Presence of Lower Cables	Absence of Lower Cables	Difference (%)
Max Deck Vertical Deflection, ft (m)	0.0614 (0.0187)	0.0193 (0.0059)	+ 218.1
Max Pylon Horizontal Deflection, ft (m)	0.0095 (0.0029)	0.0034 (0.0010)	+ 179.4
Max Deck (-ve) Moment, $k - ft$ $(kN - m)$	5992.9 (8124.9)	4442.3 (6022.7)	+ 34.9
Max Deck (+ve) Moment, $k - ft$ $(kN - m)$	4441.0 (6020.9)	2706.1 (3668.8)	+ 64.1
Max Deck Axial Force, *kips* (kN)	1749.2 (7780.4)	1040.8 (4629.5)	+ 68.1
Max Deck Shear, *kips* (kN)	322.5 (1434.5)	258.7 (1150.7)	+ 24.7
Axial Force of Upper Cable 1, *kips* (kN)	914.8 (4069.0)	800.3 (3559.7)	+ 14.3
Axial Force of Upper Cable 3, *kips* (kN)	800.7 (3561.5)	589.4 (2621.7)	+ 35.9

TABLE 4.1. Influence of Lower Cables (Comparison between Systems with and without presence of lower cables)

(i.e., higher values of moments of inertia of deck), the changes are moderate since the slopes of these curves are observed to be somewhat flatter.

Based on these figures, it is observed that as the moment of inertia of the deck under study is varied 10 % about 45 ft^4, the maximum moments of the deck and pylon and the maximum deformations of the pylon vary about 1 %. However, an approximately 7 % change is observed in the maximum deformations of the deck.

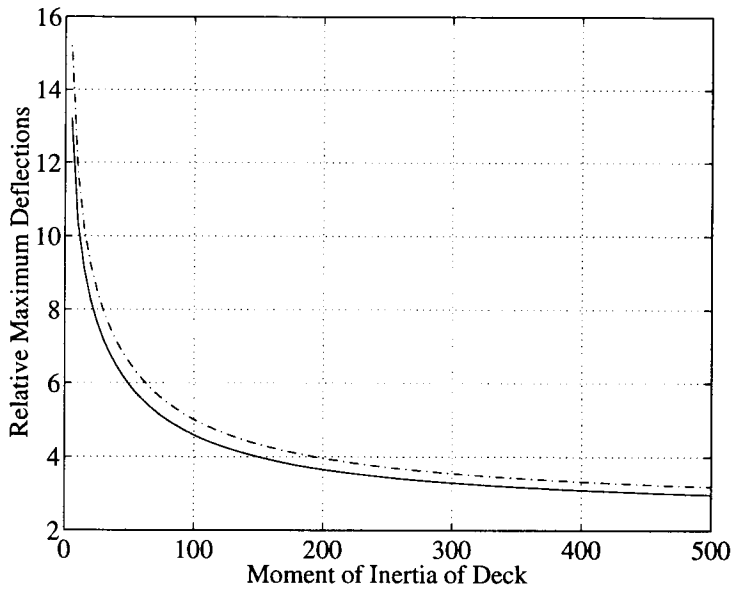

FIGURE 4.14. Influence of moment of inertia of deck on maximum relative deflection between deck and pylon with varying moments of inertia of pylon. Solid, and dash-dotted lines represent $I_{pylon} = 10$, and $400ft^4$, respectively.

4.1.7. Influence of moment of inertia of pylon

As the moment of inertia of the pylon increases, the maximum moments and the maximum absolute deflections in the deck stay almost unaffected as seen in Figures 4.15 and 4.17. It is observed that the maximum moments of the pylon increase (Figure 4.16), and the maximum deflections of the pylon (Figure 4.18) decline. As can be seen in these plots, the moment of inertia of the pylon under the range of values considered does not play a crucial role in reducing the maximum absolute deflections and the maximum moments of the deck, thus very high values are not recommended for design. This behaviour is similarly shown in [55]. This is due to the symmetrical geometry of the structure, and the fact that only the static load is considered. It may become important under dynamic loadings.

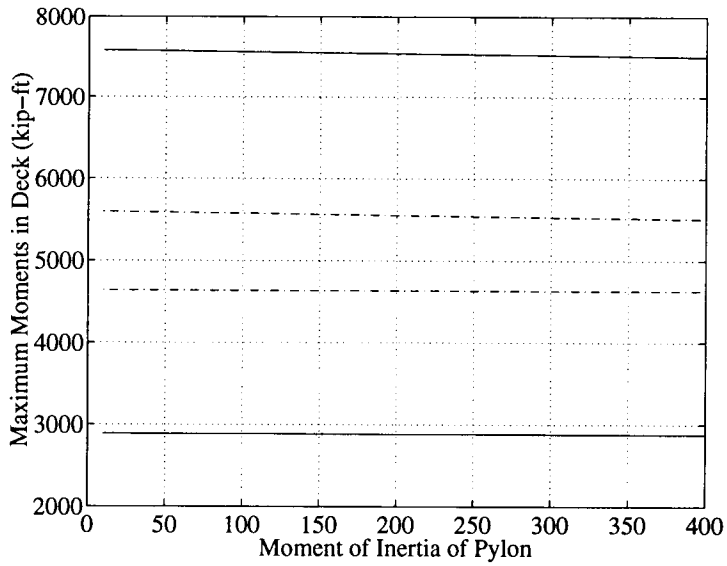

FIGURE 4.15. Influence of moment of inertia of pylon on maximum moments of deck with varying moments of inertia of deck. Solid and dashed lines represent positive and negative moments, respectively. Lower and upper curves of both solid and dash-dotted lines correspond to $I_{deck} = 5$ and 500 ft^4, respectively.

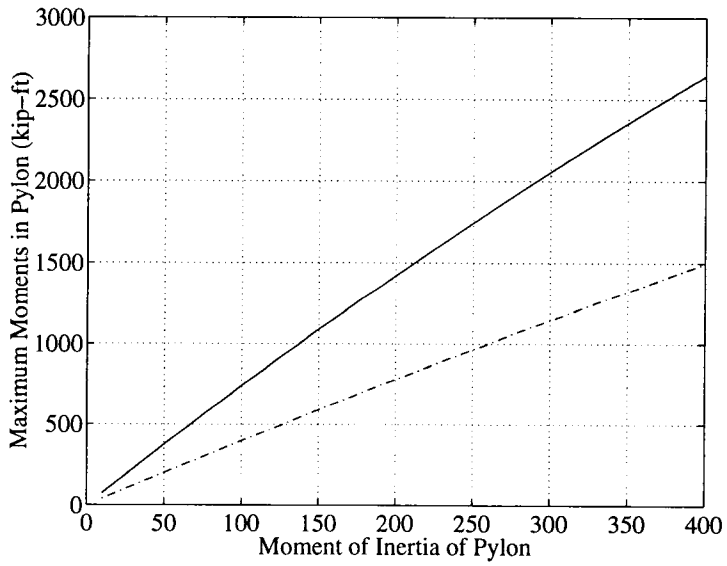

FIGURE 4.16. Influence of moment of inertia of pylon on maximum moments of pylon with varying moments of inertia of deck. Solid, and dash-dotted lines represent $I_{deck} = 5$, and $500 ft^4$, respectively.

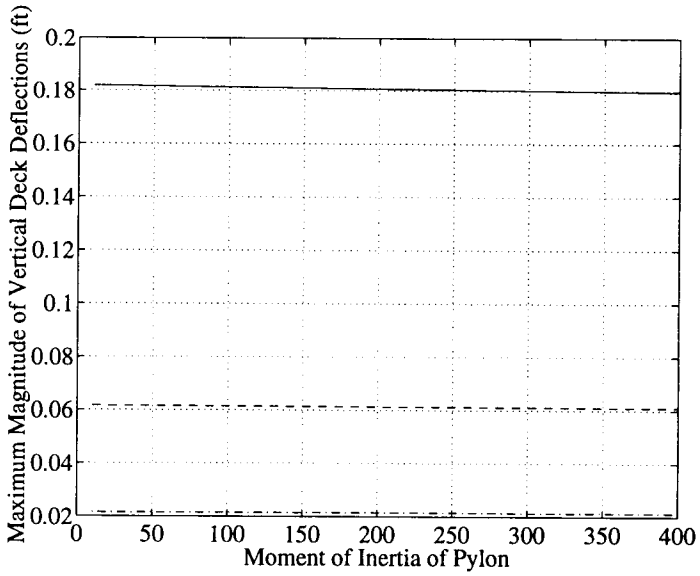

FIGURE 4.17. Influence of moment of inertia of pylon on maximum deflection of deck with varying moments of inertia of deck. Solid, dashed, and dash-dotted lines represent $I_{deck} = 5, 45$, and $500 ft^4$, respectively.

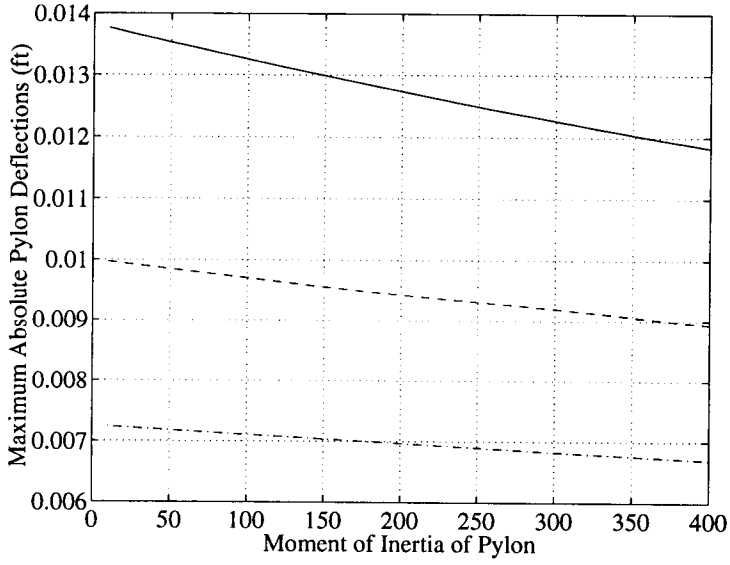

FIGURE 4.18. Influence of moment of inertia of pylon on maximum deflection of pylon with varying moments of inertia of deck. Solid, dashed, and dash-dotted lines represent $I_{deck} = 5, 45$, and $500 ft^4$, respectively.

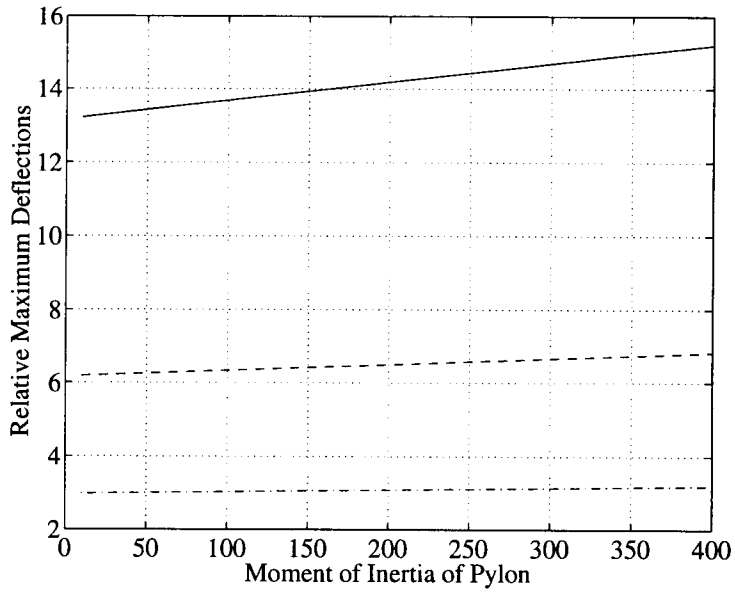

FIGURE 4.19. Influence of moment of inertia of pylon on maximum relative deflection between deck and pylon with varying moments of inertia of deck. Solid, dashed, and dash-dotted lines represent $I_{deck} = 5, 45$, and $500 ft^4$, respectively.

Based on these figures, it is seen that the maximum moment and the maximum deformations of the deck are insensitive to changes in the moment of inertia of the pylon under study (160 ft^4). However, a 10 % change in the moment of inertia of the pylon results in about 12 % change in the maximum moment, and about 4 % change in the maximum deflection of the pylon.

4.1.8. Influence of span length

An increase of the span length results in higher flexibility in the deck. In addition, as the total span length of the double-stayed bridge increases, the structure carries greater loads (uniform distributed loading is constant). One sees an increase in the maximum moment and the maximum deflection in the deck, a decrease in the

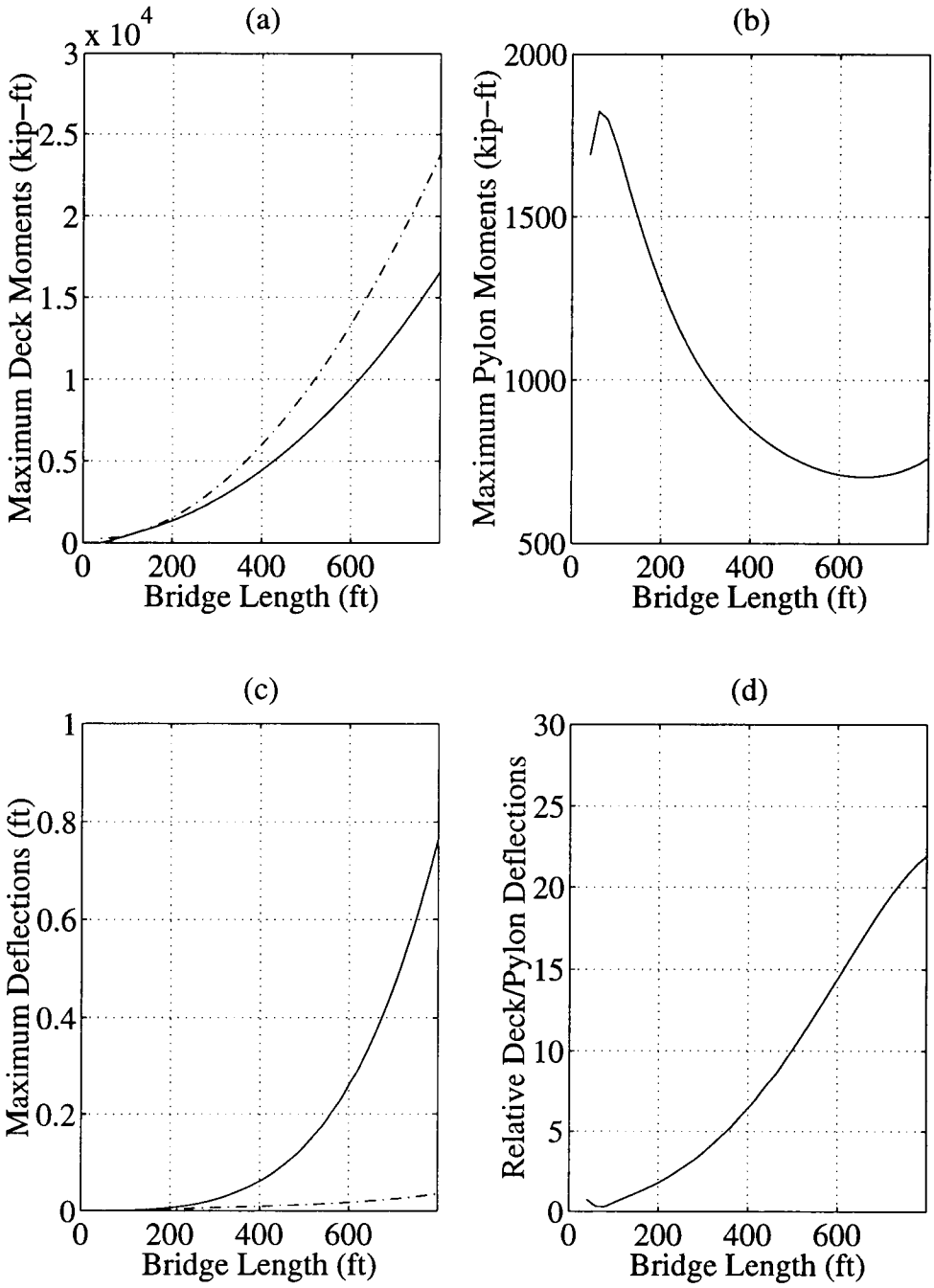

FIGURE 4.20. Influence of the structure span length. (*a*) Solid and dash-dotted lines represent positive and negative moments, respectively. (*c*) Solid and dash-dotted lines represent deck and pylon deflections, respectively.

maximum moment in the pylon, and a very slight increase in the maximum deflection of the pylon, as illustrated in Figure 4.20. Under the currently studied span length of 400 ft, the maximum deflection of the deck normalized by the maximum deflection of the pylon is at a ratio of about 6. A 10 % variation in the neighborhood of this span length causes approximately 20 % change in the maximum moment of the deck, approximately 5 % change in the maximum moment and deformation of the pylon, and about 80 % change in the maximum deflection of the deck.

4.1.9. Influence of nonlinearity

A comparison study is also conducted to observe the effects of the nonlinearities due to the sagging of the cables and the axial-bending interaction. A summary of this comparison is listed in Table 4.2. A difference of about 30 % in maximum vertical deflection of deck and over 50 % in lower cable tension show that the effect of the nonlinearity should not be neglected for this structure under the parameters listed in Table 2.1.

4.2. Uncontrolled Dynamic Parametric Study

The 1971 San Fernando earthquake is used throughout this section for the purpose of dynamic parametric studies. In this section, influences of some important properties of the structure are presented. As in the case of static parametric studies, the behaviours observed are limited to the maximum moment and the maximum absolute deflections of the deck and the pylon. In most cases, only time-series of certain nodal vertical deflections and moments of the deck are plotted for the purposes of illustration. Since the maximum responses of the double-stayed structure under study occur within the first 10 *seconds* of the Pacoima earthquake, the time

	Nonlinear Behavior	Linear Behavior	Difference (%)
Max Deck Vertical Deflection, ft (m)	0.0614 (0.0187)	0.0470 (0.0143)	+ 30.64
Max Pylon Horizontal Deflection, ft (m)	0.0095 (0.0029)	0.0090 (0.0027)	+ 5.56
Max Deck (-ve) Moment, $k - ft$ $(kN - m)$	5992.9 (8124.9)	5225.4 (7084.3)	+ 14.69
Max Deck (+ve) Moment, $k - ft$ $(kN - m)$	4441.0 (6020.9)	3827.3 (5188.9)	+ 16.03
Max Deck Axial Force, *kips* (kN)	1749.2 (7780.4)	1557.0 (6925.5)	+ 12.30
Max Deck Shear, *kips* (kN)	322.5 (1434.5)	299.1 (1330.4)	+ 7.82
Axial Force of Upper Cable 3, *kips* (kN)	800.7 (3561.5)	740.4 (3293.3)	+ 8.14
Axial Force of Lower Cable 4, *kips* (kN)	441.5 (1963.8)	279.9 (1245.0)	+ 57.73

TABLE 4.2. Influence of Nonlinearity (Comparison between Linear and Nonlinear Behavior)

history plots are only shown for that range. For the subsequent subsections, unless stated otherwise, a nonlinear static equilibrium approach combined with the linear dynamic analysis presented in Chapter 2 are carried out. In all cases considered, the rotational acceleration component of the seismic excitation is excluded.

4.2.1. Influence of mass density of deck and pylon

Under the dynamics of non-uniform support excitations from the Pacoima (1971 San Fernando) earthquake, as the mass density of the deck increases, the maximum absolute deflections of both the deck and the pylon increase with the increasing mass density of the pylon. These effects can be viewed in Figures 4.21 - 4.24.

Also based on these illustrations, a 10 % variation in the mass density of the deck of 0.018 $\frac{k-s^2}{ft^4}$ causes about 6 % variation in the maximum deflection of the deck, and about 10 % variation in the maximum deflection of the pylon. However, a 10 % change in the mass density of the pylon results in about 10 % and 13 % change in the maximum deflections of the deck and the pylon, respectively.

4.2.2. Influence of span length

As the span length of the deck increases, the maximum absolute deflections of both the deck and the pylon increase. Figure 4.25 shows that there is a moderate increase in deflections between span lengths of 200 and 450 ft, and beyond that range, the increase becomes significant. In the previous static parametric study of the span length, one observes a very slight increase in the maximum deflection of pylon as the span length increases. This is, however, not the case here. As seen in Figure 4.25, there is dynamic amplification on the order of more than 20 in the maximum deflection of the pylon for a structure span length of 800 ft over the corresponding deflection under static load. In the case of maximum deflection of the deck, under the same span length of 800 ft, the response doubles over that under static load.

4.2.3. Influence of non-uniform excitations

To observe the effects of non-uniform support excitations, the 1971 Pacoima (San Fernando) earthquake with a wave speed of 5000 ft/s is examined. With this wave speed, and the fact that the distance between the two closest supports is 200 ft apart, there would be a delay of a fraction of a second. The results are compared with the responses for the same earthquake but without any wave delay. These results are plotted and shown in Figures 4.26 - 4.27. As shown, the maximum vertical deflection at the third quarter span of the deck (node 7) is greater when subjected to this out-of-phase motion.

4.2.4. Influence of vertical excitations

To look into the effects of vertical components of this earthquake on the response of the structure, a system subjected to uniform horizontal and vertical ground motions is analyzed and compared with that without the vertical components. The results are shown in Figures 4.28 - 4.29. One notices that when the vertical components are excluded, both the maximum vertical deflection at the third quarter span of the deck (node 7) and the maximum moment in a member near midspan (member 6 at node 6) are lower. For this reason, vertical components of all three earthquakes are included in the subsequent uncontrolled and controlled response studies.

4.2.5. Influence of different analyses

A number of publications have addressed whether nonlinearity should be included in the static or dynamic analyses. These publications ([29], [53], [54]) concluded that the responses obtained by a nonlinear static and nonlinear dynamic

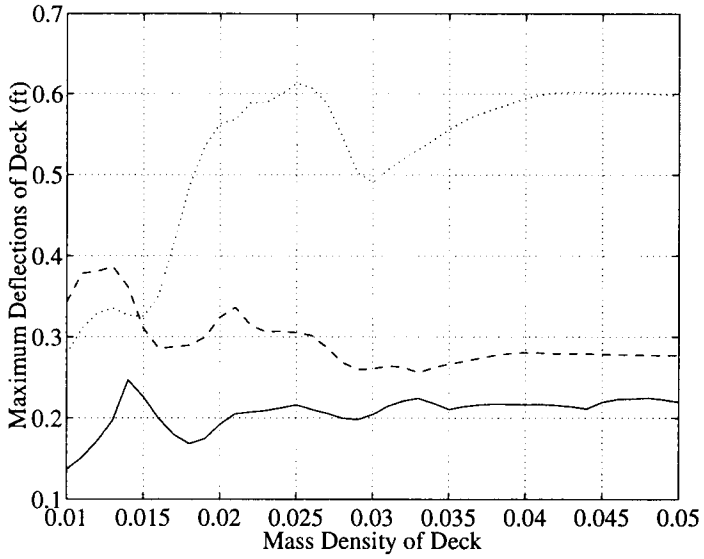

FIGURE 4.21. Influence of the mass density of deck on maximum deflections of deck subjected to nonuniform Pacoima earthquake. Solid, dashed, and dotted lines represent mass densities of pylon of 0.01, 0.02, and 0.05 $\frac{k-s^2}{ft^4}$, respectively.

analysis (NL-NL) can be well approximated by using a nonlinear static combined with a linear dynamic analysis procedure (NL-L). However, whether one can use linear static and linear dynamic analysis (L-L) depends on the degree of the nonlinearity in the system. For some systems, the responses may differ on the order of 10 % [40]; for others, the differences can be more significant. Significant nonlinearities are present for the structure under study, as shown in the previous section on the static parametric study (Table 4.2). To further illustrate the influence of different analyses methods on the dynamic response, a time history of the vertical deflection of node 7 and the moments in member 6 at node 6 are plotted and shown in Figures 4.30 - 4.31. As can be seen in Figure 4.30, the maximum vertical deflection of node 7 is underestimated by a factor of at least 1.5 using L-L analysis.

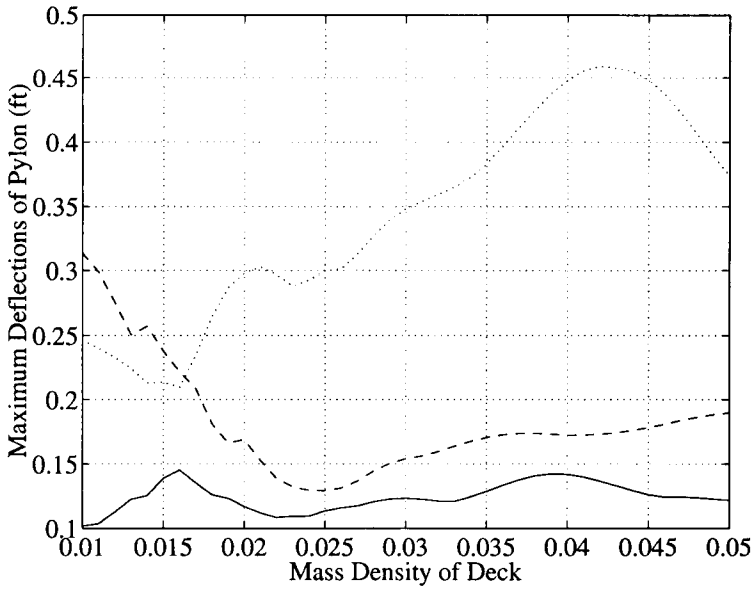

FIGURE 4.22. Influence of the mass density of deck on maximum deflections of pylon subjected to nonuniform Pacoima earthquake. Solid, dashed, and dotted lines represent mass densities of pylon of 0.01, 0.02, and 0.05 $\frac{k-s^2}{ft^4}$, respectively.

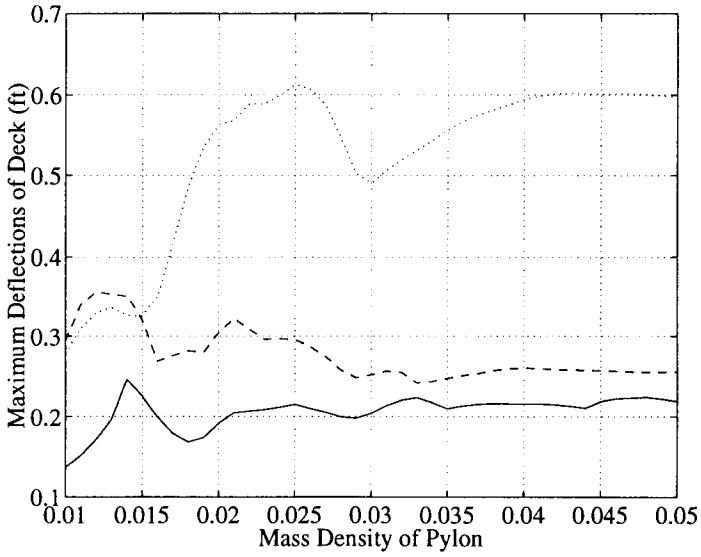

FIGURE 4.23. Influence of the mass density of pylon on maximum deflections of deck subjected to nonuniform Pacoima earthquake. Solid, dashed, and dotted lines represent mass densities of deck of 0.01, 0.018, and 0.05 $\frac{k-s^2}{ft^4}$, respectively.

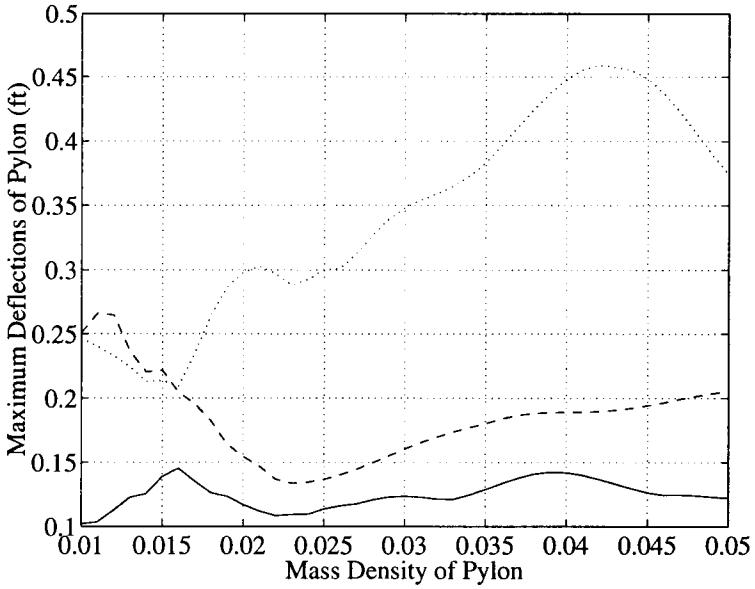

FIGURE 4.24. Influence of the mass density of pylon on maximum deflections of pylon subjected to nonuniform Pacoima earthquake. Solid, dashed, and dotted lines represent mass densities of deck of 0.01, 0.018, and 0.05 $\frac{k-s^2}{ft^4}$, respectively.

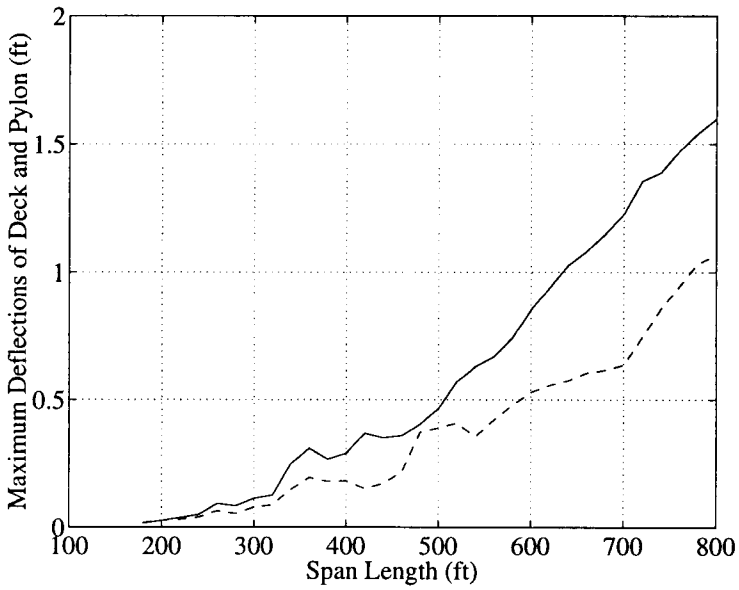

FIGURE 4.25. Influence of the span length on maximum deflections of deck (solid line) and pylon (dashed line) subjected to nonuniform Pacoima earthquake.

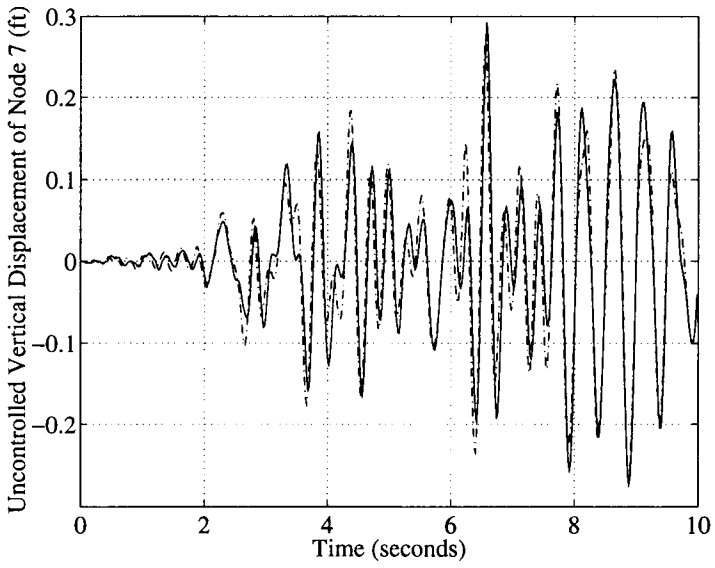

FIGURE 4.26. Comparison of uncontrolled vertical displacement time history of deck (node 7) subjected to non-uniform (solid line) and uniform (dash-dotted line) Pacoima earthquake support excitations. (Max Nonuniform = 0.2927, Max Uniform = 0.2730)

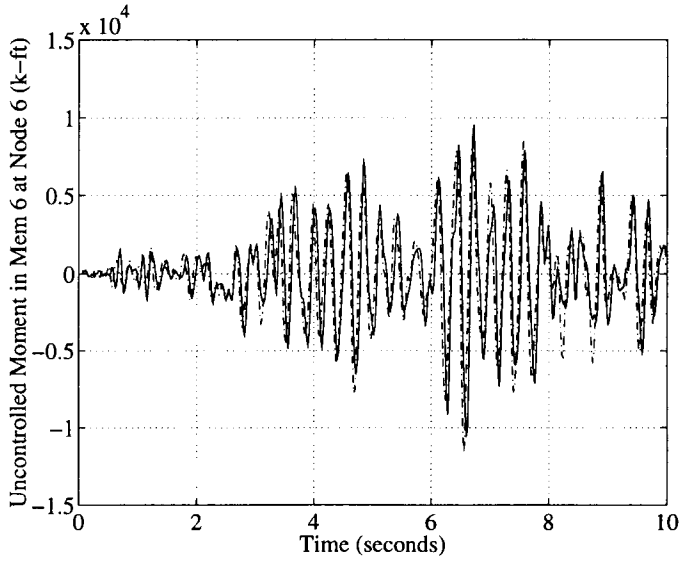

FIGURE 4.27. Comparison of uncontrolled moment time history of deck (member 6 at node 6) subjected to non-uniform (solid line) and uniform (dash-dotted line) Pacoima earthquake support excitations. (Max Nonuniform = 1.0449×10^4, Max Uniform = 1.1625×10^4)

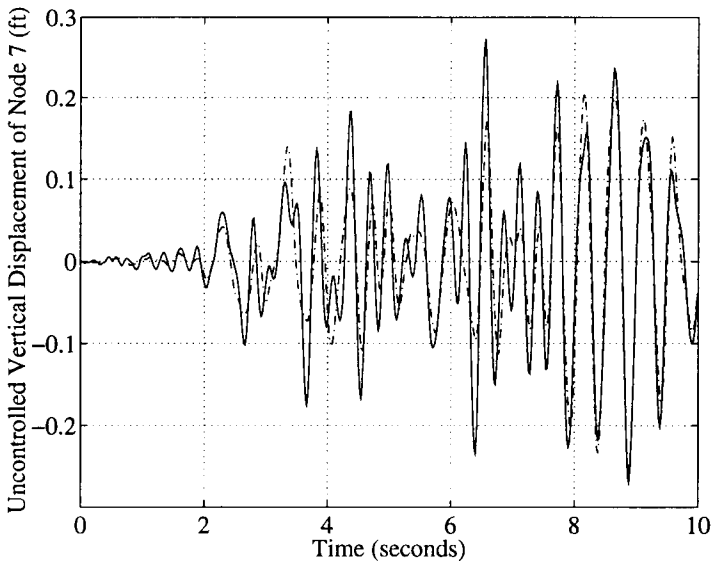

FIGURE 4.28. Comparison of uncontrolled vertical displacement time history of deck (node 7) subjected to uniform with vertical (solid line) and uniform without vertical (dash-dotted line) Pacoima earthquake support excitations. (Max with vertical = 0.2730, Max without vertical = 0.2567)

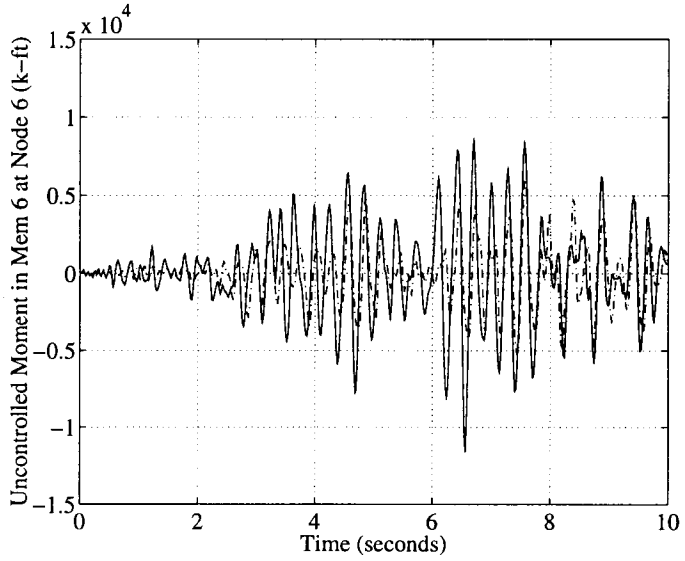

FIGURE 4.29. Comparison of uncontrolled moment time history of deck (member 6 at node 6) subjected to uniform with vertical (solid line) and uniform without vertical (dash-dotted line) Pacoima earthquake support excitations. (Max with vertical = 1.1625×10^4, Max without vertical = 0.6068×10^4)

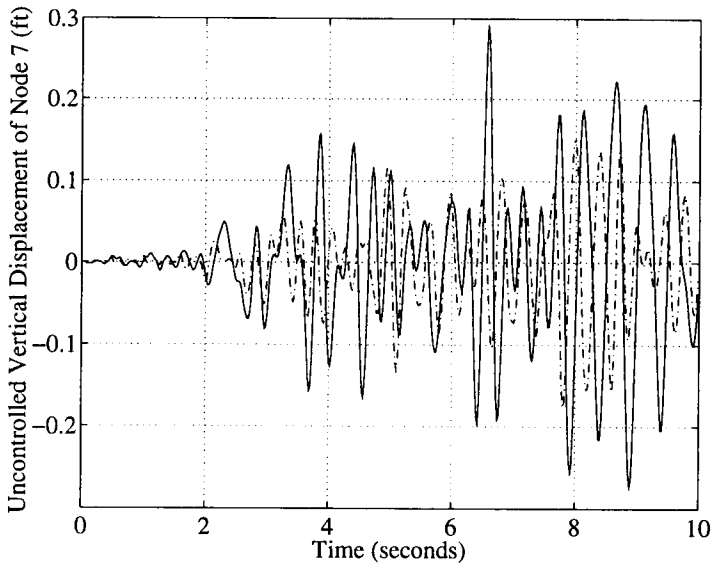

FIGURE 4.30. Comparison of uncontrolled vertical displacement time history of deck (node 7) subjected to nonuniform Pacoima earthquake support excitations using NL-L analysis (solid line) and L-L analysis (dash-dotted line). (Max NL-L = 0.2927, Max L-L = 0.1767)

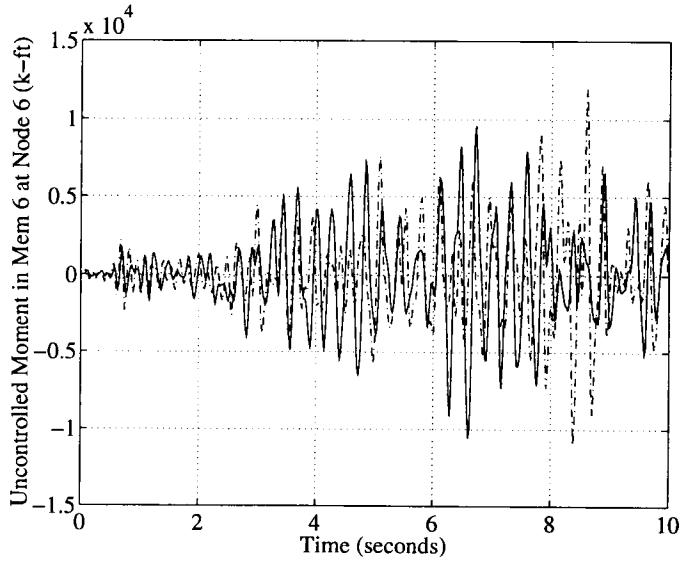

FIGURE 4.31. Comparison of uncontrolled moment time history of deck (member 6 at node 6) subjected to nonuniform Pacoima earthquake support excitations using NL-L analysis (solid line) and L-L analysis (dash-dotted line). (Max NL-L = 1.0449×10^4, Max L-L = 1.1956×10^4)

5. CONTROLLED PERFORMANCE OF THE DOUBLE-STAYED STRUCTURE

In this chapter, the dynamic performance of the controlled double-stayed structure subjected to severe nonuniform seismic excitations is evaluated. The control scheme involves the ARE-based decentralized H_∞ technique which is presented in Chapter 2. A comparative study between the controlled and uncontrolled responses is conducted to show the effectiveness of the control scheme.

The double-stayed system to be controlled is described in Figure 2.1 and the properties of which are listed in Table 2.1. All the analysis procedures used to obtain the responses are described in Chapter 2. In the analyses of both the controlled and uncontrolled responses of the system, the NL-L approach is performed. A nonlinear static equilibrium method is used to obtain the stiffness of the overall system at the static deformed state under dead load and cable pretension. To determine the uncontrolled dynamic responses of the structure, a linear dynamic analysis is performed. To determine the controlled dynamic responses of the structure, linear controllers are used. The vertical and horizontal components of three recorded earthquake ground motion data sets are considered, with a wave speed through rock of 5000 ft/s.

The vibration characteristics of the uncontrolled double-stayed structure are shown in Figure 5.1 (first three dynamic modes of the system) and Table 5.1 (uncontrolled natural frequencies). As shown, the fundamental mode vibrates at about 2 *Hertz*. As observed in Figure 5.4, when the structure is subjected to the 1971 San Fernando earthquake that has significant energy near 2 *Hertz* strong motions

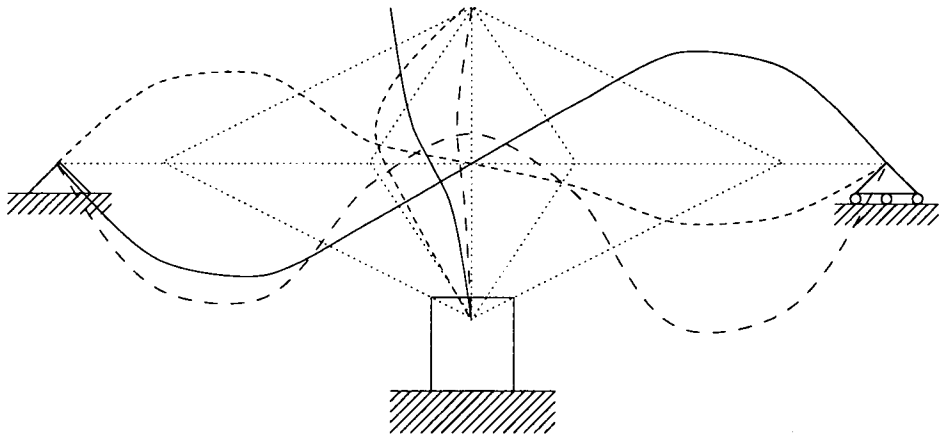

FIGURE 5.1. First three mode shapes of structure. Solid, long dashed, and short dashed lines represent the first, second, and third modes, respectively.

of the structure results. The same characteristic is also observed when the structure is excited by the 1992 Petrolia earthquake (see Figure 5.10).

To illustrate the performance of the decentralized H_∞ controllers subjected to strong earthquake motions, a comparative study between controlled and uncontrolled responses is performed using the vertical displacement time history at the third quarter of the span (node 7) and the corresponding frequency domain insights (Fourier transform). The results are plotted in Figures 5.2 through 5.11. As illustrated in these figures, reductions of 65.73 %, 47.96 %, and 44.82 % in the maximum responses are observed in the controlled system subjected to the 1971 San Fernando, the 1985 Mexico, and the 1992 Petrolia earthquakes, respectively. These response attenuations show the robustness of the control scheme, since the characteristics of these earthquakes are different in terms of intensity, duration, magnitude, and dominant frequencies (see Chapter 3). From the Fourier transform of the response time history of the controlled system, it is also noticed that there is no dominant frequency, in contrast to the uncontrolled system (see Figures 5.5 and 5.11).

Modes	Natural Frequency (rad/s)	Period (seconds)	Frequency (Hz)
1	12.4	0.5079	1.9689
2	21.7	0.2890	3.4602
3	23.0	0.2732	3.6610
4	33.0	0.1902	5.2568
5	45.8	0.1371	7.2922

TABLE 5.1. First Five Natural Frequencies, Periods, and Cyclic Frequencies of the uncontrolled system

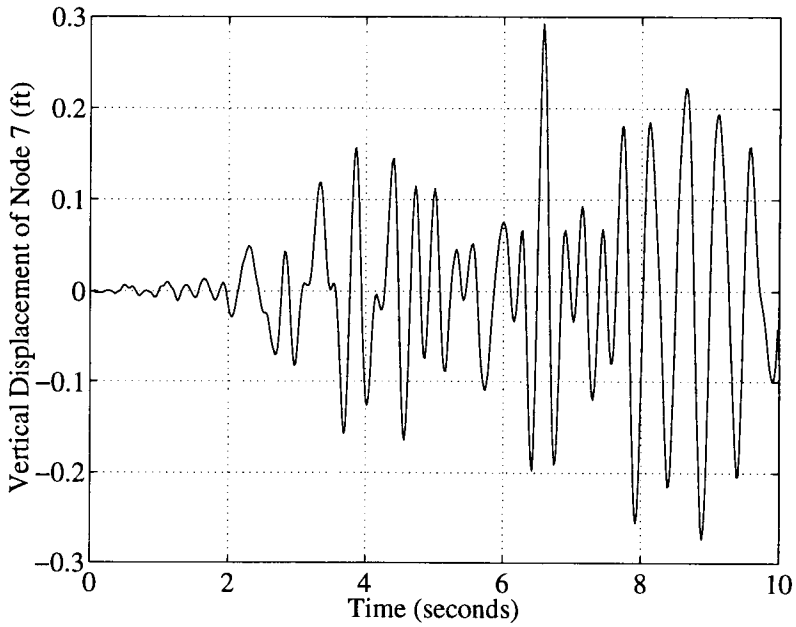

FIGURE 5.2. Uncontrolled Vertical Displacement History at the third quarter span (Node 7) due to 1971 San Fernando Earthquake. Maximum = 0.2927.

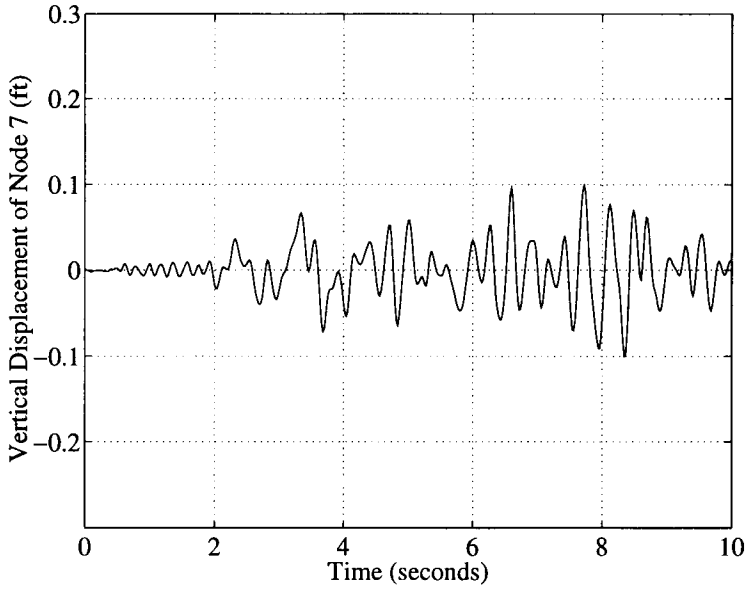

FIGURE 5.3. Controlled Vertical Displacement History at the third quarter span (Node 7) due to 1971 San Fernando Earthquake. Maximum = 0.1003.

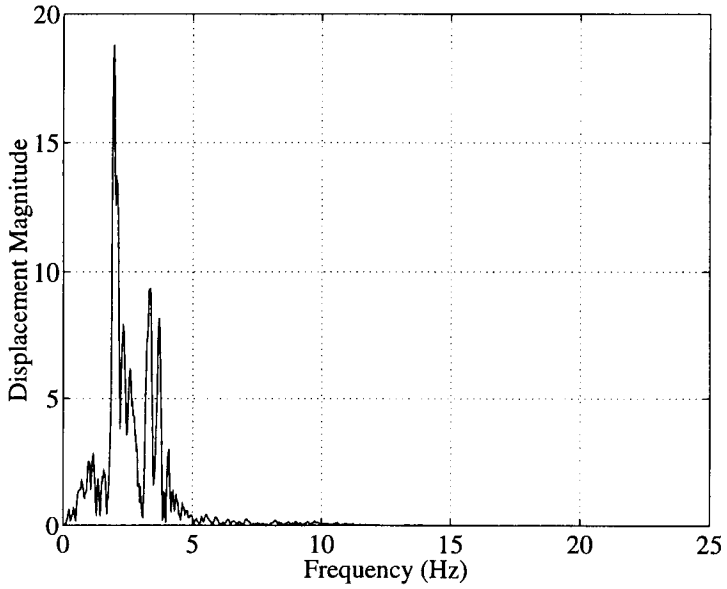

FIGURE 5.4. Fourier Transform of Uncontrolled Vertical Displacement History at the third quarter span (Node 7 - 1971 San Fernando Earthquake).

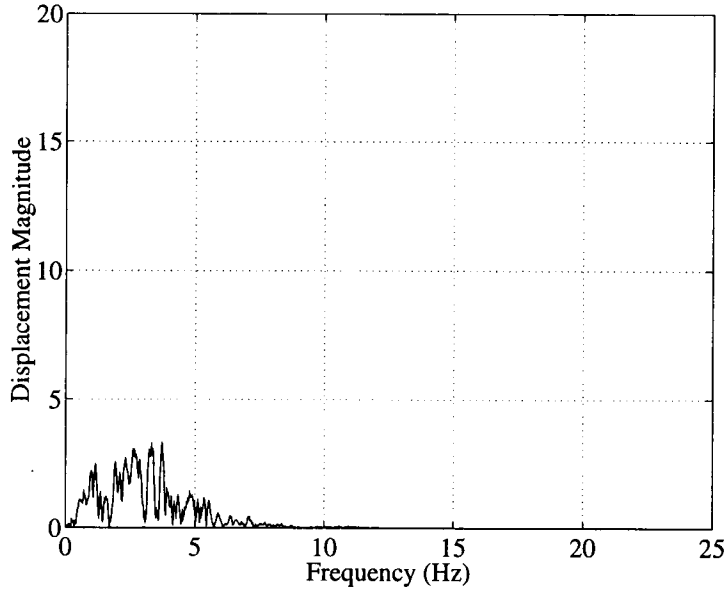

FIGURE 5.5. Fourier Transform of Controlled Vertical Displacement History at the third quarter span (Node 7 - 1971 San Fernando Earthquake).

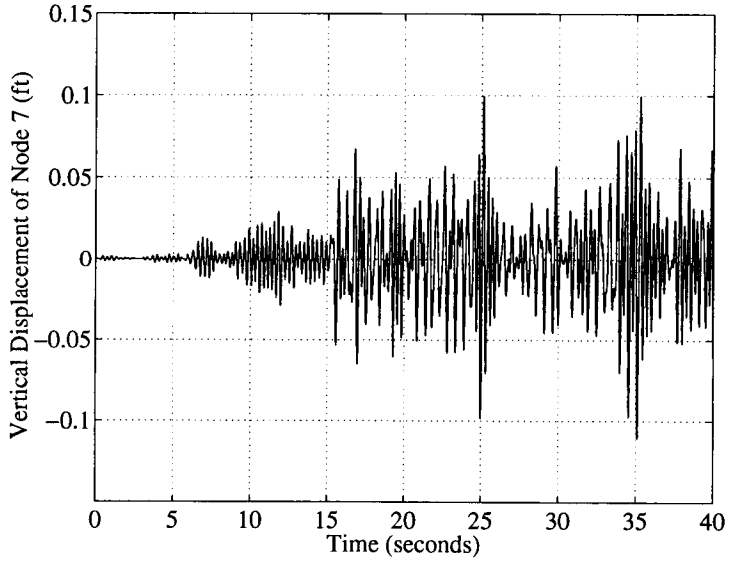

FIGURE 5.6. Uncontrolled Vertical Displacement History at the third quarter span (Node 7) due to 1985 Mexico Earthquake. Maximum = 0.1105.

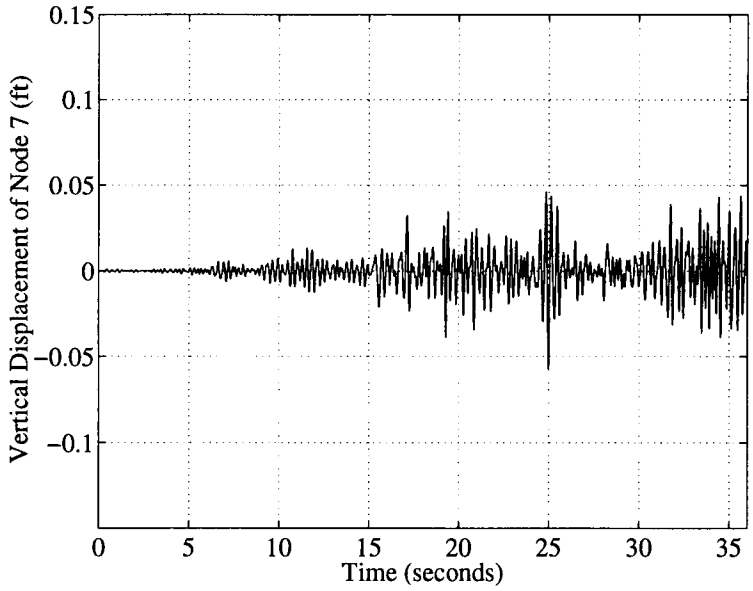

FIGURE 5.7. Controlled Vertical Displacement History at the third quarter span (Node 7) due to 1985 Mexico Earthquake. Maximum = 0.0575.

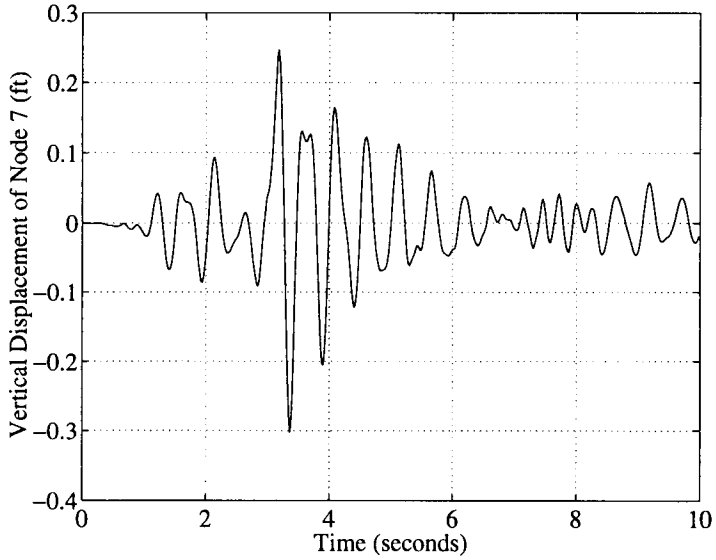

FIGURE 5.8. Uncontrolled Vertical Displacement History at the third quarter span (Node 7) due to 1992 Petrolia Earthquake. Maximum = 0.3023.

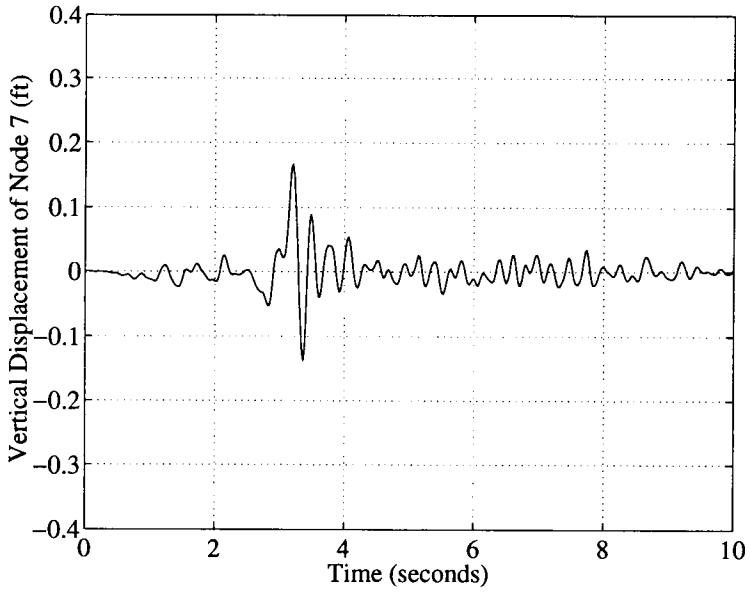

FIGURE 5.9. Controlled Vertical Displacement History at the third quarter span (Node 7) due to 1992 Petrolia Earthquake. Maximum = 0.1668.

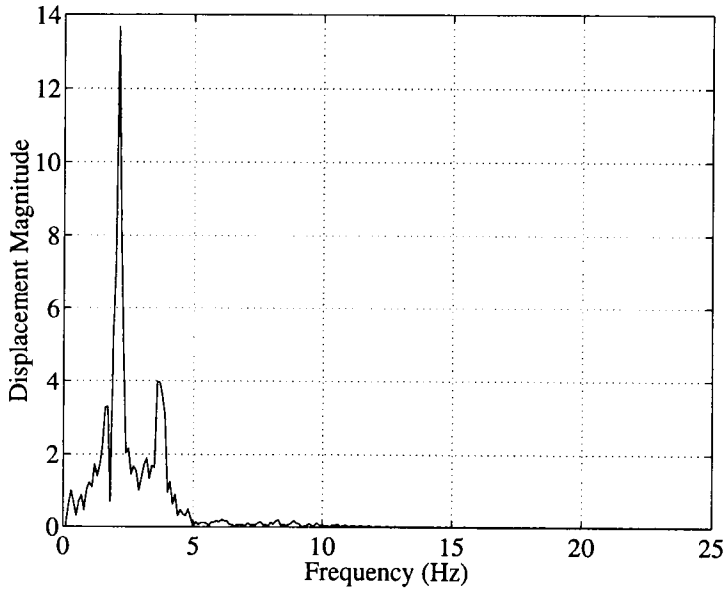

FIGURE 5.10. Fourier Transform of Uncontrolled Vertical Displacement History at the third quarter span (Node 7 - 1992 Petrolia Earthquake).

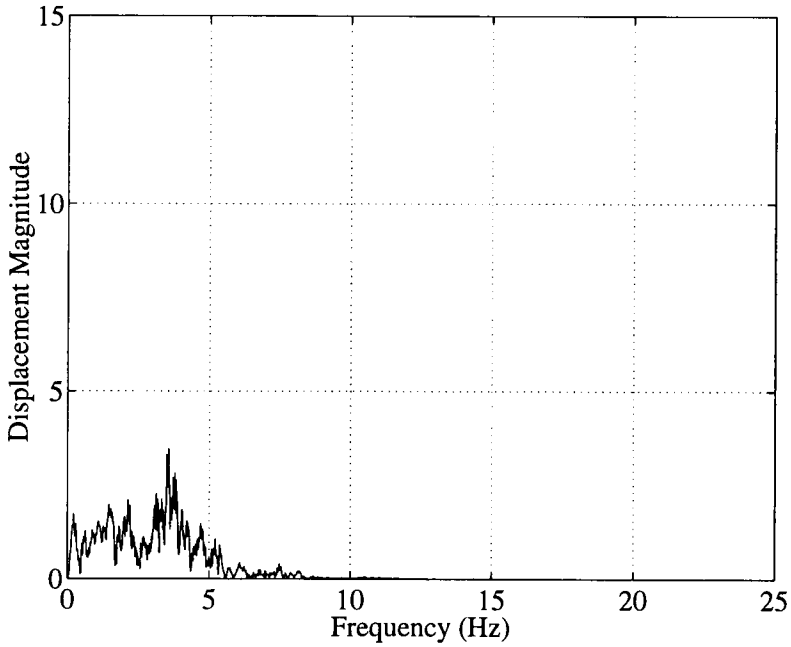

FIGURE 5.11. Fourier Transform of Controlled Vertical Displacement History at the third quarter span (Node 7 - 1992 Petrolia Earthquake).

6. DISCUSSIONS AND CONCLUSIONS

This thesis has presented the aseismic performance of a controlled and uncontrolled double-stayed structure. The controlled structure is composed of four decentralized controllers using the ARE-based H_∞ control design technique.

The ideal physical model is obtained by the finite element method. Due to the geometric nonlinearity of the cable-supported system, a nonlinear static equilibrium approach is used to obtain the stiffness of the structure at the static equilibrium deformed state. These nonlinearities originate from the sagging of the cables and the axial-bending interaction of the members. To examine the static behaviour of this structure, a series of static parametric studies have been presented. These studies have shown the effect on the structural behaviour due to variations in the pretensions of the upper and lower cables, the presence and absence of the lower cables, changes in the moments of inertia of the deck and pylon, and changes in the structure span length. The effect of the presence of nolinearities in the system is also investigated. Based on the results obtained, it may be concluded that the double-stayed system static behaviour is similar to many other cable-stayed systems. For example, [55] reports that an increase in deck moment of inertia results in an increase in moments in the deck and decreases in the moments in the pylon and the maximum deflections for some cable-stayed bridges with a variety of cable configurations. For the bridge under consideration, as the moment of inertia of the pylon increases, the moments and the deflections in the deck are reduced, and the moments in the pylon increased. The double-stayed structure has shown a similar structural behaviour. From the sensitivity studies presented, the following conclusions may also be drawn. For the structure currently under study, it is concluded that the pretensions of both the

upper and the lower cables are not sensitive to variations in their neighborhood. It may also be concluded that the presence of the lower cables causes higher maximum static responses. The maximum static responses of both the deck and pylon are observed to be insensitive to variations in the neighborhood of the moments of inertia of the deck. The same conclusion may be reached for changes in the moment of inertia of the pylon. The effect of variations in the span length of the structure is also presented and it is concluded that changes in the span length would magnify the static responses. Finally, the static responses are sensitive to the nonlinearities of the system.

The dynamic analysis of the structure is performed with a nonlinear static, linear dynamic (NL-L) approach, which is widely accepted and used by many investigators. Using this approach, the dynamic behaviours of the uncontrolled system are investigated, and a series of parametric analyses is carried out. The 1971 Pacoima Dam earthquake has been considered for the purpose of this analysis. These parametric studies have included the effects of the mass densities of the deck and pylon, the effects of the span length, the effects of the nonuniformity of the excitations, the effects of the vertical components of the excitations, and the effects of different methods of analyses. Based on the study, the following may be concluded. First, higher masses for both the deck and the pylon cause higher maximum absolute deflections in both the deck and the pylon. With the mass desities under study, the maximum deflections of the deck and pylon are somewhat sensitive to changes in the mass densities of both the deck and pylon. The longer the span length of the structure, the more flexible the structure becomes. The effect of increasing flexibility causes larger deformations in both the deck and the pylon. However, a small change in the span length does not cause a large change in the maximum deflection of the deck and no change in the maximum deflection of the pylon. Compared to the

nonuniform excitation case, uniform excitation underestimates the maximum deformation of the deck. For a conservative design, nonuniform ground motion should be included. The vertical components of an earthquake also affect the displacement response of the system. This vertical component, very often neglected in structural analysis, causes higher displacements and forces in the structure. Finally, the NL-L analysis is encouraged for the analysis of cable-stayed structure with high static nonlinearity.

To mitigate the earthquake-induced vibrations of the structure, four decentralized H_∞ controllers have been placed on the lower cables of the system. This control scheme is overviewed in detail in Chapter 2. With these controllers, the structure performs reasonably well even under severe earthquake motions. The technique effectively and robustly attenuates the displacement response of the structure. Further improvement in the effectiveness of the decentralized controller can be achieved through proper and careful design. In other words, an H_∞ norm bound can be properly chosen to maximize the performance. The control system can also be fined-tuned by optimizing the placement and number of controllers and sensors, which will lead to increasing controllability (stabilizability) and observability (detectability) of the system.

BIBLIOGRAPHY

[1] Abdel-Ghaffar, A. M., and Nazmy, A. S. (1991a). "3-D nonlinear seismic behavior of cable-stayed bridges." *J. Struct. Engrg.*, ASCE, 117(11), 3456-3476.

[2] Abdel-Mooty, M., and Roorda, J. (1991). "Time-delay compensation in active damping of structures." *J. Engrg. Mech.*, ASCE, 117(11), 2549-2570.

[3] Abdel-Mooty, M., and Roorda, J. (1994). "Optimal configuration of active-control mechanisms." *J. Engrg. Mech.*, ASCE, 120(3), 535-556.

[4] Abdel-Rohman, M., and Leipholz, H. H. (1978). "Structural control by pole assignment method." *J. Engrg. Mech. Div.*, ASCE, 104(5), 1159-1175.

[5] Abdel-Rohman, M., Quintana, V. H., and Leipholz, H. H. (1980). "Optimal control of civil engineering structures." *J. Engrg. Mech. Div.*, ASCE, 106(1), 57-73.

[6] Abdel-Rohman, M., and Leipholz, H. H. (1981). "Stochastic control of structures." *J. Struct. Engrg.*, ASCE, 107(ST7), 1313-1325.

[7] Abdel-Rohman, M. (1982). "Active control of large structures." *J. Engrg. Mech. Div.*, ASCE, 108(5), 719-730.

[8] Abdel-Rohman, M. (1987a). "Time delay effects on actively damped structures." *J. Engrg. Mech.*, ASCE, 113(11), 1709-1719.

[9] Abdel-Rohman, M. and Nayfeh, A. H. (1987b). "Passive control of nonlinear oscillations in bridges." *J. Engrg. Mech.*, ASCE, 113(11), 1694-1708.

[10] Abdel-Rohman, M. and Nayfeh, A. H. (1987c). "Active control of nonlinear oscillations in bridges." *J. Engrg. Mech.*, ASCE, 113(3), 335-348.

[11] Aida, T., Toda, S., Ogawa, N., and Imada, Y. (1992). "Vibration control of beams by beam-type dynamic vibration absorbers." *J. Engrg. Mech.*, ASCE, 118(2), 248-258.

[12] Anderson, B. O., and Moore, J. B.(1990). *Optimal control : Linear quadratic methods.* Prentice Hall, Inc., Englewood Cliffs, New Jersey.

[13] ASCE committee. (1992). "Guidelines for the design of cable-stayed bridges." *Published by ASCE.*, New York, New York.

[14] Baba, S., Ninomiya, K., and Hayashi, Y. (1989). "Active optimal control of structure under optimal observer." *J. Engrg. Mech.*, ASCE, 115(11), 2564-2581.

[15] Bachman, H., et al (1995). *Vibration problems in structures.* Birkhauser Verlag, Basel, Germany.

[16] Barmish, B. R. (1994). *New tools for robustness of linear systems.* Macmillan Publishing Company, New York, New York.

[17] Boyd, S. P., and Barratt, C. H.(1991). *Linear controller design : Limits of performance.* Prentice Hall, Inc., Englewood Cliffs, New Jersey.

[18] Brockenbrough, R. L., and Merritt, F. S. (1994). *Structural steel designer's handbook.* 2nd Edt., McGraw-Hill, Inc., New York, NY.

[19] Brogan, W. L.(1991). *Modern Control Theory.* Prentice Hall, Inc., Englewood Cliffs, New Jersey.

[20] Burdisso, R. A., Suarez, L. E., and Fuller, C. R. (1994). "Feasibility study of adaptive control of structures under seismic excitation." *J. Engrg. Mech.*, ASCE, 120(3), 580-592.

[21] Chang, J. C. H., and Soong, T. T. (1980). "Structural control using active tuned mass dampers." *J. Engrg. Mech. Div.*, ASCE, 106(6), 1091-1098.

[22] Ch'ng, G. B., Hernried, A. G., and Magana, M. (1995). "Active control of a cable-stayed guideway." *In Proceedings of the American Control Conference.*, 2359-2363, June 21-23rd, Seattle, Washington.

[23] Chung, L. L., Reinhorn, A. M., and Soong, T. T. (1988). "Experiments on active control of seismic structures." *J. Engrg. Mech.*, ASCE, 114(2), 241-256.

[24] Chung, L. L., Lin, R. C., Soong, T. T., and Reinhorn, A. M. (1989). "Experimental study of active control for MDOF seismic structures." *J. Engrg. Mech.*, ASCE, 115(8), 1609-1627.

[25] Chung, L. L., Lin, C. C., and Chu, S. Y. (1993). "Optimal direct output feedback of structural control." *J. Engrg. Mech.*, ASCE, 119(11), 2157-2173.

[26] Clough, R. W., and Penzien, J. (1993). *Dynamics of stuctures.* 2nd Ed., McGraw-Hill, Inc., New York, NY.

[27] Doyle, J. C. et al. (1989). "State-space solutions to standard H_2 and H_∞ control problems." *IEEE Transactions on Automatic Control.*, vol.34, No.8, 831-846.

[28] Doyle, J. C., Francis, B. A., and Tannenbaum, A. R. (1992). *Feedback control theory.* Macmillan Publishing Company, New York, New York.

[29] Fleming J. F., and Egeseli, E. A.(1980). "Dynamic behaviour of a cable-stayed bridge." *Earthquake Eng. Struct. Dyn.* 8, 1-16.

[30] Gimsing, N. J. (1983). *Cable supported bridges : concept and design.* John Wiley & Sons, Inc., New York, NY.

[31] Green, M., and Limebeer, D. J. N. (1995). *Linear robust control.* Prentice Hall, Inc., Englewood Cliffs, New Jersey.

[32] Gupta, R. K. (1980). "Dynamic loading of highway bridges." *J. Engrg. Mech. Div.*, ASCE, 106(2), 377-394.

[33] Harichandran, R. S., and Wang, W. (1988). "Response of simple beam to spatially varying earthquake excitation." *J. Engrg. Mech.*, ASCE, 114(9), 1526-1541.

[34] Hegab, H. I. A. (1986). "Energy analysis of cable-stayed bridges." *J. Struct. Engrg.*, ASCE, 112(5), 1182-1195.

[35] Hutton, D. V. (1993). "Dynamic analysis of active-control, cable-stayed guideway." *J. Struct. Engrg.*, ASCE, 119(8), 2403-2420.

[36] Igusa, T., and Kiureghian, A. D. (1985). "Dynamic response of multiply supported secondary systems." *J. Engrg. Mech.*, ASCE, 111(1), 20-41.

[37] Jain, S. K. (1984). "Continuum models for dynamics of buildings." *J. Engrg. Mech.*, ASCE, 110(12), 1713-1730.

[38] Khalifa, M. A. (1993). "Parametric study of cable-stayed bridge response due to traffic-induced vibration." *Computers & Structures.*, 47(2), 321-339.

[39] Koh, C. G., and See, L. M. (1994). "Identification and uncertainty estimation of structural parameters." *J. Engrg. Mech.*, ASCE, 120(6), 1219-1236.

[40] Lazar, B. E. (1972). "Stiffness analysis of cable-stayed bridges." *J. Struct. Div.*, ASCE, 98(ST7), 1605-1612.

[41] Livesley, R. K. (1975). *Matrix methods of structural analysis.* 2nd Edt., Pergamon Press, Oxford, London.

[42] Logan, D. L. (1992). *A first course in the finite element method.* 2nd Ed., PWS-KENT Publishing Company, Boston, Massachusetts.

[43] Lutes, L. D., and Lilhanand, K. (1979). "Frequency content in earthquake simulation." *J. Engrg. Mech. Div.*, ASCE, 105(1), 143-158.

[44] Meirovitch, L., and Silverberg, L. M. (1983). "Control of structures subjected to seismic excitation." *J. Engrg. Mech.*, ASCE, 109(2), 604-618.

[45] Meirovitch, L., and Ghosh, D. (1987). "Control of flutter in bridges." *J. Engrg. Mech.*, ASCE, 113(5), 720-736.

[46] Melosh, R. J., and Smith, H. A. (1989). "New formulation for vibration analysis." *J. Engrg. Mech.*, ASCE, 115(3), 543-554.

[47] Miller, R. K., Masri, S. F., Dehghanyar, T. J., and Caughey, T. K. (1988). "Active vibration control of large civil structures." *J. Engrg. Mech.*, ASCE, 114(9), 1542-1570.

[48] Morris, N. F. (1974). "Dynamic analysis of cable-stiffened structures." *J. Struct. Div.*, ASCE, 100(ST5), 971-981.

[49] Morris, N. F. (1976). "Analysis of cable-stiffened space structures." *J. Struct. Div.*, ASCE, 102(ST3), 501-513.

[50] Mote, S. H., and Chu, K. H. (1978). "Cable trusses subjected to earthquake." *J. Struct. Div.*, ASCE, 104(ST4), 667-680.

[51] Naeim, F. (1989). *The seismic design handbook.* Van Nostrand Reinhold, New York, New York.

[52] Naeim, F., and Anderson, J. C.(1993). *Classification and evaluation of earthquake records for design* . The 1993 NEHRP Professional Fellowship Report, EERI.

[53] Nazmy, A. S., and Abdel-Ghaffar, A. M.(1990a). "Non-linear earthquake-response analysis of long-span cable-stayed bridges : Theory." *Earthquake Eng. Struct. Dyn.* 19, 45-62.

[54] Nazmy, A. S., and Abdel-Ghaffar, A. M.(1990b). "Non-linear earthquake-response analysis of long-span cable-stayed bridges : Applications." *Earthquake Eng. Struct. Dyn.* 19, 63-76.

[55] Podolny, W. Jr., and Scalzi, J. B. (1986). *Construction and design of cable-stayed bridges.* 2nd Edt., John Wiley and Sons, Inc., New York, New York.

[56] Pu, J., and Hsu, D. (1988). "Optimal control of tall building." *J. Engrg. Mech.*, ASCE, 114(6), 973-989.

[57] Raoof, M., and Huang, Y. P. (1991). "Upper-bound prediction of cable damping under cyclic bending." *J. Engrg. Mech.*, ASCE, 117(12), 2729-2747.

[58] Rodellar, J., Barbat, A. H. and Martin-Sanchez, J. M. (1987). "Predictive control of structures." *J. Engrg. Mech.*, ASCE, 113(6), 797-812.

[59] Rodellar, J., Chung, L. L., Soong, T. T., and Reinborn, A. M. (1989). "Experimental digital control of structures." *J. Engrg. Mech.*, ASCE, 115(6), 1245-1261.

[60] Roorda, J. (1975). "Tendon control of tall structures." *J. Struct. Div.*, ASCE, 101(ST3), 505-521.

[61] Rugh, W. J.(1993). *Linear system theory.* Prentice Hall, Inc., Englewood Cliffs, New Jersey.

[62] Sae-Ung, S., and Yao, J. T. P. (1978). "Active control of building structures." *J. Engrg. Mech. Div.*, ASCE, 104(2), 335-349.

[63] Safak, E. (1989a). "Adaptive modeling, identification, and control of dynamic structural systems : I. Theory." *J. Engrg. Mech.*, ASCE, 115(11), 2386-2405.

[64] Safak, E. (1989b). "Adaptive modeling, identification, and control of dynamic structural systems : II. Applications." *J. Engrg. Mech.*, ASCE, 115(11), 2406-2426.

[65] Samali, B., Yang, J. N., and Yeh, C. T. (1985). "Control of lateral-torsional motion of wind-excited buildings." *J. Engrg. Mech.*, ASCE, 111(6), 777-796.

[66] Shahian, B., and Hassul, M. (1993). *Control system design using MATLAB.* Prentice Hall, Inc., Englewood Cliffs, New Jersey.

[67] Singh, J. P., and Tabatabaie, M. (1991). "Strong motion data - Application to multiple support structures." *Geotechnical News.*, March, 38-41.

[68] Singh, M. P., and Ghafory-Ashtiany, M. (1984). "Structural response under multicomponent earthquakes." *J. Engrg. Mech. Div.*, ASCE, 110(5), 761-775.

[69] Sirlin, S., Paliou, S. M., Longman, R. W., Shinozuka, M., and Samaras, E. (1986). "Active control of floating structures." *J. Engrg. Mech.*, ASCE, 112(9), 947-965.

[70] Spencer Jr, B. F., Suhardjo, J., and Sain, M. K. (1994). "Frequency domain optimal control strategies for aseismic protection." *J. Engrg. Mech.*, ASCE, 120(1), 135-158.

[71] Starossek, U. (1991). "Dynamic stiffness matrix of sagging cable." *J. Engrg. Mech.*, ASCE, 117(12), 2815-2829.

[72] Starossek, U. (1993). "Reduction of dynamic cable stiffness to linear matrix polynomial." *J. Engrg. Mech.*, ASCE, 119(10), 2132-2136.

[73] Stefani, R. T., Savant, C. J., Shahian, B., and Hostetter, G. H.(1994). *Design of feedback control systems.* 3rd Ed., Saunders College Publishing, Boston.

[74] Stoorvogel, A. (1992). *The H_∞ control problem.* Prentice Hall, Inc., London, United Kingdom.

[75] Tang, M. C. (1971). "Analysis of cable-stayed bridges." *J. Struct. Div.*, ASCE, 97(ST5), 1481-1496.

[76] Tang, M. C. (1971). "Design of cable-stayed girder bridges." *J. Struct. Div.*, ASCE, 98(ST8), 1789-1802.

[77] Triantafyllou, M. S., and Howell, C. T. (1992). "Nonlinear impulsive motions of low-tension cable." *J. Engrg. Mech.*, ASCE, 118(4), 807-830.

[78] Troitsky, M. S. (1994). *Planning and design of bridges.* John Wiley & Sons, Inc., New York, NY.

[79] Udwadia, F. E. (1994). "Methodology for optimal sensor locations for parameter identification in dynamic systems." *J. Engrg. Mech.*, ASCE, 120(2), 368-390.

[80] Veillette, R. J.(1990). *Reliable control of decentralized systems : An ARE-based H_∞ approach.* Ph.D Thesis, University of Illinois at Urbana-Champaign, Illinois.

[81] Vilnay, O. (1984). "Active control of machinery foundation." *J. Engrg. Mech. Div.*, ASCE, 110(2), 273-281.

[82] Walther, R., et al. (1988). *Cable-stayed bridges.* Thomas Telford, London, United Kingdom.

[83] Warnitchai, P., Fujino, Y., Pacheco, B. M., and Agret, R. (1993). "An experimental study on active tendon control of cable-stayed bridges." *Earthquake Eng. Struct. Dyn.*, 22, 93-111.

[84] Wilson, H. B., and Gupta, S. (1992). "Math software package simplifies structural analysis." *Sound and Vibration*, August, 24-29.

[85] Wong, H. L., and Luco, J. E. (1991). "Structural control including soil-structure interaction effects." *J. Engrg. Mech.*, ASCE, 117(10), 2237-2250.

[86] Xu, Y. L., Samali, B., and Kwok, K. C. S. (1992). "Control of along-wind response of structures by mass and liquid dampers." *J. Engrg. Mech.*, ASCE, 118(1), 20-39.

[87] Yang, J. N. (1975). "Application of optimal control theory to civil engineering structures." *J. Engrg. Mech. Div.*, ASCE, 101(6), 819-838.

[88] Yang, J. N., and Giannopoulos, F. (1978). "Active tendon control of structures." *J. Engrg. Mech. Div.*, ASCE, 104(3), 551-568.

[89] Yang, J. N., and Giannopoulos, F. (1979a). "Active control and stability of cable-stayed bridge." *J. Engrg. Mech. Div.*, ASCE, 105(4), 677-694.

[90] Yang, J. N., and Giannopoulos, F. (1979b). "Active control of two-cable-stayed bridge." *J. Engrg. Mech. Div.*, ASCE, 105(5), 795-810.

[91] Yang, J. N., and Lin, M. J. (1982a). "Optimal critical-mode control of building under seismic load." *J. Engrg. Mech. Div.*, ASCE, 108(6), 1167-1185.

[92] Yang, J. N. (1982b). "Control of tall buildings under earthquake excitation." *J. Engrg. Mech. Div.*, ASCE, 108(5), 833-849.

[93] Yang, J. N., and Lin, M. J. (1983). "Building critical-mode control : Nonstationary earthquake." *J. Engrg. Mech.*, ASCE, 109(6), 1375-1389.

[94] Yang, J. N., Akbarpour, A. and Ghaemmaghami, P. (1987). "New optimal control algorithms for structural control." *J. Engrg. Mech.*, ASCE, 113(9), 1369-1386.

[95] Yang, J. N., and Akbarpour, A. (1990). "Effect of system uncertainty on control of seismic- excited buildings." *J. Engrg. Mech.*, ASCE, 116(2), 462-478.

[96] Yao, J. T. P. (1972). "Concept of structural control." *J. Struct. Div.*, ASCE, 98(7), 1567-1574.

[97] Zames, G. (1981). "Feedback and optimal sensitivity : Model reference transformation, multiplicative seminorms and approximate inverses." *IEEE Transactions on Automatic Control*, AC-26, 301-320.